Extraction and Upgrading of Bio-Crude and Bio-Residue from Hydrothermal Liquefaction of Agricultural Biomass

A Thesis Submitted to the College of Graduate and Postdoctoral Studies
in Partial Fulfilment of the Requirements for the

Degree of Master of Science

in the Department of Chemical and Biological Engineering
University of Saskatchewan
Saskatoon, SK, Canada

By

RISHAV CHAND

PERMISSION TO USE

In presenting this thesis towards the partial fulfilment of the requirements for Master of Science degree from the University of Saskatchewan, the author agrees that the libraries of the University of Saskatchewan may make it freely available for reference. The author further agrees that the copying of this thesis in any manner, entirely or partially, for academic purpose may be granted by Dr. Ajay Dalai who supervised this thesis work, or in his absence, by the Head of the Department of Chemical and Biological Engineering or by the Dean of the College of Graduate Studies and Research at the University of Saskatchewan. However, it is understood that any copying or publication or use of this thesis or parts thereof for financial gains shall not be permitted without the author's written approval. It is also understood that the author would be recognized and so will the University of Saskatchewan be for any scholarly use of any material available in this thesis.

Request for permission to copy or to make other use of the material in this thesis in whole or in part should be addressed to:

Head of the Department

Chemical and Biological Engineering

University of Saskatchewan

57 Campus Drive

Saskatoon, Saskatchewan S7N 5A9 Canada

OR

Dean

College of Graduate and Postdoctoral Studies

University of Saskatchewan

Room 116 Thorvaldson Building, 110 Science Place

Saskatoon, Saskatchewan S7N 5C9 Canada

ABSTRACT

Fossil-based sources of energy have conventionally driven the human civilization till date. However, in the wake of an unprecedented population explosion, these conventional sources of energy are falling short of meeting the increased global demand due to the finite nature of their reserves. Moreover, they have increasingly caused the environment to deteriorate due to the pollutants that are released into the atmosphere as a result of their utilization. This has caused researchers to look for alternative renewable sources of energy which would also be environmentally benign. Bio-crude is one such alternative which can potentially substitute the use of fossil-based fuels such as petroleum crude. Bio-crude can be produced via two main processes: fast pyrolysis and hydrothermal liquefaction (HTL). Due to certain inherent drawbacks of the pyrolysis process, the focus is currently on producing bio-crude from the HTL process. In the present study, three different solvents – ethyl acetate, tetrahydrofuran and petroleum ether – were used to extract bio-crude from a hydrothermal liquefaction product mixture obtained from canola meal and waste wheat flour. The bio-crude yields and the ease of extraction were compared for each of the solvents to evaluate the efficacy of the solvent-extraction process and to determine the most suitable solvent for the same. The extracted bio-crude and bio-residue fractions were characterized in detail so as to determine their physicochemical properties and identify the samples that would be ideal for further upgrading processes. The bio-crude thus produced has a high percentage of oxygen and thus, needs to be upgraded to make it comparable with diesel fuel for utilization in different applications. Therefore, the report further focusses on decreasing the amount of oxygen present in HTL bio-crude via catalytic hydrodeoxygenation (HDO). To serve the purpose, carbon-supported molybdenum carbide catalysts were synthesized via Carbothermal Hydrogen Reduction (CHR) method using three different carbon supports – commercial activated carbon, commercial multi-walled carbon nanotubes and bio-residue obtained during solvent-extraction. The catalysts were screened for their oxygen reduction efficiency using a blend of bio-crude in hydrotreated heavy gas oil and the efficiency of the best-performing catalyst was compared with that of commercial hydrotreating catalysts. The synthesized catalysts were characterized in order to explain their oxygen reduction percentages and a parametric study was carried out for the best-performing catalyst to determine the effects of process parameters such as temperature, pressure, reaction time and catalyst loading on oxygen reduction efficiency.

ACKNOWLEDGEMENT

I would like to express my sincere gratitude to my supervisor, Dr. A. K. Dalai for providing encouragement, support and guidance on my thesis work. His timely advices and vast expertise over the research subject helped me fine-tune my research, gain new perspectives on the topic and develop healthy research habits that enabled me to compile the current manuscript. I would remain forever grateful to him for providing me with an environment that fosters research and learning. I would also like to thank my advisory committee members – Dr. Jafar Soltan and Dr. Hui Wang for their time and valuable suggestions that helped me design my research, correct my mistakes and above all, gain more knowledge about my research than any book could ever provide.

I am also thankful to Dr. Venu Babu Borugadda for being a friend, a guide and an elder brother to me. He guided me at every step with a smile on his face and his reassuring presence both inside the laboratory and outside of it played a crucial part in shaping the research the way it is. I would like to mention Dr. Philip Boahene and Mr. Girish Kamath and thank them for their ever-readiness in answering my queries and helping me to operate reactor systems and certain characterization instruments. I would also like to express my gratitude to Ms. Heli Eunike and Mr. Richard Blondin for teaching me laboratory skills, helping me with my characterizations and for being constant sources of support inside the laboratory.

I would like to gratefully acknowledge the financial support received from the Natural Sciences and Engineering Research Council of Canada (NSERC) towards completion of the current research work. My gratitude also goes to Mr. Michael Qiu and NULIFE Green Tech for providing the HTL product mixture and to Saskatchewan Structural Sciences Centre (SSSC) for providing the NMR and XPS facilities.

Finally, I would like to state my humble gratitude towards my parents, my younger sister and my friends, both near and far, for their constant encouragement and motivation throughout the duration of my research work. Their selfless cooperation and unwavering support were priceless in ensuring that all my efforts culminated in the form of this thesis.

TABLE OF CONTENTS

LIST OF TABLES

LIST OF FIGURES

NOMENCLATURE

AC	Activated Carbon
BC	Bio-crude
BET	Brunauer-Emmett-Teller
BJH	Barret-Joyner-Halenda
BR	Bio-residue
CHR	Carbothermal Hydrogen Reduction
CNF	Carbon Nanofiber
CNT	Carbon Nanotube
CP/TOSS	Cross-Polarization/Total Suppression of Sidebands
DCO	Decarbonylation
DCO_2	Decarboxylation
DMDS	Dimethyl Disulphide
DTG	Derivative Thermogravimetry
EA	Ethyl Acetate
FAME	Fatty Acid Methyl Esters
FTIR	Fourier Transform Infrared Spectroscopy
GC-MS	Gas Chromatography-Mass Spectrometry
HAS	Hemi-spherical Analyzer
HDA	Hydrodearomatization
HDM	Hydrodemetallization
HDN	Hydrodenitrogenation
HDO	Hydrodeoxygenation
HDS	Hydrodesulphurization
HGO	Heavy Gas Oil
HHGO	Hydrotreated Heavy Gas Oil
HHV	Higher Heating Value
HTL	Hydrothermal Liquefaction

HVGO	Heavy Vacuum Gas Oil
HYD	Hydrogenation
IP	Induction Period
LGO	Light Gas Oil
LVGO	Light Vacuum Gas Oil
MWCNT	Multi-walled Carbon Nanotube
NMR	Nuclear Magnetic Resonance
PE	Petroleum Ether
RGO	Reduced Graphene Oxide
Sim-Dist	Simulated Distillation
SMA	Spherical Mirror Analyzer
TGA	Thermogravimetric Analysis
THF	Tetrahydrofuran
TPD	Temperature Programmed Desorption
TPR	Temperature Programmed Reduction
XPS	X-ray Photoelectron Spectroscopy
XRD	X-ray Diffraction

1. INTRODUCTION

1.1 Research Background

Fossil fuels, such as petroleum crude, are non-renewable sources of energy and their reserves are fast depleting in the wake of increased global demand (Sorrell et al., 2010, Mortensen et al., 2011). Under the circumstances, biomass-derived fuels (bio-fuels), such as bio-crude, can prove to be promising substitutes for the conventional fossil-based fuels. Bio-fuels can be produced within a relatively short cycle and unlike fossil fuels, they maintain a closed carbon cycle, i.e., the net increase in CO_2 levels in the atmosphere is almost negligible. Biomass, in the form of green plants, absorb carbon from the atmosphere in order to promote their growth and development, and upon combustion of derived bio-fuels, the absorbed carbon is eventually emitted back to the atmosphere (Mortensen et al., 2011, Xiu and Shahbazi, 2012). Moreover, as plant biomass contains negligible amounts of sulphur, combustion of bio-crude would not generate much SO_x emissions. NO_x emissions also go down by more than 50% when bio-crude is used in place of diesel oil in a gas turbine. Thus, bio-crude has less adverse effects on the environment as compared to petroleum crude oil (Xiu and Shahbazi, 2012).

There are two main conversion technologies by which biomass can be converted into bio-crude: biochemical and thermochemical conversion (Gollakota et al., 2018). Biochemical conversion technologies have certain disadvantages such as requirement of pre-processing stages, longer processing times, inferior space-time yields and energy-intensive downstream processing, which restrict their application (Gollakota et al., 2018, Singh et al., 2015). Thermochemical conversion technologies can be broadly classified into four categories: direct combustion, gasification, pyrolysis and hydrothermal liquefaction (Gollakota et al., 2018, Dimitriadis and Bezergianni, 2017). Direct combustion is mostly used for generating heat energy to produce electricity. Gasification yields a gaseous product and it would require an auxiliary process to convert that into liquid hydrocarbons (Dimitriadis and Bezergianni, 2017). Fast pyrolysis and hydrothermal liquefaction (HTL) are two comparable thermochemical conversion technologies that yield significant amounts of an energy-rich liquid product termed as bio-crude.

However, the bio-crude produced by either of the methods has some undesired properties such as high moisture content, high viscosity, high ash content, high oxygen content and high acidity or corrosiveness. These unwanted characteristics need to be eliminated before the bio-crude can be either utilized for co-processing in refineries alongside petroleum crude oil or used as a direct drop-in biofuel that can be applied to the existing transportation infrastructure (Xiu and Shahbazi, 2012, Jensen et al., 2016). Some of the current techniques used for upgrading bio-crude include hydrotreating, hydrocracking, solvent addition/esterification, emulsification, etc. (Xiu and Shahbazi, 2012, Lian et al., 2017). Among these, the hydrotreating method is widely used at present in all refineries for upgrading petroleum crude. Co-processing (hydrotreating) of bio-crude alongside petroleum crude is the preferred modus operandi to ensure an efficient and economic phase-in of bio-crude utilization in the existing refinery infrastructure (Sauvanaud et al., 2018). Hence, the primary focus of this work will be on hydrotreating the HTL bio-crude after blending it with a refinery intermediate.

The present study uses a post-HTL product mixture as the feedstock and attempts to extract bio-crude from it via solvent-extraction method using three different solvents: ethyl acetate (EA), tetrahydrofuran (THF) and petroleum ether (PE). The study further attempts to upgrade the extracted bio-crude (which is most suitable for bio-diesel applications) using synthesized and commercial catalysts and thereafter, determine the desirable reaction conditions for carrying out the upgrading process. The HTL product mixture used originated from a combination of canola meal (agricultural waste) and waste wheat flour (food waste). Canola is one of the most widely grown crops in Canada; in 2018, approximately 20,342,600 metric tonnes of canola was produced in Canada (Statistics Canada, 2019). Therefore, utilizing canola meal as a feedstock is a reasonably sustainable approach (Casséus, 2009). Also, large amounts of wheat flour are wasted during the production process and during transportation (Baloch, 1999, Khader et al., 2019). Presently, in Saskatchewan (a Western Canadian province), NULIFE Green Tech carries out hydrothermal liquefaction of a combination of the aforementioned feedstocks for commercial purposes. Therefore, in order to complement industrial activities, the current research aims at utilizing the HTL product mixture procured from NULIFE Green Tech.

1.2 Knowledge Gaps

Based on the literature review discussed in Chapter 2, the following knowledge gaps were identified:

1) To the best of the author's knowledge, no study has been carried out on extraction of bio-crude from a hydrothermal liquefaction (HTL) product mixture obtained from a combination of canola meal and waste wheat flour feedstocks. Additionally, the characterization studies carried out for bio-crude and bio-residue fractions in previous reports are fairly limited and have seldom been attempted in a single study.

2) Limited number of studies have been done on metal carbide catalysts for the hydrodeoxygenation process and even fewer studies have focussed on incorporating carbon-supported molybdenum carbide catalysts for the hydrodeoxygenation of bio-crude. A handful of studies have been carried out which separately investigate the hydrodeoxygenation of individual oxygenates present in bio-crude such as phenolic compounds, carboxylic acids and heterocyclic compounds like furfural, benzofuran, etc. However, the hydrodeoxygenation of HTL bio-crude as a whole is scarcely reported in literature.

1.3 Hypotheses

1) Extraction of bio-crude from a post-HTL product mixture and characterization of the resultant bio-crude and bio-residue fractions would help in evaluating the potential for further upgrading processes and subsequent applications as bio-diesel (for bio-crude) or carbon-based catalyst supports (for bio-residue).

2) Carbon-supported molybdenum carbide catalysts would not be suffering from the inherent drawbacks of conventional metal sulphide catalysts and hence, would work better than commercial hydrotreating catalysts for the hydrodeoxygenation of HTL bio-crude. In addition, the superior textural properties of carbon support materials would be favourable towards enhancing the catalytic activity of molybdenum carbide catalysts. Compared to γ-Al_2O_3 supports, carbon supports have higher tolerance towards moisture which results in lower deactivation rates for the catalyst. Moreover, carbon supports are much cheaper and therefore, they are sustainable in the long run.

1.4 Research Objectives

1) Phase 1: To extract bio-crude from an HTL product mixture via solvent-extraction process using three different solvents – ethyl acetate (EA), tetrahydrofuran (THF) and petroleum ether (PE) – and to compare the bio-crude yields and the ease of extraction for each of the solvents in order to determine the most suitable solvent for carrying out the extraction process. Thereafter, the extracted bio-crude and bio-residue fractions would be characterized using different analytical techniques so as to determine their physicochemical properties and identify the samples that would be ideal for further upgrading processes.

2) Phase 2: To synthesize carbon-supported metal carbide catalysts by using molybdenum as the active metal and three different types of carbon supports – commercial activated carbon (AC), commercial multi-walled carbon nanotubes (MWCNT) and bio-residue (BR) obtained during Phase 1 of research. The synthesized catalysts would be characterized and used for hydrodeoxygenation (HDO) of bio-crude blends. Based on preliminary screening tests for oxygen reduction efficiency, the best-performing catalyst would then be used for a comparative study with commercial hydrotreating catalysts such as $CoMo/\gamma\text{-}Al_2O_3$ (3 wt. % Co, 13 wt. % Mo) and $NiMo/\gamma\text{-}Al_2O_3$ (3 wt. % Ni, 13 wt. % Mo). Lastly, the best-performing catalyst would be used for carrying out hydrodeoxygenation reactions at different conditions in order to determine the effect of process parameters such as temperature (250-350 °C), pressure (3-7 MPa), reaction time (1-5 h) and catalyst loading (1-5% w/w) on the oxygen reduction percentage.

2. LITERATURE REVIEW

2.1 Thermochemical Conversion Routes for Biomass

2.1.1 Pyrolysis

In a broad sense, all plants (flora) and other living organisms (fauna) which are directly or indirectly dependent on the photosynthetic ability of these plants to convert sunlight and CO_2 into chemical energy constitute biomass. Biomass resources include wood and wood-processing residues, short-rotation woody crops, food crops, energy crops, aquatic plants, algae, animal wastes and cooking wastes, among many others (Lian et al., 2017, Akhtar and Amin, 2011). Depending on the species of origin, vegetative biomass can have varying compositions of lignin, cellulose and hemicelluloses (Akhtar and Amin, 2011).

Biomass pyrolysis is a very complex endothermic process which involves the thermal degradation of solid organic matter into mostly liquids and gases when heated in a non-reactive environment, i.e., in the absence of air/oxygen. The long-chain hydrocarbons present in biomass decompose into smaller compounds under pyrolysis conditions, and both the rate and extent of decomposition depend on the variations in pyrolysis temperature, rate of heating, pressure of the system, configuration of the reactor, nature of the feedstock, etc. Depending on the operating conditions, biomass pyrolysis has been classified into three categories: slow pyrolysis, fast pyrolysis and flash pyrolysis (Jahirul et al., 2012).

Among all the three pyrolysis processes, fast pyrolysis technology is currently the most popular option due to its high bio-oil yield and fewer associated drawbacks. Fast pyrolysis of a biomass is carried out at atmospheric pressure and high temperatures in the range of 400-600 °C for approximately 1 second. The bio-crude thus produced has a high oxygen content of 35-40 wt. % and a low energy content of 16-19 MJ/kg. The presence of oxygen in high quantities leads to inferior thermal stability of the bio-crude as well as increased costs of upgrading (Tzanetis et al., 2017).

All the pyrolysis techniques require biomass feedstocks that have low (<40%) moisture contents and in order to achieve a positive energy balance, the feedstock needs to be dried via an energy-consuming process before it can be subjected to pyrolysis (Akhtar and Amin,

2011). Therefore, much of the recent research has shifted towards investigating the characteristics of hydrothermal liquefaction as an improvement over the pyrolysis processes.

2.1.2 Hydrothermal Liquefaction (HTL)

Also known as hydrous pyrolysis, hydrothermal liquefaction process is carried out at lower temperatures and lower heating rates than conventional pyrolysis methods. Hydrothermal liquefaction involves the use of wet biomass and hence, no excess energy is required for drying the feedstock (Filippis et al., 2016). Consequently, a wide variety of feedstocks having high moisture contents can be used for this process. Hydrothermal liquefaction involves the treatment of biomass in an aqueous environment at moderate temperatures in the range of 280-380 °C and high pressures in the range of 7-25 MPa (sub- or super-critical state) for 10-60 minutes (Tzanetis et al., 2017, Filippis et al., 2016). The bio-crude produced from this process has a lower oxygen content (5-10 wt. %) and a higher energy content (30-40 MJ/kg) than pyrolysis oil (Jin, 2014, Demirbas, 2011).

Effects of Temperature

Biomass depolymerization takes place when the temperature is sufficiently larger than the activation energies for bond breakage. Hydrolysis and re-polymerization are the two main competing reactions that take place during pyrolysis or hydrothermal liquefaction. During the initial stages of the process, hydrolysis and depolymerization of biomass is the dominant reaction while in the later stages, re-polymerization reactions dominate which lead to the formation of bio-char (Akhtar and Amin, 2011).

Biomass liquefaction is endothermic at low temperatures but exothermic at high temperatures and hence, the process is thermodynamically unfavourable. At low temperatures, the bio-oil yield increases with increasing temperature and reaches a maximum value. Thereafter, any further increase in temperature leads to an increasingly reduced bio-oil yield due to inhibition of biomass liquefaction (Akhtar and Amin, 2011).

At high temperatures, the concentration of free radicals increases which results in a higher probability of re-polymerization reactions to take place and form bio-char (Akhtar and Amin, 2011). In addition, secondary decompositions and the Boudouard reaction contribute to the formation of gases at such high temperatures (El-Rub et al., 2004). It is not advisable to carry

out the HTL process at extremely high temperatures because it would lead to high operational costs and reduced bio-oil yields. It has been observed that higher amounts of bio-oil are produced at intermediate temperatures in the range of 300-350 °C (Akhtar and Amin, 2011).

Effects of Pressure

Both sub- and super-critical HTL conditions require a highly pressurized system to maintain a single-phase media throughout the duration of the process. Two-phase systems require large heat inputs to maintain the reaction temperature and therefore, the liquefaction media should not be allowed to undergo any phase change during the process (Akhtar and Amin, 2011, Goudriaan et al., 2000). The pressure must be maintained above the critical pressure value for the medium so as to facilitate the production of liquid bio-fuels via thermodynamically favourable reaction pathways. In addition, pressure increases the density of the medium. As a result, the solvent efficiently penetrates into the biomass molecules and enhances decomposition and extraction processes (Akhtar and Amin, 2011). However, the properties of water or the aqueous phase in super-critical state are negligibly affected by changes in pressure. Hence, in super-critical liquefaction, variation in pressure has no significant effect on the overall yield of bio-oil (Akhtar and Amin, 2011, Sangon et al., 2006).

Effects of Solvent Density (Solvent-to-Biomass Ratio)

Water is the most commonly used solvent for thermo-chemical liquefaction processes. During the HTL process, water functions as a solvent, as a reactant and also as a catalyst (Dimitriadis and Bezergianni, 2017, Chornet and Overend, 1985). The weight ratio of biomass to water (inverse of solvent density) is regarded as an important parameter for controlling the bio-oil yield (Akhtar and Amin, 2011).

Increasing the biomass-to-water ratio results in a decrease in the bio-oil yield. At high biomass-to-water ratios, there are fewer solvent molecules available per unit volume of biomass molecules. This hinders the extraction and dissolution of biomass components by the solvent. Hence, a higher solvent density can lead to a higher bio-oil yield. However, this result comes at the expense of increased in-process energy consumption and elevated costs for processing the downstream wastewater (Akhtar and Amin, 2011, Qu et al., 2003). Moreover, beyond a certain threshold, increasing the solvent density actually leads to a

decrease in the production of bio-oil (Boocock and Sherman, 1985). Generally, in an HTL process, the biomass-to-water weight ratio is kept in the range of 0.1-0.2 (Filippis et al., 2016).

2.2 Separation of Hydrothermal Liquefaction Products

In addition to bio-crude, a typical HTL process also results in the formation of aqueous phase by-products containing dissolved organics, gaseous products and a solid residue (bio-residue). After releasing the gaseous products, an organic solvent is added to the HTL product mixture. The bio-crude dissolves in the organic solvent and forms an organic liquid phase. The organic phase is then separated from the product mixture and the solvent evaporated to obtain liquid bio-crude. Thereafter, the solid residue is removed from the aqueous phase and water is evaporated from the remaining aqueous mixture to recover dissolved organics (Valdez et al., 2011).

Different authors have reported different variations of the aforementioned process for separating the HTL products (Valdez et al., 2011, Kader et al., 2015, Ross et al., 2010, Yang et al., 2014, Zou et al., 2009). Moreover, different organic solvents such as acetone, chloroform, dichloromethane, tetrahydrofuran, ethyl acetate, petroleum ether, cyclohexane, hexane, methoxy-cyclopentane, etc., have been employed in these studies for carrying out the separation process. It has been further suggested that the yield and composition of bio-crude and bio-residue fractions might be influenced by the specific solvent that is used for the extraction process (Valdez et al., 2011).

2.3 Upgrading of Hydrothermal Liquefaction Bio-crude

2.3.1 Hydrotreating Process Overview

Hydrotreating is a catalytic process used extensively to reduce sulphur and other undesirable compounds such as nitrogen, metals, oxygen, aromatics and unsaturated hydrocarbons from refinery processing streams. These compounds adversely affect the stability and performance of the oil, contribute to catalyst poisoning in downstream unit operations and make the oil incompatible with respect to environmental regulations (Badoga, 2015, Mapiour, 2009). Hydrotreating includes variety of processes such as hydrodesulphurization (HDS), hydrodenitrogenation (HDN), hydrodearomatization (HDA), hydrodemetallization (HDM)

hydrodeoxygenation (HDO), and olefin saturation. In this process, hydrogen is used at high pressure and temperature in the presence of a metal catalyst to achieve the removal of unwanted constituents from crude oil. For lighter feedstock such as naphtha, the hydrotreating process is carried out at temperatures ranging from 260 °C to 343 °C and pressures ranging from 1.4 MPa to 3.4 MPa. On the other hand, for heavier feedstocks, the hydrotreating process requires temperatures in the range of 343-427 °C and pressures in the range of 6.9-13.8 MPa (Mapiour, 2009, Botchwey, 2003).

2.3.2 Hydrotreating Reactions

The hydrotreating reaction (2.1) is represented as:

$$\text{Feed} + H_2 \rightarrow \text{Hydrocarbon} + H_2S + NH_3 + H_2O \quad (2.1)$$

Hydrogen reacts with the hydrocarbon feedstock in the presence of a suitable catalyst to produce saturated hydrocarbons, H_2O, hydrogen sulphide (H_2S) and ammonia (NH_3) (Mapiour, 2009). All the hydrotreating reactions are exothermic in nature which causes an increase in the reaction temperature as the feed passes through the catalyst bed. It has been reported that the values of K_{eq} for HDS and HDN are positive over a wide range of temperatures (on the commercial scale). This indicates that hydrotreating reactions are basically irreversible and can proceed to completion if hydrogen is present in stoichiometric quantity. For all practical purposes, n^{th} order kinetics with respect to the total concentration of the heteroatom is used for the hydrotreating process. The n-value depends on various factors: a) type and concentration of the heteroatom, b) properties of the catalyst, c) nature of the feed, d) operating conditions, etc., and it has been observed that the value of n for most hydrotreating reactions is typically greater than 1 (Fundamentals of Hydrotreating Part 1, 2019).

2.3.3 Hydrotreating Catalysts

As is the case with many other chemical reactions, hydrotreating also requires suitable catalysts to speed up the process. Hydrotreating catalysts consist of three main constituents:

a) An active component – Molybdenum (Mo) is most commonly used but occasionally, tungsten (W) is also used (Mapiour, 2009).

b) A promoter – It is also a metal (other than the active component) which helps to stabilize

the catalyst and thus, improves the overall catalytic activity. Cobalt (Co) or nickel (Ni) are normally used to promote molybdenum catalysts (Mapiour, 2009).

c) A support – Gamma alumina (γ-Al_2O_3) is normally used as the support material. Its main purpose is to impart mechanical strength to the catalyst (Satterfield, 1996). The acidity of the support material and the corresponding metal-support interactions lead to an increase in the catalytic activity of the hydrotreating catalyst. Furthermore, the addition of small amounts of phosphorous or silica to the support has been found to enhance its acidity (Mapiour, 2009, Gruia, 2006).

At present, NiMo/γ-Al_2O_3 and CoMo/γ-Al_2O_3 are the most widely used commercial hydrotreating catalysts (Rana, 2016). CoMo catalysts are the most popular and economic choice for desulphurization. NiMo catalysts are used in place of CoMo catalysts when more refractory sulphur compounds need to be removed (Badoga, 2015, Stanislaus et al., 2010). NiMo catalysts are also the primary choice for both de-nitrogenation and de- aromatization (Girgis and Gates, 1991, Gary et al., 2007). Though NiW is the most efficient catalyst for such cases, it is much more expensive than NiMo and hence, is seldom used (Gary et al., 2007).

2.3.4 Hydrodeoxygenation of Bio-crude

Owing to their origin from ligno-cellulosic biomass feedstocks, HTL bio-crudes have been found to possess significantly low amounts (< 0.5 wt. %) of sulphur and nitrogen (Jensen et al., 2016). Nonetheless, the amount of oxygen present in HTL bio-crude is pretty high compared to petroleum crude. Therefore, hydrodeoxygenation (HDO) is the primary objective of hydrotreating in the present case. In petroleum crude, the heteroatom (N, S, O, etc.) content is a function of boiling point, i.e., the majority of N and S content is found in the high-boiling fractions while their concentration in the low-boiling fractions is almost negligible (Gary et al., 2007). On the other hand, such distribution is not observed in the case of HTL bio-crude; the oxygenates have been found to exist in significant quantities in different fractions of the bio-crude. The oxygenates comprise of phenols, alcohols, carbonyls, carboxylic acids, ketones, ethers, etc. These compounds have different hydrodeoxygenation reactivities and consume different amounts of hydrogen during deoxygenation (Jensen et al., 2016).

2.3.5 Deoxygenation Reactions

Deoxygenation can proceed through hydrogenation (HYD) followed by hydrodeoxygenation (HDO) reactions if the HTL bio-crude contains large numbers of hydroxyl and carbonyl groups. Besides, decarboxylation and decarbonylation reactions can also occur if carboxylic acids and aldehydes are present in the bio-crude (Jensen et al., 2016).

i) Hydrodeoxygenation (HDO): Hydrogen is used as a reducing agent to react with oxygen-containing compounds and remove the oxygen atom in the form of H_2O. A typical hydrodeoxygenation process has been shown in reaction (2.2):

$$(CH_2O) + H_2 \rightarrow (CH_2) + H_2O \quad (2.2)$$

ii) Decarboxylation (DCO_2): Carboxyl groups present in the bio-crude undergo decomposition and the oxygen atom is removed in the form of CO_2. The O-H bond breaks and results in the formation of hydrogen ions and carboxylate anions. Carbon dioxide is then formed from the carboxylate anions and the residual alkyl anions couple with H^+ ions to generate hydrocarbons (Li et al., 2018). The decarboxylation process has been shown in reactions (2.3), (2.4) and (2.5):

$$RCOOH \leftrightharpoons RCOO^- + H^+ \quad (2.3)$$

$$RCOO^- \leftrightharpoons R^- + CO_2 \quad (2.4)$$

$$R^- + H^+ \rightarrow R\text{-}H \quad (2.5)$$

iii) Decarbonylation (DCO): In this process, the C-C bonds present in carboxylic acids or aldehydes undergo breakage and the oxygen atom is removed in the form of CO (Li et al., 2018). The reaction (2.6) yields unsaturated hydrocarbons as shown:

$$RCHO \rightarrow R\text{-}H + CO \quad (2.6)$$

However, in the presence of H_2, the process would yield saturated aliphatic hydrocarbons as shown in reactions (2.7) and (2.8):

$$RCOOH + H_2 \rightarrow R\text{-}H + HCOOH \quad (2.7)$$

$$HCOOH \rightarrow CO + H_2O \quad (2.8)$$

Both decarboxylation and decarbonylation reactions involve C-C bond cleavage that results in the formation of hydrocarbons having one less carbon atom than the reactant. Moreover, pollutants such as CO and CO_2 are formed as by-products in the aforementioned reactions. Under the reaction conditions, these by-products may undergo further hydrogenation to produce methane. This would result in a higher H_2 consumption than that in the case of hydrodeoxygenation. On the other hand, hydrodeoxygenation produces hydrocarbons having the same carbon-number as the reactant. In addition, the process yields H_2O as the only by-product and is thus more environment-friendly (Li et al., 2018).

2.3.6 Hydrodeoxygenation Catalysts

Over the years, metal sulphide catalysts such as NiMo/γ-Al_2O_3 and CoMo/γ-Al_2O_3 have been the preferred choice for use in HDO processes (Gutierrez et al., 2009). Toba et al. (2011) investigated the hydrodeoxygenation of waste cooking oil over three sulphide catalysts: NiMo/Al_2O_3, CoMo/Al_2O_3 and NiW/Al_2O_3. The catalysts exhibited similar hydrocarbon yields (~ 100%) and high selectivity for the formation of saturated hydrocarbons. It was also observed that the NiW/Al_2O_3 catalyst facilitated both decarboxylation and decarbonylation reaction pathways and produced more olefins. However, these conventional catalysts are prone to rapid deactivation by leaching of sulphur in the presence of trace quantities of water. Due to low sulphur content of the feedstock, sulphur leaching takes place and brings about changes in the micro-structure of the active sites. This eventually leads to deactivation of the catalyst (Li et al., 2018). Moreover, the addition of sulphating reagents such as H_2S, CS_2 and DMDS can contaminate the final products formed during the HDO process (Hachemi et al., 2016, Kimura et al., 2013). Therefore, recent studies have predominantly focussed on developing sulphur-free hydrodeoxygenation catalysts.

Noble-metal catalysts are known to be efficient in activating molecular hydrogen atoms and hence, they exhibit better catalytic activity and stability on different support materials (Gollakota et al., 2016). Wildschut et al. (2009) compared the HDO efficiency of Ru/C,

Ru/TiO_2, Ru/Al_2O_3, Pd/C and Pt/C catalysts with that of conventional metal sulphide catalysts. The authors reported that the performance of Ru/C catalyst, in terms of oxygen elimination and hydrocarbon yield, was better than all the other catalysts used in the study. Gollakota et al. (2016) mentioned the use of Fe/SiO_2 catalyst for the hydrodeoxygenation of guaiacol. Benzene and toluene were the products obtained in this process. Nickel-based catalysts such as Ni/Al_2O_3 have been shown to achieve an HDO degree of 95% while bi-metallic Ni-Cu catalysts such as $Ni\text{-}Cu/Al_2O_3$ can achieve even better HDO degree of 99.2% (Gollakota et al., 2016). In Table 2.1, some of the HDO catalysts that are found in literature have been summarized.

Table 2.1 Summary of HDO catalysts from literature.

Feed	T (°C)	P (MPa)	Catalyst	Reference
Carbonyl, carboxylic and guaiacyl groups	260-300	7	$CoMo/Al_2O_3$ and $NiMo/Al_2O_3$	Laurent and Delmon, 1994.
Cellulose	300-520	10	$NiMo/Al_2O_3$	Rocha et al., 1996.
Ortho-, meta- and para-cresols	360	7	$NiMo/Al_2O_3$	Wandas et al., 1996.
Guaiacol	280	1	Pt/ZrO_2 and Rh-Pt/ZrO_2	Gutierrez et al., 2009.
4-methyl-acetophenol, ethyl decanoate guaiacol	280	7	CoMo/C	Puente et al., 1999.
Pyrolysis oil	175-300	5-15	Pd/C	Chaiwat et al., 2013.
Eugenol	240	5	Pd/C combined with HZSM-5	Zhang et al., 2014.
Fast pyrolysis oil	150-350	1-10	$Ni\text{-}Cu/Al_2O_3$	Ardiyanti et al., 2012.
Pine saw dust oil	300	3	Ru/Al_2O_3	Xu et al., 2012.
Solvolysed ligno-cellulosic biomass	300	8	MoS_2, MoO_2, Mo_2C and WS_2	Grilc et al., 2015.

2.3.7 Metal Carbide Hydrodeoxygenation Catalysts

Due to the introduction of carbon into the metal lattice, metal carbides exhibit high catalytic activity for HDO similar to noble metals (Furimsky, 2003). Molybdenum carbide (Mo_2C) is the most widely used catalyst in this category. Mo_2C is usually dispersed over alumina, zeolite or carbon supports. The carbon support can be of different structures e.g., carbon nanotube (CNT), carbon nanofiber (CNF), activated carbon (AC) and graphene. In general, metal

carbide catalysts can be prepared via different methods such as temperature programmed reduction (TPR), carbothermal hydrogen reduction (CHR) and microwave-assisted method (Li et al., 2018).

Mo_2C catalysts are highly oxophilic in nature. The adsorption of oxygen atoms on the Mo_2C catalyst during HDO reaction has been shown to result in high deoxygenation selectivity and low hydrogenation selectivity (Wang et al., 2016, Lee et al., 2014). Mo_2C catalysts show preference towards HDO reaction pathway over decarboxylation and decarbonylation because they exhibit high selectivity towards C-O/C=O bond cleavage instead of C-C bond breakage (Ren et al., 2013). Phenolic compounds are considered to be the most refractory species present in bio-oil (Wang et al., 2016). Based on this fact, Jongerius et al. (2012) carried out the HDO reaction for guaiacol using Mo_2C catalysts at 350 °C and 55 bar H_2. The authors observed high selectivity for phenol (45%) and methylated phenols (13%). Lee et al. (2014) also used unsupported Mo_2C catalysts to study the HDO process for anisole and reported impressive selectivity for benzene (> 90%). Han et al. (2011) used Mo_2C/CNT catalyst for deoxygenation of methyl palmitate and vegetable oils, and reported high activity and preference for the HDO pathway. Kim et al. (2015) also observed higher hydrocarbon yield and reduced deactivation for the Mo_2C/RGO catalyst in comparison to commercial $CoMo/Al_2O_3$ catalysts. This was attributed to the uniform dispersion of Mo_2C nanoparticles over the support, more thermodynamically favourable adsorption of hydrogen gas on Mo_2C surfaces and easier mass transport of reactant molecules due to large pore sizes present in the RGO support (Li et al., 2018). In this study, the hydrocarbon yield increased with increasing Mo content in the catalyst till it reached the maximum value of 84.6% at 17 wt. % Mo loading. Thereafter, the hydrocarbon yield decreased with increasing Mo loading. This can be attributed to an increase in the particle size of Mo_2C and a decrease in the number of exposed active sites (Kim et al., 2015). In Table 2.2, the performances of some of the molybdenum carbide HDO catalysts that are found in literature have been summarized.

Due to the high moisture content in bio-oil, the γ-Al_2O_3 support suffers from thermal instability which leads to high coke deposition rates when sulphided $NiMo/\gamma$-Al_2O_3 or $CoMo/\gamma$-Al_2O_3 catalysts are used for HDO reactions. Moreover, isomerization reactions

adversely affect the selectivity for the HDO process due to the acidity of γ-Al_2O_3 supports. It has been observed that the surface area and pore volume of γ-Al_2O_3 supports decrease during the HDO process. In comparison, carbon supports are neutral and inert in nature and have better tolerance towards moisture. They have superior surface area, meso-porosity, pore volume and thermal stability as compared to γ-Al_2O_3 supports. Due to the hydrophobic nature of carbon supports, the water formed during the HDO process does not get adsorbed on the active sites. This significantly reduces the rate of catalyst deactivation (Wang et al., 2016, Patel and Kumar, 2016).

Table 2.2 Summary of molybdenum carbide HDO catalysts from literature.

Feed	T (°C)	P (MPa)	Catalyst	Reaction Characteristics	Reference
Anisole	420-520	0.1	Mo_2C	Conversion: 100% Selectivity: > 90%	Lee et al., 2014.
Ethyl caprate	280	6	MoC-SiO_2	Yield: 96 mol. % Selectivity: 90%	Smirnov et al., 2017.
Furfural	250	0.1	Co/Mo_2C	Yield: ~ 90% Conversion: ~ 98% Selectivity: ~ 95%	Lin et al., 2018.
Anisole, m-cresol, guaiacol, 1, 2-	260-280	0.1	Mo_2C	Yield: > 90% Conversion: 95% Selectivity: ~ 95%	Chen et al., 2016.
Guaiacol	340	2.8	Mo_2C/C (graphite)	Conversion: 76.3% Selectivity: 93.5%	Li et al., 2016b.
Oleic acid	350	5	Mo_2C/RGO	Yield: 84.6% Conversion: ~ 72% Selectivity: > 95%	Kim et al., 2015.
Soybean oil	400	4.5	NiMoC/Al-SBA-15	Yield: 96% Conversion: 100% Selectivity: 97%	Wang et al., 2013.
Guaiacol	300	3	Mo_2C/AC	Conversion: 97% Selectivity: 39.4%	Cai et al., 2017.
Benzofuran	250	5.1	β-Mo_2C	Conversion: 97% Selectivity: 96%	Dhandapani et al., 1998.
Phenol	350	2.5	Mo_2C/TiO_2	Conversion: ~ 60% Selectivity: > 90%	Boullosa-Eiras et al., 2014.

3. EXPERIMENTAL

3.1 Properties of Feedstocks

As previously stated in Chapter 1, the HTL product mixture used in the present study is obtained from a combination of canola meal and wheat flour. Proximate and ultimate analysis of the canola meal and wheat flour feedstocks have been presented in Table 3.1. From Table 3.1, it can be seen that wheat flour has higher carbon, hydrogen, oxygen, and calorific values than canola meal.

Table 3.1 Ultimate and proximate analysis of canola meal and wheat flour feedstocks used for HTL process.

		Feedstock	
		Canola Meal	Wheat Flour
Proximate Analysis (wt. %)	Moisture	3.8 ± 0.1	13.1 ± 0.3
	Ash Content	59.0 ± 0.83	0.6 ± 0.01
	Volatile Matter	36.3 ± 0.2	74.0 ± 0.5
	Fixed Carbon	0.9 ± 0.1	12.3 ± 0.2
Ultimate Analysis (wt. %)	C	27.5 ± 0.8	38.9 ± 0.7
	H	3.8 ± 0.1	5.4 ± 0.3
	N	< 0.01	1.6 ± 0.08
	S	0.5 ± 0.05	< 0.01
	O*	5.5 ± 0.4	40.4 ± 0.7
Calorific Value (MJ/kg)		13.8 ± 0.4	18.7 ± 0.6

* Calculated by difference

3.2 Extraction of Bio-crude

The highly viscous (semi-solid) hydrothermal liquefaction (HTL) product mixture provided by NULIFE Green Tech contained bio-crude, water and solids. Bio-crude was then recovered from the product mixture using solvent-extraction method. In the present research work, six different solvents – methanol, acetone, ethyl acetate, tetrahydrofuran, toluene and petroleum ether - were used individually for the extraction process to investigate the bio-crude yields as part of a pre-screening study. All the solvents were purchased from Fisher Scientific, Edmonton, Canada and they were used as received. The solvents were chosen based on their relative polarities. Relative polarity is defined as the polarity of a solvent with respect to water. The relative polarity of water is specified as '1' and the relative polarities of other

solvents are determined with reference to water. The values for relative polarity were obtained from literature (Reichardt, 2003). The HTL product was first heated in an oven at 100 °C for 24 hours to remove water from the mixture. Following that, the solvent was added to the HTL product and the mixture was magnetically stirred at room temperature for 6 hours to ensure proper dissolution of the bio-crude in the solvent and achieve efficient extraction of bio-crude. The liquid fraction (bio-crude and solvent) was separated from the solid fraction (bio-residue) using vacuum filtration. The filter papers (slow flow, 18.5 cm) were purchased from VWR International, Mississauga, Canada. The liquid mixture was then heated under vacuum in a rotary evaporator to separate the solvent from the bio-crude fraction. After complete separation and collection of the solvent, bio-crude was obtained as the final product. The bio-crude yields for the six solvents have been presented in Table 3.2. From the pre-screening study, it was found that ethyl acetate (EA), tetrahydrofuran (THF) and petroleum ether (PE) resulted in the highest bio-crude yields among the six solvents. Therefore, these three solvents were selected for further comparative studies. In general, these three solvents don't have an absolute and specific advantage over the other solvents used in the pre-screening study of the current work or elsewhere. The choice of solvent depends on the nature (polarity) of compounds present in the HTL product mixture which in turn is characteristic of the feedstock used for the purpose. Thus, if there is prior information available regarding the type of compounds present in a given feedstock, then the solvents required for extracting bio-crude can be chosen accordingly. Depending upon the solvent (EA, THF or PE) that was used for the extraction process, the bio-crude (BC) samples were labelled as BC-EA, BC-THF and BC-PE while the bio-residue (BR) samples were named as BR-EA, BR-THF and BR-PE.

Table 3.2 Bio-crude and bio-residue yields for solvent-extraction method.

Solvent	Relative Polarity	Bio-crude Yield (%)	Bio-residue Yield (%)
Methanol	0.762	10.8 ± 0.4	86.9 ± 0.7
Acetone	0.355	14.7 ± 0.5	82.8 ± 0.5
Ethyl Acetate	0.228	31.8 ± 0.6	66.4 ± 0.3
Tetrahydrofuran	0.207	37.8 ± 0.5	59.8 ± 0.8
Toluene	0.099	10.4 ± 0.3	88.4 ± 0.4
Petroleum Ether	~ 0.01	17.5 ± 0.5	81.8 ± 0.6

3.3 Characterization of Bio-crude and Bio-residue

Simulated Distillation (Sim-Dist) Analysis

Simulated distillation technique was used to estimate the boiling point distribution of the extracted bio-crudes. The bio-crude samples were analyzed using a Varian CP-3800 gas chromatograph (Varian, Inc., Walnut Creek, CA, USA) and the simulated distillations were modelled after ASTM D-2887 method (ASTM International, 2018). The bio-crude samples were dissolved in CS_2 (Fisher Scientific, Canada) to prepare the solutions for Sim-Dist analysis.

Karl-Fischer Coulometric Titration

The moisture content in the bio-crude samples was determined via Karl-Fischer (KF) coulometric titration. The analysis was carried out using a Mettler-Toledo DL32 Karl Fischer Coulometer (Mettler-Toledo, LLC, Columbus, OH, USA). The bio-crude samples were dissolved in methanol (HPLC grade; Fisher Scientific, Canada) to prepare the solutions for KF coulometric titration and Hydranal^{TM} – Coulomat AG (Honeywell Fluka^{TM}, Canada) was used as the reagent (anolyte solution) for the same.

CHNS Elemental Analysis

The amounts of carbon, nitrogen, hydrogen and sulphur in the bio-crude and bio-residue samples were determined using a Vario EL III CHNS elemental analyzer (Elementar Americas, Inc., Ronkonkoma, NY, USA). The amount of oxygen in the samples was calculated by difference. Further, the (H/C) ratios for all the bio-crude and bio-residue samples were calculated according to the following equation:

$$(H/C) = (H/1.008) / (C/12.011) \quad (3.1)$$

Where C and H are the weight percentages of carbon and hydrogen, respectively.

Ash Content Analysis

The ash content analysis for the bio-crude and bio-residue samples was carried out according to the ASTM D482-13 standard test method (ASTM International, 2013).

Gas Chromatography-Mass Spectrometry (GC-MS) Analysis

The GC-MS analysis was carried out to identify different compounds present in the bio-crude samples and it was performed using a Trace 1310 Gas Chromatograph and a TSQ Duo Mass

Spectrometer (Thermo Fisher Scientific, Waltham, MA, USA). The source temperature was set at 250 °C and the helium flow rate was 1.2 mL/min. One μL of each sample was injected at 250 °C with a split ratio of 50:1 and split flow of 60 mL/min. The oven temperature was initially set to 40 °C with a hold time of 1 min, then increased to 150 °C at 5 °C/min and finally, increased to 320 °C at 10 °C/min and held constant for 5 min. The bio-crude samples were dissolved in acetone (Anachemia – VWR International, Canada) to prepare the test samples for GC-MS analysis. The mass spectral data for the bio-crude samples were acquired from 50 to 650 m/z and the peaks were identified after comparison against the standard NIST (National Institute of Standards and Technology) library using Chromeleon™ 7.2 Chromatography Data System (CDS) software.

Fourier Transform Infrared (FTIR) Spectroscopy

The FTIR spectra of bio-crude and bio-residue samples were obtained to qualitatively determine the functional groups present in them. The spectroscopic analysis was carried out using a Bruker Vertex 70 FTIR spectrometer (Bruker Corporation, Billerica, MA, USA). A diamond ATR (attenuated total reflection) crystal was used in the spectrometer to obtain the infrared spectra in the range of 4500-400 cm^{-1} for bio-crude samples and 4000-500 cm^{-1} for bio-residue samples.

Oxidation Stability Analysis

The oxidative stability of bio-crude samples was determined by an accelerated oxidation/ageing test (Rancimat method) carried out at 110 °C according to the EN 14112 standard test procedure (European Committee for Standardization, 2003). A Metrohm 743 Rancimat (Metrohm AG, Herisau, Appenzell Ausserrhoden, Switzerland) was used to conduct the stability tests and Millipore water was used as the measuring solution.

Solid-state ^{13}C Cross-Polarization/Total Suppression of Sidebands (CP/TOSS) Nuclear Magnetic Resonance (NMR) Spectroscopy

Quantitative information about the composition of bio-residue samples was obtained using a Bruker Avance 500 MHz NMR spectrometer. The instrument was used to conduct ^{13}C CP/TOSS NMR experiments at a spinning frequency of 6 kHz. Proton-to-carbon CP TOSS was used to increase the carbon sensitivity with a cross polarization time equal to 2 ms. The

total time for CP/TOSS with decoupling experiments was typically 90 minutes with 2048 scans.

^{13}C Nuclear Magnetic Resonance (NMR) Spectroscopy

^{13}C NMR spectral analysis was performed for all the bio-crude samples using a Bruker Avance 500 MHz NMR spectrometer equipped with 5 mm broadband inverse probe. The samples for analysis were prepared by dissolving 5 mg of a bio-crude sample in $CDCl_3$ (Merck, Germany) followed by filtration using 0.2 µm non-pyrogenic sterilized disc filters (VWR, Canada). During the analysis, ^{13}C NMR spectra were referenced to $CDCl_3$ solvent at 77.3 ppm and the experimental data were processed through TopSpin version 3.5 software. All the spectra resulted from 2048 scans and the components of the bio-crude samples were quantified by integrating the chemical shifts based on the carbon bonding behavior of their functional groups such as: paraffinic C–H, C–H_2, C–H_3; aromatic C–H; ether, phenolic, carboxylate and carbonyl.

Particle Size Analysis

The particle size distributions in the bio-residue samples were determined using a Malvern Mastersizer particle size analyzer (Malvern Instruments, Malvern, Worcestershire, UK). The particles were scanned for sizes in the range of 4-3500 µm.

X-ray Diffraction (XRD) Analysis

The structural phases in the bio-residue samples along with their crystal parameters were determined by X-ray diffraction crystallography. The analysis was carried out using a Bruker D8 Advance Series II X-ray Powder Diffractometer (Bruker Corporation, Billerica, MA, USA). The diffractometer was fitted with a Cu K-α radiation source (λ = 1.5406 Å) and was operated at 40 kV voltage and 40 mA current. Powder XRD data were collected in the two-theta range of 10-90° (wide-angle XRD) at a scan rate of 1.36° per minute and step size of 0.02°. Thereafter, the peaks and corresponding phases present in the bio-residue samples were identified from the XRD patterns using X'Pert HighScore Plus (version 2.2.2) software (Degen et al., 2014).

Brunauer-Emmett-Teller (BET) and Barret-Joyner-Halenda (BJH) Analysis

The specific surface areas of the bio-residue samples were calculated from the BET method while the pore sizes and pore volumes were estimated from the BJH method. The analysis was carried out by the adsorption and desorption of N_2 at 77K using a Micromeritics ASAP 2020 surface area and porosity analyzer (Micromeritics Instrument Corporation, Norcross, GA, USA). Prior to degassing at 300 °C under vacuum, the samples were heated overnight at 315 °C to remove the traces of oil present in the samples post extraction.

Thermogravimetric Analysis (TGA)

The thermal stability of bio-residue samples was evaluated via thermogravimetric analysis (TGA) method using a TGA Q500 instrument (TA Instruments – Waters LLC, New Castle, DE, USA). The samples (8-10 mg) were heated from room temperature till 800 °C at a ramping rate of 10°C/min. All the measurements were carried out in a nitrogen (flow rate: 60 mL/min) atmosphere. Nitrogen was also used as the purge gas at a flow rate of 40 mL/min.

3.4 Catalyst Synthesis

The carbon-supported molybdenum carbide catalysts were synthesized via Carbothermal Hydrogen Reduction (CHR) method (Wang et al., 2018, Liang et al., 2002, Liang et al., 2016). Three different carbon supports were used for synthesizing the catalysts: commercial activated carbon (AC), commercial multi-walled carbon nanotubes (MWCNT) and bio-residue (BR) obtained during Phase 1 of research. The bio-residue was heated overnight at 315 °C to remove the traces of bio-crude present in the sample post extraction. The supports were separately pre-treated with 6M HNO_3 at 80 °C for 3 hours in order to introduce oxygen functional groups on the surface. Individual mixtures were then cooled, filtered and washed with distilled water several times till the pH of the filtrate became neutral. After that the samples were dried overnight under vacuum at 100 °C. Molybdenum was then impregnated onto the supports via incipient wetness impregnation method. Ammonium heptamolybdate was used as the precursor for the same. The precursor was dissolved in deionized water and the solution was added drop-wise to the supports to achieve 13 wt. % Mo loading. For catalyst synthesis, 5 g of catalyst was taken as the basis. To achieve a 13 wt. % molybdenum loading, 1.146 g of ammonium heptamolybdate tetrahydrate ($(NH_4)_6Mo_7O_{24}.4H_2O$) was dissolved in 1.88 mL

(for bio-residue support) of water and the precursor solution was then added dropwise to 4.793 g of support. The amount of water required for preparing the precursor solutions for the supports was calculated from the pore volume data (please see Table 5.3 for reference) of the support materials. The precursor-impregnated supports were then dried overnight under vacuum at 100 °C and thereafter, calcined under N_2 flow at 500 °C for 3 hours. Following that, the samples were heated till 700 °C with a H_2 flow of 100mL/min in a tubular furnace at a rate of 10 °C/min. The samples were held and reduced at this temperature for 3 hours. Finally, the catalyst samples labelled as Mo/AC, Mo/MWCNT and Mo/BR were quenched to room temperature under nitrogen flow and passivated in a 200 mL/min flow of 1% O_2 in N_2 for 45 minutes.

3.5 Catalyst Characterization Techniques

N_2 Physisorption and CO Chemisorption Analyses

A Micromeritics ASAP 2020 instrument (previously discussed in section 3.3) was used to carry out the physisorption and chemisorption analyses. N_2 physisorption was carried out to determine the specific surface areas (BET method) and pore sizes and pore volumes (BJH method) of the carbon supports and the synthesized catalysts. The metal dispersion over the synthesized catalysts was determined via CO chemisorption. The pre-treatment for the catalyst samples was carried out in the instrument using Helium gas at 110 °C for 60 min. Thereafter, the samples were reduced in-situ using a flow of H_2 gas at 350 °C for 2 h. Finally, the samples were cooled to 35 °C and CO gas was injected into the sample tube for starting the analysis.

Thermogravimetric Analysis (TGA) and X-ray Diffraction (XRD) Analysis

A TGA Q500 instrument was used to evaluate the thermal stability of the synthesized catalysts via thermogravimetric analysis while a Bruker D8 Advance Series II X-ray Powder Diffractometer was used to identify the structural phases in the synthesized catalyst samples. The details of both the analyses have been previously discussed in section 3.3.

Ammonia Temperature Programmed Desorption (NH_3-TPD) Analysis

The strength and abundance of acidic sites on the surface of synthesized catalysts were determined via temperature programmed desorption of a gaseous base such as ammonia. The

analysis was carried out using a Micromeritics AutoChem HP chemisorption analyzer (Micromeritics Instrument Corporation, Norcross, GA, USA). The catalyst samples were purged in-situ with helium at 400 °C for 1 h to remove moisture and volatile impurities. Thereafter, the samples were cooled down and exposed to a 30 mL/min flow of 3% (v/v) NH_3/He gas mixture for 2 h. The physisorbed ammonia was removed by passing He over the samples at 100 °C for 1 h and following that, NH_3-TPD analysis was carried out by heating the catalyst samples from 100 °C to 800 °C at a rate of 10 °C/min.

X-ray Photoelectron Spectroscopic (XPS) Analysis

The surface elemental composition and abundance of different oxidation states of the impregnated metal in the synthesized catalysts were determined via X-ray photoelectron spectroscopy. The XPS analysis was carried out using a Kratos AXIS Supra (Kratos Analytical Ltd, Manchester, UK) spectrometer at the Saskatchewan Structural Sciences Centre (SSSC). The spectrometer comes equipped with a 500 mm Rowland circle monochromated Al K-α (1486.6 eV) source and a combination of hemi-spherical analyzer (HSA) and spherical mirror analyzer (SMA). A spot size of 300x700 microns (hybrid mode) was used for the analysis. The survey scan spectra for the catalyst samples were collected in the 0-1200 eV binding energy range in steps of 1 eV using a pass energy of 160 eV. Additionally, high-resolution scans of different regions were obtained using steps of 0.05 eV with a pass energy of 20 eV. An accelerating voltage of 15 keV and an emission current of 15 mA were used for analyzing the synthesized catalysts.

3.6 Preparation of Bio-crude Blend and Sulphidation of Commercial Catalysts

For reaction runs using synthesized catalysts, 5 g of extracted bio-crude and 45 g of 'hydrotreated heavy gas oil' (HHGO) were taken in a glass beaker and magnetically stirred at 120 °C for 5.5 hours to achieve a 10 wt. % blend of bio-crude in HHGO. The total weight of the feed in the reactor vessel was thus 50 g. However, for reaction runs using commercial catalysts, 16.67 g of bio-crude and 150.03 g of HHGO were mixed together to obtain 10 wt. % bio-crude blend. In this case, the total weight of feed in the reactor vessel was 166.7 g. The bio-crude blend has lower viscosity and better flowability than the pure bio-crude which

facilitates handling of the feed during the upgrading process. An already hydrotreated refinery intermediate was chosen for blending in order to minimize its contribution towards the total concentration of heteroatoms in the final calculation.

The sulphiding solution for commercial catalysts was prepared by mixing 2.9 vol.% butanethiol in straight run gas oil (VOLTESSO 35) inside the fume hood. 200 mL of the prepared solution was then added to the reactor vessel for sulphiding the catalyst. The commercial catalysts were sulphided in two stages: at 193 °C for 4 hours and then at 343 °C for 4 hours. The temperature was increased from room temperature till 180 °C at a ramping rate of 2.5 °C/min. Thereafter, the temperature was slowly increased to 193 °C in steps of 2-3 °C, allowing the temperature to equilibrate before changing the set point each time. After sulfidation at 193 °C for 4 hours, the temperature was again increased to 333 °C at a ramping rate of 2.5 °C/min. Finally, the temperature was increased to 343 °C in steps of 2-3 °C, allowing the temperature to equilibrate before changing the set point each time. The pressure was maintained at 1300 psi and the stirring speed was kept at 400 RPM throughout the sulfidation process (Badoga, 2015, Mapiour, 2009, Rana, 2016).

Unlike the synthesized catalysts, the commercial catalysts were loaded inside a catalyst basket in order to carry out the sulphidation process and the subsequent hydrotreating reaction. The catalyst basket was loaded in such a way that the catalyst remains sandwiched between layers of glass beads and SiC. At first, the catalyst basket was filled with glass beads up to a height of 10 mm. Thereafter, 10 mm of 16 mesh SiC was added to the catalyst basket. 0.5 g of catalyst (3% w/w with respect to the amount of bio-crude in the feed) was then weighed and added above the layers of glass beads and SiC. 10 mm of 16 mesh SiC, followed by 10 mm of glass beads were finally added above the layer of catalyst and the basket was sealed.

3.7 Hydrotreating Reaction and Screening of Synthesized Catalysts

For screening studies using synthesized catalysts, the hydrodeoxygenation of bio-crude was carried out in a Parr batch reactor system having five 100 mL reactors connected in parallel (Fig. 3.1) while the hydrotreating reaction runs using commercial catalysts were carried out in a 450 mL Parr batch reactor equipped with a catalyst basket (Fig. 3.2).

Fig. 3.1 100 mL Parr batch reactor system (5 reactors connected in parallel).

Fig. 3.2 450 mL Parr batch reactor system (sulphidation in progress).

The 10 wt. % blend of bio-crude in hydrotreated heavy gas oil (HHGO) was hydrotreated at 300 °C for 3 hours with a catalyst loading of 3% w/w. The temperature was increased to 290 °C at a ramping rate of 2.5 °C/min. Thereafter, the temperature was slowly increased to 300 °C in steps of 2-3 °C, allowing the temperature to equilibrate before changing the set point each time. The pressure was maintained at 725 psi (5 MPa) and the stirring speed was kept at 400 RPM throughout the reaction. The screening conditions were selected based on the literature review discussed in Chapter 2. After completion of the reaction, the heating was switched off and the reactor vessel was allowed to cool down to room temperature. Thereafter, the product was collected in a glass bottle and N_2 was gently bubbled through the product to remove the trapped gases that were produced during the reaction. The synthesized catalysts were in powder form and black in colour. The hydrodeoxygenation reaction also yielded coke which was black in colour. As a result, it was not possible to distinguish the catalysts from coke particles and separate the catalysts from the reaction mixture. However, the catalyst and coke particles were separated out from the hydrodeoxygenated bio-crude blend samples using a 0.2 μm syringe filter before analysing the blends.

3.8 Parametric Study

Four different process parameters such as temperature (250–350 °C), pressure (3–7 MPa), reaction time (1–5 h) and catalyst loading (1–5% w/w with respect to the amount of bio-crude in the feed) were studied for the hydrodeoxygenation process using the best-performing synthesized catalyst. The range of values for each parameter was again determined from the literature review discussed in Chapter 2. The parameters were studied individually (keeping the other parameters fixed for a given set of reactions) to determine the maximum extent of hydrodeoxygenation (percentage of oxygen removal) achieved within the specified ranges. The desirable conditions were obtained corresponding to the overall highest percentage of oxygen removal. The bio-crude blend before hydrodeoxygenation was simply labelled as ‘Blend’ while the bio-crude blend obtained after carrying out hydrodeoxygenation at the desirable conditions using the best-performing catalyst was labelled as ‘HDO Blend’ and used for subsequent characterization studies.

3.9 Feed and Product Analyses

^{1}H and ^{13}C Nuclear Magnetic Resonance (NMR) Spectroscopy

The bio-crude blends before and after hydrodeoxygenation (feed and product) were analysed using a Bruker Avance 500 MHz NMR spectrometer equipped with a 5mm broadband inverse (BBI) probe. The ^{1}H NMR spectra were referenced to $CDCl_3$ solvent at 7.26 ppm and the experimental data were processed using TopSpin (version 3.5) software. The ^{13}C NMR spectra were also obtained using the aforementioned spectrometer and the details of the analysis have already been provided in section 3.3.

Simulated Distillation (Sim-Dist) Analysis and Karl-Fischer Coulometric Titration

Simulated distillation was carried out for the feed and product blends using a Varian CP-3800 gas chromatograph to investigate their boiling point distribution while a Mettler-Toledo DL32 Karl Fischer Coulometer was used to determine the moisture content in the said bio-crude blends. The details of both the analyses have been previously discussed in section 3.3.

4. A COMPREHENSIVE ANALYSIS OF BIO-CRUDE AND BIO-RESIDUE FROM HYDROTHERMAL LIQUEFACTION OF AGRICULTURAL BIOMASS

Most of the content in this chapter has been published as a journal article: *Chand R, Borugadda VB, Qiu M, Dalai AK. Evaluating the potential for bio-fuel upgrading: A comprehensive analysis of bio-crude and bio-residue from hydrothermal liquefaction of agricultural biomass. Applied Energy 2019; 254; 113679. DOI: https://doi.org/10.1016/j.apenergy.2019.113679*. Elsevier holds the copyright and the permission to use the aforementioned article in this thesis has been obtained from Elsevier (see Appendix A). The contribution of the M.Sc. candidate to the published article included a) extracting bio-crude and bio-residue via solvent-extraction, b) characterizing the extracted bio-crude and bio-residue in detail, c) analyzing the results and providing explanations for the same, and d) writing the article and replying to reviewers' comments. Dr. V. B. Borugadda (post-doctoral fellow) reviewed the aforementioned extraction and characterization methods, helped in analyzing the characterization results (especially, for NMR) and provided support in finalizing the layout of the article. Mr. M. Qiu (NULIFE GreenTech) supplied the HTL product mixture to carry out the extraction studies and provided information on the properties of feedstocks used for the HTL process. Dr. A. K. Dalai (supervisor) provided overall guidance, reviewed the research methodology and characterization results, submitted the article and monitored the research progress throughout.

4.1 Solvent-extraction of Bio-crude and Bio-residue

A mass balance was carried out for the extraction processes and it was observed that THF-assisted extraction yielded the maximum amount of bio-crude (37.8 ± 0.5 wt. %) and the least amount of bio-residue (59.8 ± 0.8 wt. %), while PE-assisted extraction exhibited the opposite trend (bio-crude: 17.5 ± 0.5 wt. % and bio-residue: 81.8 ± 0.6 wt. %). EA-assisted extraction produced intermediate values for both bio-crude and bio-residue yields (31.8 ± 0.6 wt. % and 66.4 ± 0.3 wt. %, respectively). The unaccounted fractions in the yield calculations – THF-assisted extraction: 2.4 ± 0.3 wt. %, EA-assisted extraction: 1.8 ± 0.3 wt. % and PE-assisted extraction: 0.7 ± 0.1 wt. % – can be attributed to material losses during the extraction process. All calculations were done on dry basis, i.e., after the removal of excess water, free moisture and other volatiles by heating the HTL product mixture at 100 °C for 24 hours. Yang et al. (2014) have also reported a similar trend in the yield of bio-crude fractions extracted using

THF, EA and PE as the solvents. Ethyl acetate and tetrahydrofuran are moderately polar solvents and have similar values of relative polarity – 0.228 and 0.207, respectively. On the other hand, petroleum ether is a highly non-polar solvent having a relative polarity of ~ 0.01. Therefore, the higher bio-crude yields observed in the case of EA- and THF-assisted extractions suggest the presence of moderately polar compounds in larger proportions in the given HTL product mixture. Even though the nature of compounds present in an HTL product mixture is characteristic of the feedstock used for the purpose, the aforementioned correlation between solvent polarity and bio-crude yield can be generalized for a wider range of feedstocks, provided that there is prior information available regarding the type of compounds present in them.

All the bio-crude samples – BC-EA, BC-THF and BC-PE – were black in colour and the bio-residue samples – BR-EA, BR-THF and BR-PE – were brownish-black in colour. However, the bio-crude samples varied quite distinctively in their viscosities and flowability: upon visual inspection and at room temperature, BC-PE had the lowest viscosity (highest flowability), BC-THF behaved as a hard and sticky dough-like solid (highest viscosity, no flowability) and BC-EA had intermediate viscosity and appreciable flowability. Thus, even though THF-assisted extraction exhibited the highest bio-crude yield and the lowest bio-residue yield, the resultant bio-crude (BC-THF) was difficult to handle due to its extremely high viscosity and poor flowability. On the other hand, EA-assisted extraction exhibited quite preferable values for both bio-crude and bio-residue yields and, to top it off, the resultant bio-crude (BC-EA) was much easier to handle due to more favourable viscosity and flow properties.

Besides having the lowest purchase price, ethyl acetate also has the highest boiling point (~ 77 °C) among the three solvents that were used for extraction of bio-crude. Consequently, it was observed that the percentage (40.5 ± 1.5%) of solvent recovery was the highest in case of EA-assisted extraction. In comparison, THF-assisted extraction and PE-assisted extraction exhibited solvent recovery percentages of 35.5 ± 0.5% and 28.0 ± 1.0%, respectively. The loss of solvent could be happening at two points during the extraction process:

1) Vacuum filtration – Due to the volatile nature of solvents, they are prone to faster evaporation when vacuum is applied to facilitate filtration.

2) Rotary evaporation – This method is not 100% efficient in recovering all the solvent from the liquid mixture that contains bio-crude and the said solvent. As a result, some amount of solvent is likely to be left behind in the mixture and that would result in a lower percentage of solvent recovery.

Table 4.1 Energy and cost requirements for solvent recovery in the bio-crude extraction process.

Solvent	Time required for solvent recovery (min)	Total electrical energy consumed (kWh)	Total cost of energy (CA$) [a]	Amount of solvent recovered (mL) [b]	Energy cost per unit recovered solvent (CA$/L)
EA	85	3.07	0.46	405	1.14
THF	77	2.78	0.42	355	1.18
PE	74	2.68	0.40	280	1.43

[a] Utility rates set by the City of Saskatoon; [b] Calculated on a 1000 mL solvent basis

Additionally, the energy and cost requirements for solvent recovery in the bio-crude extraction process have been presented in Table 4.1. It was calculated that the cost for recovering a unit volume of solvent was the lowest for ethyl acetate. All these factors suggested that among the current selection of solvents, ethyl acetate would be the most suitable for extracting bio-crude from HTL product mixture.

4.2 Characterization of Extracted Bio-crude

4.2.1 CHNS Elemental analysis and Ash Content Analysis

From the CHNS elemental analysis (Table 4.2), the amounts of carbon, hydrogen, nitrogen and sulphur in the bio-crude and bio-residue samples were determined directly. The amount of oxygen in these samples was determined by the method of difference from the whole. It was found that BC-EA contained the highest amounts of carbon and hydrogen as well as the lowest amounts of sulphur and oxygen among the three bio-crude samples. However, the amount of nitrogen in the aforementioned sample was intermediate.

The CHNS elemental data was further used to calculate the (H/C) ratios (Eq. 3.1) for all the bio-crude and bio-residue samples. Table 4.2 summarizes the elemental composition, gross calorific values, (H/C) ratios and the ash content for all the samples.

For the bio-crude samples, it was observed that BC-EA had the highest gross calorific value, while BC-PE had the lowest value for the same. However, the (H/C) ratios and ash content values for both samples were quite close to each other and more favourable than the values obtained for BC-THF. Preferably, a hydrocarbon fuel should have a high (H/C) ratio and a low ash content value. During combustion, a higher (H/C) value results in increased yield of hydrocarbon products and decreased formation of coke (Wang et al., 2015). The ash content of a fuel is an estimate of the amount of inorganic non-combustible matter present in it. In bio-fuels, this inorganic matter may be present in the form of minerals of K, Mg, P, Ca, Fe, Al, Si, Ti and Mn. The presence of these minerals results in many operational and environmental problems during the combustion of bio-fuels, such as low combustion efficiency, increased agglomeration, slagging, fouling, corrosion, contamination of water and soil, and difficulty in waste disposal, among others (Vassilev et al., 2013).

4.2.2 Moisture Content Analysis

The presence of moisture in bio-crude is an undesirable property as it adversely affects the calorific value of bio-crude and the ease of further upgrading processes. As previously stated in sections 3.2 and 4.1, the HTL product mixture was heated in an oven at 100 °C for 24 hours to remove the excess water and free moisture from the material prior to the extraction process. However, the aforementioned drying method doesn't ensure the removal of bound moisture which might still be present in the HTL product mixture after the heating process. Furthermore, there is a possibility that some amount of moisture might be introduced into the material during subsequent extraction steps. The presence of moisture in bio-crude results in unwanted oxidation reactions and bacterial growth that reduce the quality of bio-crude and create additional problems during upgrading. Therefore, moisture content analysis was carried out for the bio-crude samples to evaluate the extent of moisture removal and to verify if the final products have sufficiently low amounts of moisture. The moisture content in the bio-crude samples was determined by Karl-Fischer coulometric titration and the results were reported as weight percentages of moisture. It was found from the analysis that BC-EA contained the least

amount of moisture (0.02 ± 0.002 wt. %) while BC-THF had the highest moisture percentage by weight (0.14 ± 0.001 wt. %). BC-PE contained an intermediate amount of moisture (0.05 ± 0.004 wt. %) by comparison. However, all the values for moisture content were pretty low and this corroborated the efficacy of the extraction process.

4.2.3 Boiling Point Distribution Analysis

The boiling point distributions of the bio-crude samples have been compared in Fig. 4.1. The Sim-Dist data was calibrated using n-alkane standards and it was observed that all the samples contained a majority of C_{24} compound irrespective of the solvent used.

However, there was distinct variation in the amounts of C_{24} n-alkanes present in each of the bio-crude samples. BC-PE contained the highest amount (67.6 wt. %) of C_{24} n-alkane while BC-THF had the lowest amount (52.7 wt. %) of the same. BC-EA consisted of 55.1 wt. % of C_{24} n-alkane which is an intermediate value. Thus, irrespective of variations, all the bio-crude samples contained a majority of n-alkanes in the heavy gas oil (HGO) fraction (Table 4.3).

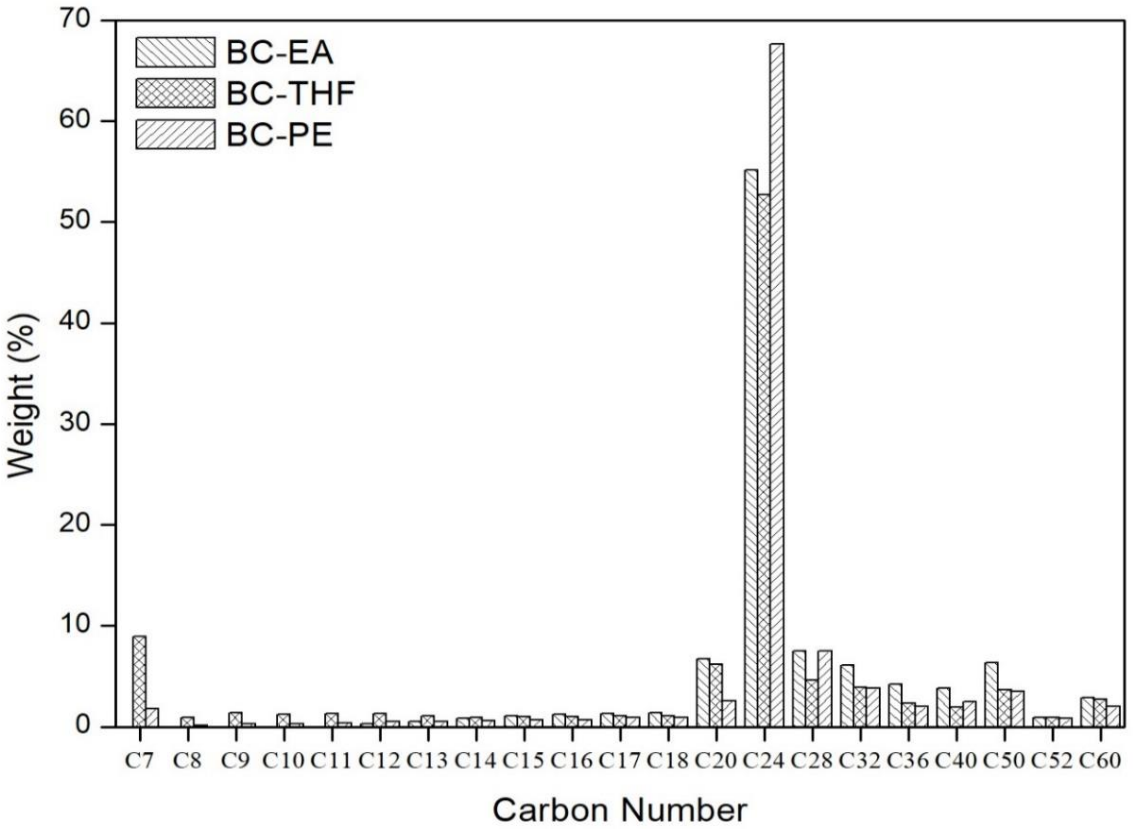

Fig. 4.1 Distribution of n-alkanes in bio-crude samples extracted using EA, THF and PE.

Table 4.2 Elemental composition, higher heating values (HHV), (H/C) ratios and ash content values for bio-crude and bio-residue samples.

Sample	C (wt. %)	H (wt. %)	N (wt. %)	S (wt. %)	O (wt. %) *	HHV (MJ/kg)	(H/C) [a] Ratio	Ash Content (wt. %)
BC-EA	78.5 ± 1.3	10.4 ± 0.3	1.8 ± 0.1	0.1 ± 0.01	9.2 ± 1.5	46.0 ± 0.5	1.6	0.1 ± 0.01
BC-THF	76.4 ± 0.1	9.4 ± 0.1	2.2 ± 0.1	0.2 ± 0.01	10.9 ± 0.1	44.3 ± 0.9	1.5	1.0 ± 0.06
BC-PE	69.8 ± 1	9.6 ± 0.3	0.6 ± 0.1	0.7 ± 0.10	18.9 ± 0.7	39.6 ± 1	1.7	0.3 ± 0.01
BR-EA	39.6 ± 0.2	4.8 ± 0.2	2.2 ± 0.1	0.4 ± 0.04	13.0 ± 0.4	17.6 ± 1.2	1.5	40.0 ± 0.87
BR-THF	32.0 ± 0.5	4.0 ± 0.1	2.0 ± 0.1	0.3 ± 0.01	8.7 ± 0.5	12.5 ± 1.5	1.5	53.0 ± 1.05
BR-PE	40.3 ± 0.6	4.6 ± 0.3	2.0 ± 0.1	0.3 ± 0.02	7.2 ± 1.0	15.3 ± 0.8	1.4	45.5 ± 0.62

*Calculated by difference; [a] Calculated using average values of C and H (Eq. 3.1)

Further, it was also revealed that BC-EA did not contain any n-alkanes in the C_7-C_{11} range. On the other hand, BC-THF comprised of a significant proportion of its n-alkanes in the given carbon range, while BC-PE had a much smaller fraction of n-alkanes in this range.

Table 4.3 Boiling point distribution of bio-crude samples based on cut points for crude oil distillate fractions.

Distillate Fraction	Boiling Point (BP) Range (Eser, 2019)	Carbon Number Range	Weight (%)		
			BC-EA	BC-THF	BC-PE
Heavy Naphtha	88-193 °C	$C_7 – C_{10}$	0.0	12.4	2.5
Kerosene	193-271 °C	$C_{11} – C_{15}$	2.7	5.6	2.7
Light Gas Oil	271-321 °C	$C_{16} – C_{18}$	3.9	3.2	2.5
Heavy Gas Oil	321-425 °C	$C_{19} – C_{27}$	61.8	58.9	70.2
Light Vacuum Gas Oil	425-510 °C	$C_{28} – C_{37}$	17.8	10.8	13.3
Heavy Vacuum Gas Oil	510-564 °C	$C_{38} – C_{47}$	3.7	1.9	2.5
Vacuum Residue	> 564 °C	$C_{48} – C_{60}$	10.1	7.2	6.3

Fig. 4.2 clearly shows that among the three bio-crude samples, BC-THF had the highest percentage (21.2 wt. %) of low-boiling n-alkanes (BP < 321 °C) corresponding to heavy naphtha, kerosene and light gas oil (LGO) fractions, whereas BC-PE consisted of the greatest amount (86.0 wt. %) of mid-boiling n-alkanes (BP: 321-564 °C) which belong to heavy gas oil (HGO), light vacuum gas oil (LVGO) and heavy vacuum gas oil (HVGO) fractions. Similarly, BC-EA was found to contain the largest fraction (10.1 wt. %) of high-boiling n-alkanes (BP > 564 °C) which are related to the vacuum residue fraction. Nonetheless, BC-EA was composed of around 68 wt. % (second only to 74.5 wt. % of BC-PE) of n-alkanes in the C_{13}-C_{24} carbon range and more importantly, the highest amount (11.7 wt. %) of n-alkanes in the C_{15}-C_{20} carbon range. As discussed in section 4.2.1, it was observed that BC-EA contained the least amount of oxygen among all the bio-crude samples. Thus, the properties mentioned in the current section along with the aforementioned observation suggest that BC-EA would be the most suitable candidate for bio-diesel applications (Bharti et al., 2014). Further, BC-EA contained the highest fraction (61.8 wt. %) of its n-alkanes in the heavy gas oil range and thus, it could

be used for blending with heavy gas oil fraction of petroleum crude and subjected to co-processing operations for fuel upgrading. Utilizing blends of bio-crude and petroleum crude in varying proportions would ensure a gradual introduction of renewables in transportation fuels without significantly disrupting the current petroleum industry and infrastructure.

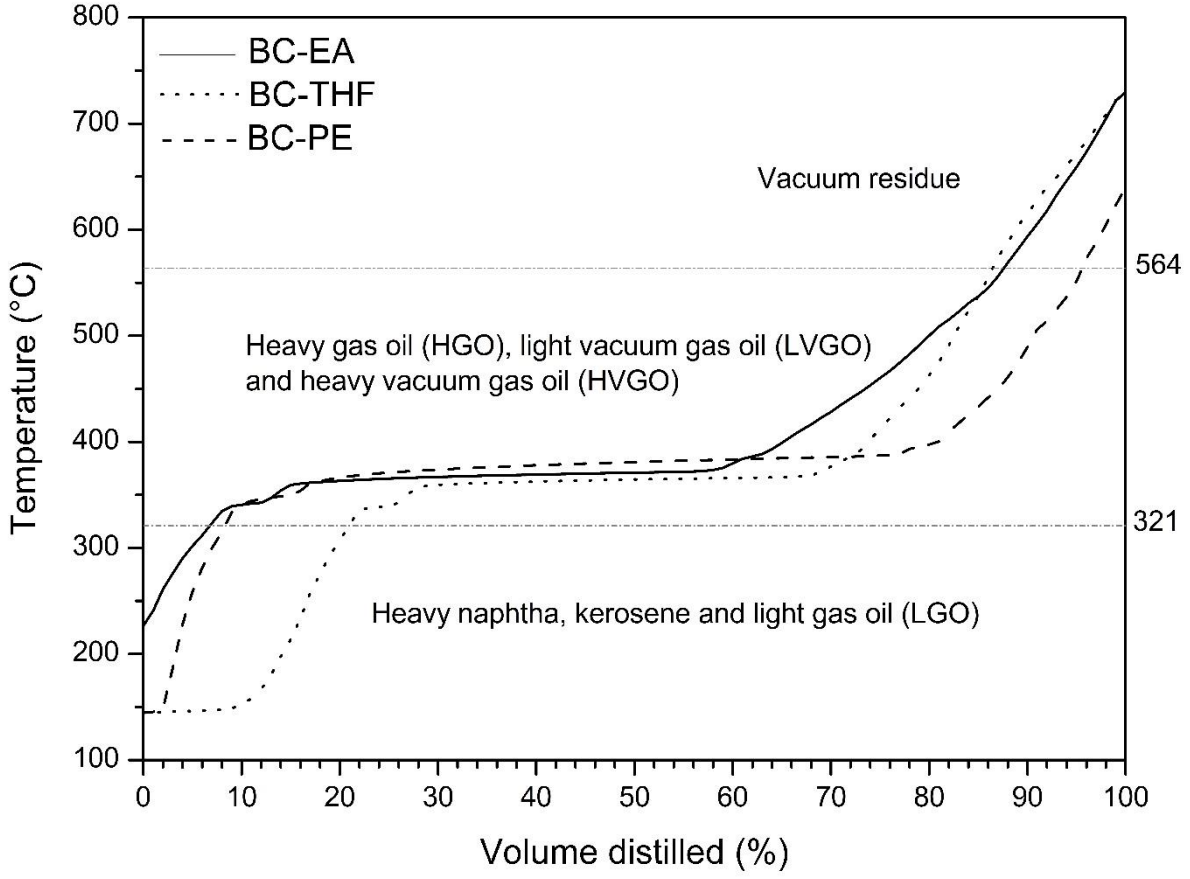

Fig. 4.2 Change in volume of bio-crude samples as a function of boiling point.

4.2.4 FTIR Spectroscopic Analysis

Table 4.4 summarizes the infrared frequency ranges corresponding to the peaks in the FTIR spectra for both bio-crude and bio-residue samples and the functional groups they are associated with (Yang et al., 2007, Reusch, 2013, Vardon et al., 2011, Li et al., 2016a, Domingues et al., 2017). It was observed that the FTIR spectra of the bio-crude samples (Fig. 4.3) were almost identical to each other. Thus, from Table 4.4, it was found that all the bio-crude samples most likely consisted of long-chain alkanes, aromatics, carboxylic acids and esters. Kumar et al. (2010) and Santos et al. (2015) have reported the presence of similar

compounds and functional groups in bio-oil samples produced by pyrolysis of eucalyptus wood and mangaba seed, respectively. Additionally, Yang et al. (2014) and Gai et al. (2014) have shown the same to be also true for bio-crude fractions produced *via* hydrothermal liquefaction of *Salix Psammophila* and *Chlorella Pyrenoidosa*, respectively. Thus, both pyrolysis and HTL bio-crude fractions have largely identical classes of compounds and functional groups. However, the aforementioned bio-crude fractions might differ with respect to the type of specific compounds present and the relative abundance of each category of compounds and the compounds themselves.

Table 4.4 Identification of functional groups present in extracted bio-crude and bio-residue samples.

Wavenumber (cm^{-1})	Assignment	Functional Group
3000-2850 cm^{-1}	2922 cm^{-1} – CH_2 asymmetrical stretch,	n-Alkanes
	2852 cm^{-1} – CH_2 symmetrical stretch	
1470-1450 cm^{-1}	C-H scissoring or CH_3 asymmetrical bending	
1390-1370 cm^{-1}	C-H rock or CH_3 symmetrical bending	
725-720 cm^{-1}	C-H rock or CH_2 symmetrical bending	Long-chain alkanes (7 or more carbon atoms)
3100-3000 cm^{-1}	C-H stretch	Aromatics
2000-1665 cm^{-1}	Overtones	
1500-1400 cm^{-1}	C-C in-ring stretch	
1760-1690 cm^{-1}	C=O stretch	Carboxylic Acids
1440-1395 cm^{-1}	O-H bend	
950-910 cm^{-1}		
1320-1210 cm^{-1}	C-O stretch	
1300-1000 cm^{-1}	C-O stretch	Esters
1680-1600 cm^{-1}	C=C stretch	Alkenes
850-780 cm^{-1}	=C-H out-of-plane bend	

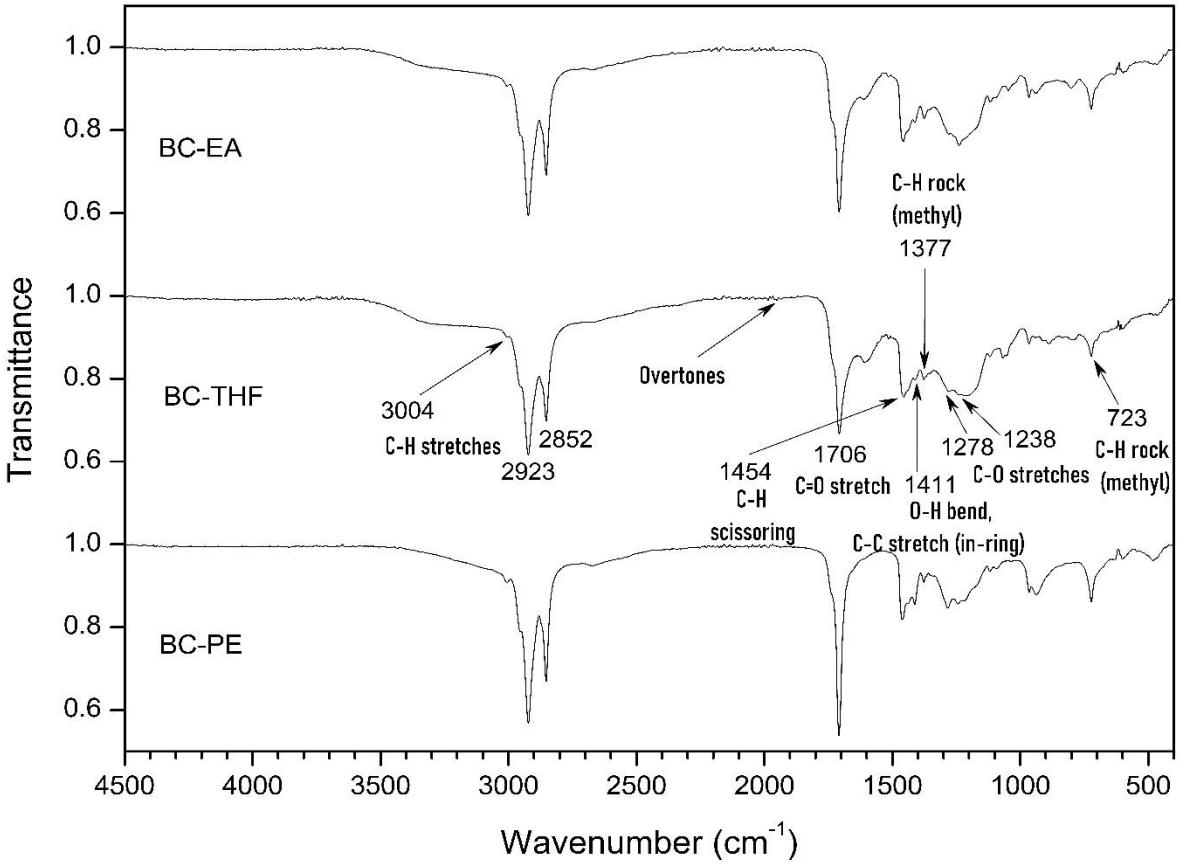

Fig. 4.3 FTIR spectra for bio-crude samples extracted using EA, THF and PE.

4.2.5 Chemical Composition by GC-MS Analysis

From the GC-MS analysis, it was found that all the bio-crude samples predominantly consisted of fatty acid methyl esters (FAME), aromatics and carboxylic acids. This observation corroborated the data from FTIR spectroscopic analysis that was discussed earlier in section 4.2.4. The chromatograms of all the bio-crude samples have been represented in Fig. 4.4. It was observed that the chromatograms in Fig. 4.4 are largely similar to one another and they are characteristic of the feedstocks used herein. The major peak in each of the three chromatograms was associated with the presence of 9-Octadecenoic acid (Z)-, methyl ester (FAME) molecules. Due to the presence of FAME molecules in significant proportions, the bio-crude samples can be effectively used for bio-diesel production upon undergoing suitable upgrading processes (Borges et al., 2011, Shang et al., 2012). Table 4.5 provides an exhaustive list of all the compounds that were identified in the bio-crude samples via GC-MS analysis. Each of the identified compounds had a match factor in the range of 750-900.

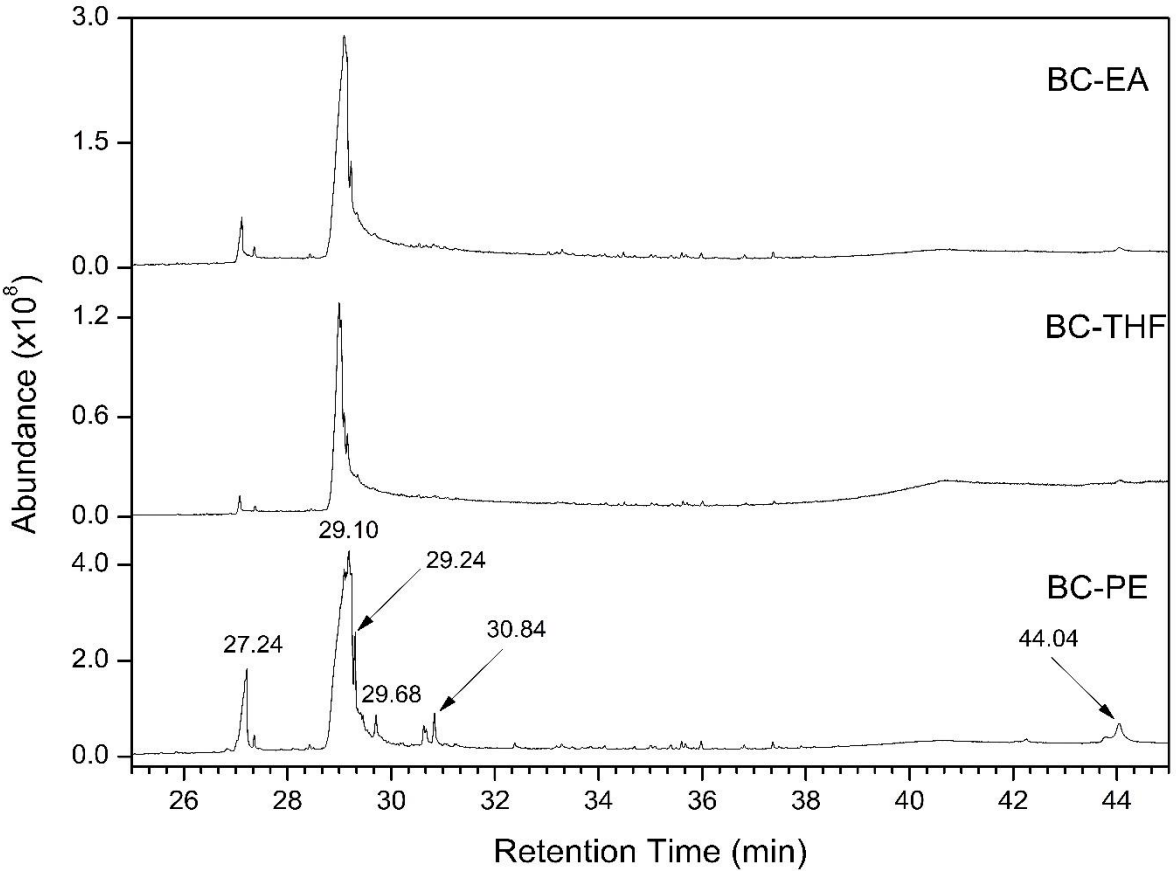

Fig. 4.4 Gas chromatograms of bio-crude samples extracted using EA, THF and PE.

4.2.6 ^{13}C NMR Spectroscopic Analysis

The ^{13}C NMR spectra of the three different bio-crude samples are shown in Fig. 4.5 and their respective chemical components on quantitative percentage basis (based on integration) are reported in Table 4.6. Table 4.6 provides the detailed carbon content within a specified chemical shift range, thus rendering selective information on types of chemical functional groups that are present in the specified range and their relative quantities.

The ^{13}C NMR spectra obtained by extraction of bio-crude with three different solvents was divided into four major regions (as shown in Table 4.6) based on the chemical shifts of respective carbon types. The peak identification and assignments of the ^{13}C NMR spectra were established by the works of Joseph et al. (2010) and Ingram et al. (2008) which offer the identification of types of chemical functional groups present in bio-crude samples. The prominent spectral region of 6-55 ppm represented aliphatic (primary: 6-24 ppm, secondary and tertiary: 25-35 ppm) carbons bonded to hydrogen atoms.

Table 4.5 Volatile compounds identified in bio-crude samples via GC-MS analysis.

Retention Time (min)	Name of the Chemical Compound	Molecular Formula	Area (%)			Molecular Structure
			BC-EA	BC-THF	BC-PE	
27.14	n-Hexadecanoic acid	$C_{16}H_{32}O_2$	4.40	2.58	3.66	
27.24	Pentadecanoic acid	$C_{15}H_{30}O_2$	0.57	0.53	1.52	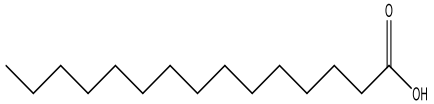
27.36	Octanoic acid, ethyl ester	$C_{10}H_{20}O_2$	0.52	0.53	0.52	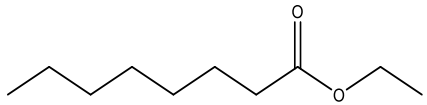
29.10	9-Octadecenoic acid (Z)-, methyl ester	$C_{19}H_{36}O_2$	53.27	49.85	55.48	
29.24	Octadecanoic acid	$C_{18}H_{36}O_2$	22.80	17.46	13.05	

29.66	1,3-Isobenzofurandione, 4,5,6,7-tetrachloro	$C_8Cl_4O_3$	0.10	9.35	0.09	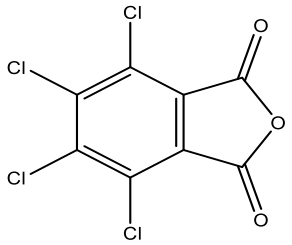
29.68	Benzenethiol, pentachloro-	C_6HCl_5S	1.94	2.52	4.56	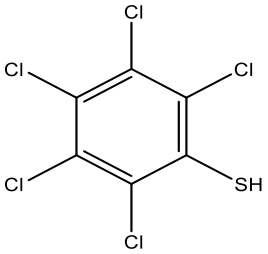
30.20	2-Pyridinecarboxylic acid, 4-amino-3,5,6-trichloro-	$C_6H_3Cl_3N_2O_2$	1.17	0.57	0.80	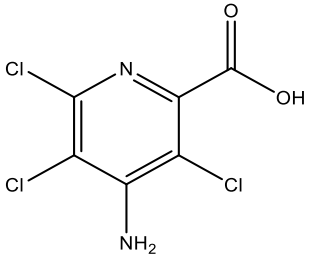
30.84	Ricinoleic acid	$C_{18}H_{34}O_3$	0.57	0.48	2.41	

36.17	Cholesterol	$C_{27}H_{46}O$	0.39	0.43	0.41	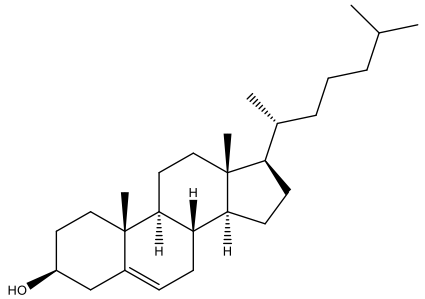
40.60	Dehydrocholic acid	$C_{24}H_{34}O_5$	0.10	0.36	0.31	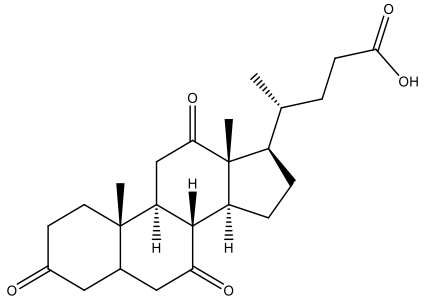
44.04	Digitoxin	$C_{41}H_{64}O_{13}$	1.72	1.35	4.82	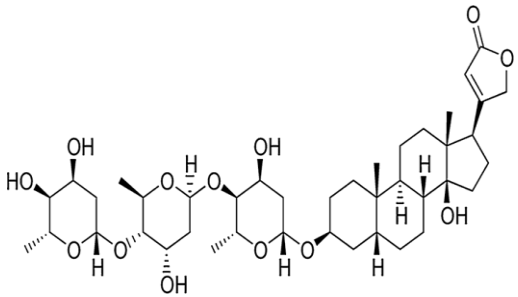
	Total		87.55	86.01	87.63	

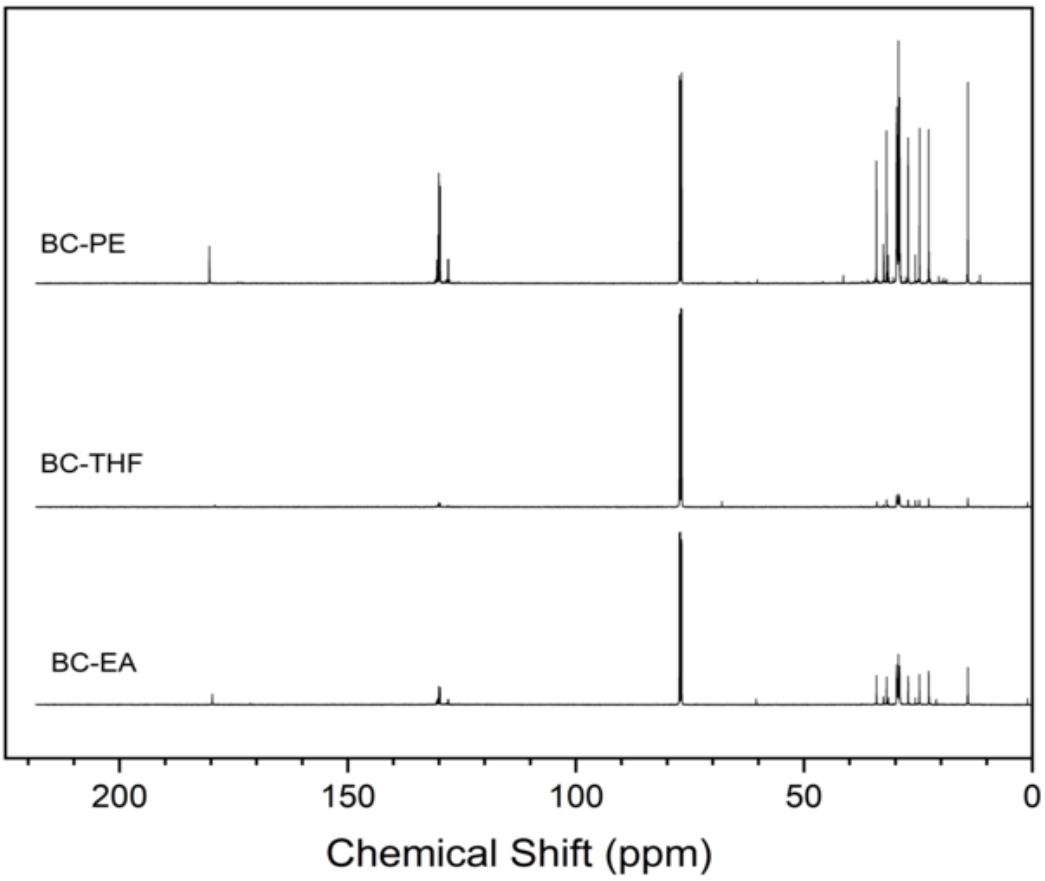

Fig. 4.5 ^{13}C NMR spectra of bio-crude samples extracted using EA, THF and PE.

The higher mass percentage (78.75-88.38 wt. %) of the aliphatic compounds represented higher amounts of heavy oil and the presence of higher oxygen containing compounds. Boateng et al. (2008) and Ingram et al. (2008) reported that aliphatic carbon atoms contribute significantly to the energy content (higher heating value - HHV) which is of primary interest when bio-oil is used for fuel applications.

The next important portion of the ^{13}C NMR spectrum was 120-145 ppm which represented the carbon atoms attached to the protons of aromatic –CH and indicated the presence of medium weight oil (11.53-18.16 wt. %). Further, the spectral region from 170-180 ppm was attributed to carboxylic acids which were present in less quantities in both BC-PE (0.08 wt. %) and BC-EA (1.57 wt. %) samples. On the other hand, there were no detectable carboxylic acids present in the BC-THF sample. The spectral region of 205-225 ppm was assigned to the esters and carbonyl compounds which were present in miniscule amounts in both BC-THF (3.07 wt. %)

and BC-EA (0.71 wt. %). However, no peaks were detected corresponding to these compounds in the BC-PE sample. There were also no ether and phenolic compounds present in any of the bio-crude samples analysed in the present study and these results are in coherence with the FTIR and GC-MS results reported in previous sections 4.2.4 and 4.2.5. These results are consistent with the earlier reports by Lin et al. (2015) and Torri et al. (2016).

Table 4.6 Quantitative percentages of various functional groups present in the bio-crude samples based on ^{13}C NMR spectra.

Sample	Carbon type (wt. %)			
	Aliphatic 6-55 ppm	Aromatic –CH 120-145 ppm	Carboxylic acids 170-180 ppm	Esters 205-225 ppm
BC-THF	78.75	18.16	BD	3.07
BC-PE	88.38	11.53	0.08	BD
BC-EA	82.99	14.71	1.57	0.71

*BD: Below Detection

In all the bio-crude samples, aliphatic carbons were found to be the major fraction followed by aromatic carbons. Carboxylic acids and esters were found to be the predominant oxygen-containing compounds present in these bio-crude samples. Therefore, the extracted bio-crude samples need to undergo a suitable hydrotreatment process in order to reduce the oxygen content and enhance the heating value for subsequent application as liquid transportation fuels.

4.2.7 Oxidation Stability Analysis

In the current study, the Rancimat method was carried out for all the bio-crude samples at three different temperatures: 100 °C, 110 °C and 120 °C. The oxidation stability at each of these temperatures was measured in terms of induction period (IP) and a graph between the natural logarithm of induction period was plotted against the temperatures used for stability study (Fig. 4.6). Using the plots in Fig. 4.6, the oxidation stability for each of the bio-crude samples was forecasted at room temperature, i.e., at 25 °C. The induction periods at both 110 °C and 25 °C have been presented in Table 4.7 for all the bio-crude samples.

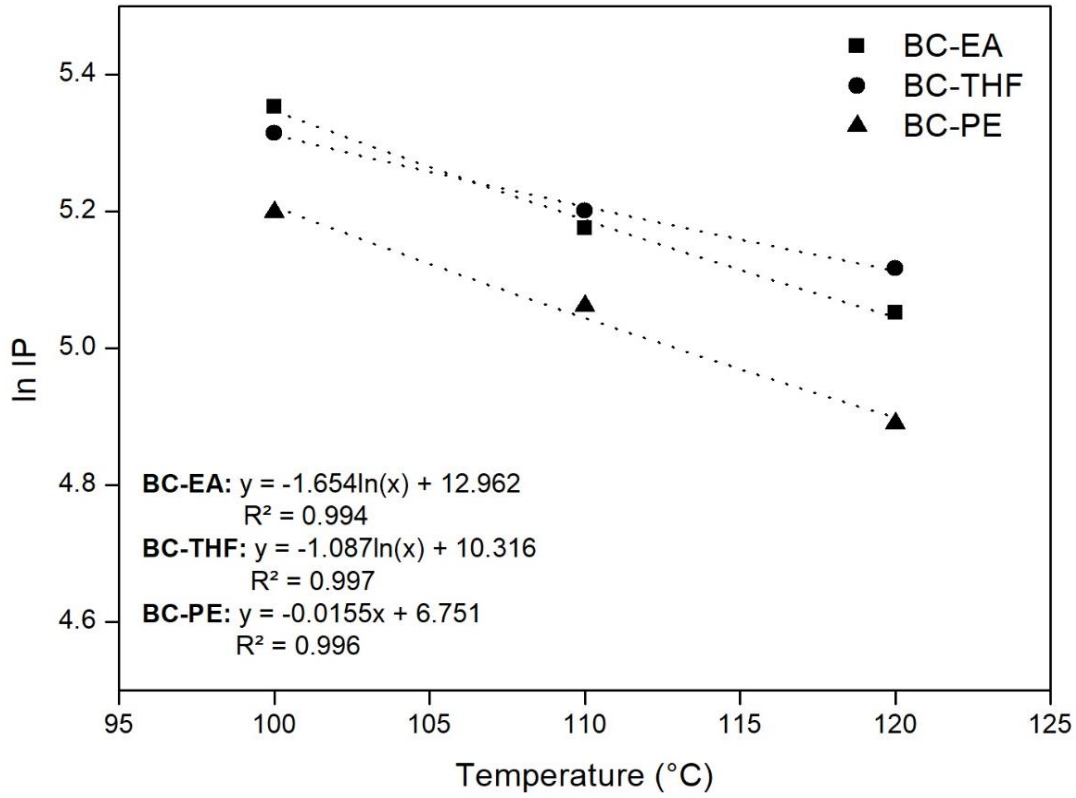

Fig. 4.6 Correlation between the natural logarithm of the induction period (IP) for bio-crude samples and the temperature used for stability study.

From the tabulated induction periods, it was observed that BC-EA exhibited the highest oxidation stability at room temperature (25 °C) even though BC-THF had a slightly higher stability than BC-EA at 110 °C. On the other hand, BC-PE exhibited the lowest oxidation stability at both the temperatures (110 °C and 25 °C).

Table 4.7 Oxidation stability of bio-crude samples at 110 °C and the forecasted stability at room temperature (25 °C).

Sample	Induction Period (IP)	
	At 110 °C	At 25 °C
BC-EA	176.9 ± 3.2 h (7.4 ± 0.1 days)	2075.6 h (86.5 days)
BC-THF	181.5 ± 2.8 h (7.6 ± 0.1 days)	913.3 h (38.1 days)
BC-PE	157.9 ± 5.8 h (6.6 ± 0.2 days)	580.3 h (24.2 days)

4.3 Characterization of Extracted Bio-residue

4.3.1 CHNS Elemental Analysis and Ash Content Analysis

Among the bio-residue samples, BR-EA and BR-PE contained similar amounts of all the five elements (Table 4.2). However, BR-THF contained lower amounts of carbon and hydrogen than both BR-EA and BR-PE samples. The amounts of oxygen in the bio-residue samples followed the exact opposite trend to what was observed for the bio-crude samples. The amounts of sulphur and nitrogen in BR-THF were comparable to those of other two samples.

Furthermore, BR-THF had the lowest gross calorific value and the highest ash content. On the other hand, the gross calorific values for BR-EA and BR-PE were quite similar to each other with BR-EA having the lower ash content between the two. It was also observed that the amounts of carbon, hydrogen, nitrogen and sulphur in all the bio-residue samples were quite comparable to those in the wheat flour feedstock. Moreover, the gross calorific values for all the bio-residue samples and the wheat flour feedstock were quite close to each other. Therefore, the bio-residue samples could be further subjected to another stage of HTL processing to possibly recover more bio-crude.

4.3.2 FTIR Spectroscopic Analysis

It was observed that the FTIR spectra of the bio-residue samples (Fig. 4.7) were also quite similar to each other and that all the bio-residue samples most likely consisted of alkanes, alkenes, esters and carboxylic acids. Lu et al. (2012), Lee et al. (2010), Suguihiro et al. (2013) and Zhao et al. (2017) had previously reported the presence of similar functional groups and compounds in bio-char samples produced from sewage sludge, corn stover, castor oil cake and apple tree branch, respectively. For both bio-crude and bio-residue samples, esters and carboxylic acids were the only oxygen-containing functional groups that were identified via FTIR spectroscopic analysis.

4.3.3 Solid-state ^{13}C CP/TOSS NMR Spectroscopic Analysis

The solid state ^{13}C CP/TOSS NMR spectroscopic analysis was employed to identify the carbon functionality and aromaticity of the bio-residue fractions. Previous studies have reported that the chemical structure of bio-residue depends upon the thermochemical process rather than the process temperature, heating rate, or the nature of the biomass (Bardet et al., 2007). The ^{13}C CP/TOSS NMR spectra of bio-residue samples obtained using different solvents are shown in Fig. 4.8.

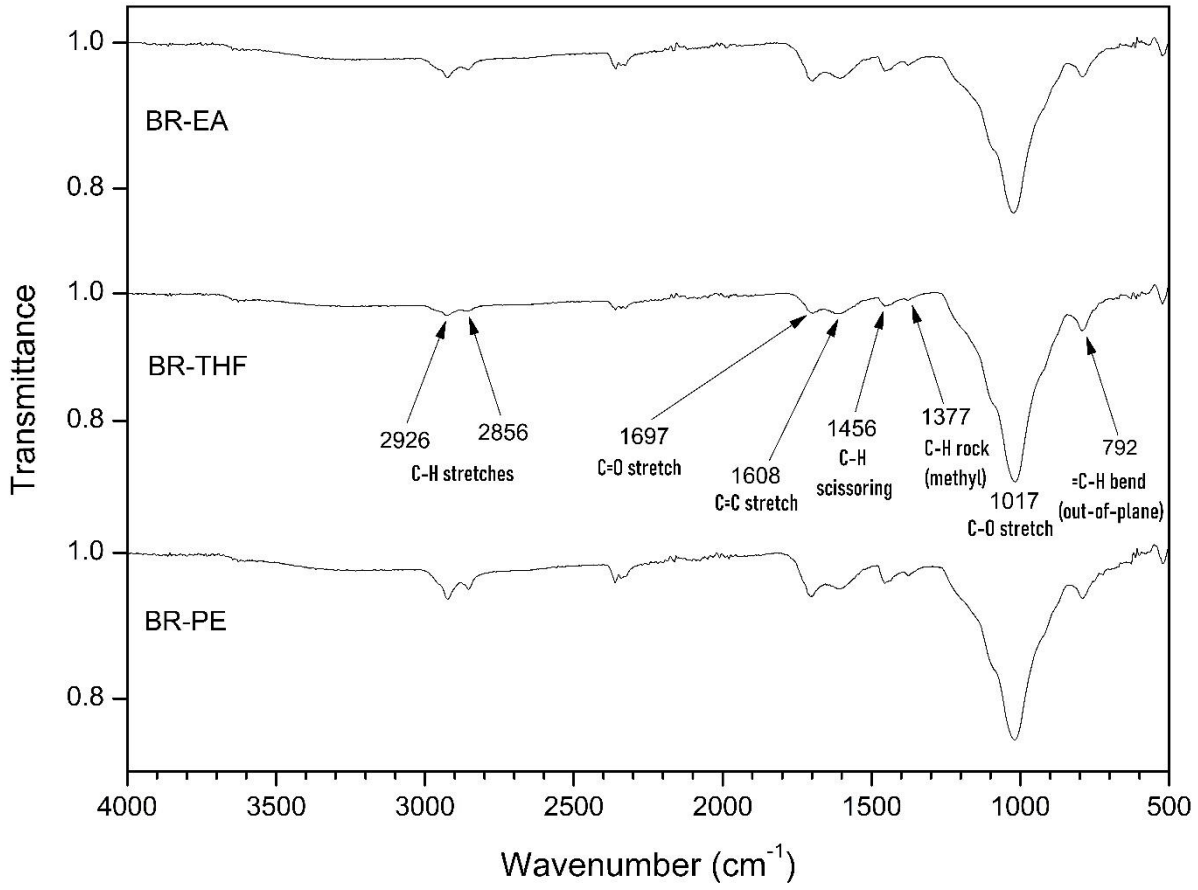

Fig. 4.7 FTIR spectra for bio-residue samples obtained using EA, THF and PE.

In the spectral plots, the range of 0-45 ppm belonged to non-polar alkyl groups such as CCH_3 (14.4 ppm), CCHC and CCH_2C (29.5 ppm). The spectral region for N-alkyl carbons and methoxyl carbons overlays the 46-65 ppm region. The shoulder around 55 ppm was mainly attributed to the NCH group of peptides or proteins; likewise, the peaks found within the range of 65-101 ppm were assigned to carbohydrates. Further, the band observed in the 110-165 ppm range was attributed to aromatic C-O groups which mostly originated from lignin. The band present in the 166-183 ppm range was ascribed to carboxylic acids (-COO-) or peptides/proteins (Cao et al., 2011). Based on detailed analysis of all the solid-sate ^{13}C CP/TOSS NMR spectra, non-polar alkyl (46.85-53.96 wt. %) and aromatic C-O (39.76-46.10 wt. %) groups were found to be the major components in all the bio-residue samples along with the presence of small amounts of methoxyl and N-alkyl carbons (3.45-5.49 wt. %), and peptides/proteins and carboxylic acids (0.86-2.07 wt. %). Regmi et al. (2012) also reported similar outcomes for hydrothermally carbonized bio-char from switchgrass.

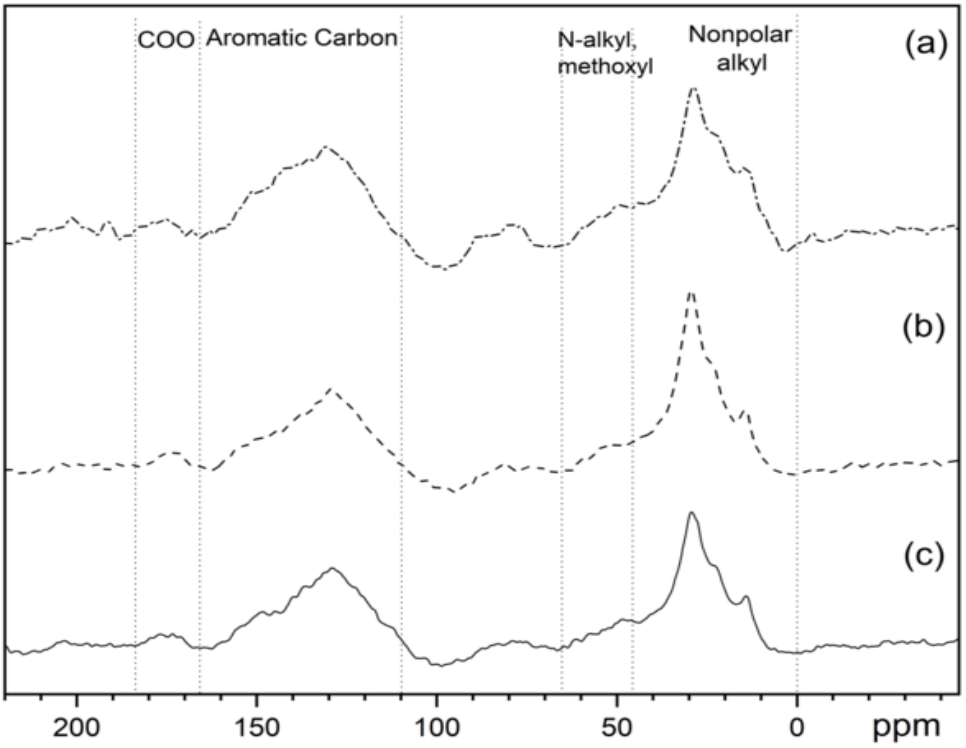

Fig. 4.8 ^{13}C CP/TOSS spectra for (a) BR-THF; (b) BR-PE and (c) BR-EA.

The quantitative percentages of different compounds present in the bio residues based on ^{13}C CP/TOSS spectra are compiled in Table 4.8.

Table 4.8 Quantitative percentages of various functional groups present in the bio-residue samples based on ^{13}C CP/TOSS.

Sample	Functional group/compound (wt. %)			
	Non-polar alkyl 0 – 45 ppm	N-alkyl, methoxyl 46 – 65 ppm	Aromatic C 110 – 165 ppm	Peptides/proteins or carboxylic acids 166 – 183 ppm
BR-THF	49.57	3.45	46.1	0.86
BR-PE	53.96	4.46	39.76	1.8
BR-EA	46.85	5.49	45.57	2.07

Owing to the presence of higher aromatic and non-polar alkyl groups, these bio-residue fractions can be utilized as potential feedstocks to make conductors and electrical circuits

(Manya, 2012). Further, addition of bio-residue to soils enhances certain soil properties such as the structure, pore size distribution, texture and bulk density, aeration, soil workability, water holding capacity and cation exchange capacity due to negative surface charges, all of which aid in plant growth (Manya, 2012).

4.3.4 Particle Size Distribution Analysis

The distribution of particles in BR-EA, BR-THF and BR-PE across different diameter ranges have been presented in Table 4.9.

Table 4.9 Particle size distribution across different diameter ranges in bio-residue samples.

Particle Diameter Range (μm)	Volume (%)		
	BR-EA	BR-THF	BR-PE
4-100	35.7	54.7	23.9
100-600	44.1	39.2	37.5
600-1900	20.2*	6.1**	38.6

*No particles above 1400 μm.

**No particles above 1200 μm.

BR-THF had the maximum number of particles in the 4-100 μm diameter range, while BR-PE had the maximum number of particles in the 600-1900 μm diameter range. These represented the extremities of the particle size spectrum: BR-THF had no particles which had sizes above 1200 μm, while BR-PE had particles which had sizes up to 1900 μm. In comparison, BR-EA had the maximum number of particles in the 100-600 μm diameter range. Further, there were no particles which had sizes above 1400 μm. In BR-EA, the particles in the 550-750 μm diameter range had the highest volume percentages which was characterized by the higher peak in the particle size distribution plot (Fig. 4.9). Similar conclusions were also drawn for the other two bio-residue samples: in BR-THF, the particles in the 50-150 μm diameter range and in BR-PE, the particles in the 700-900 μm diameter range had the highest volume percentages. These were characterised by the highest peaks in the respective particle size distribution plots (Fig. 4.9). In summary, the average particle sizes of the three bio-residue samples follow the order: BR-PE > BR-EA > BR-THF. As discussed in section 4.1, THF-assisted extraction had the highest bio-crude yield, followed by EA-assisted extraction and further followed by PE-

assisted extraction. This could mean that the amount of unrecovered bio-crude present in each of the bio-residue samples follows the order: BR-PE > BR-EA > BR-THF. The presence of bio-crude might cause the particles in the bio-residue samples to agglomerate and form larger units. Further, the degree of agglomeration would depend on the amount of unrecovered bio-crude present in each of bio-residue samples; higher amount of bio-crude would result in a higher degree of agglomeration and larger average particle size, and vice-versa. This could explain why the average particle sizes of the three bio-residue samples follow the aforesaid order.

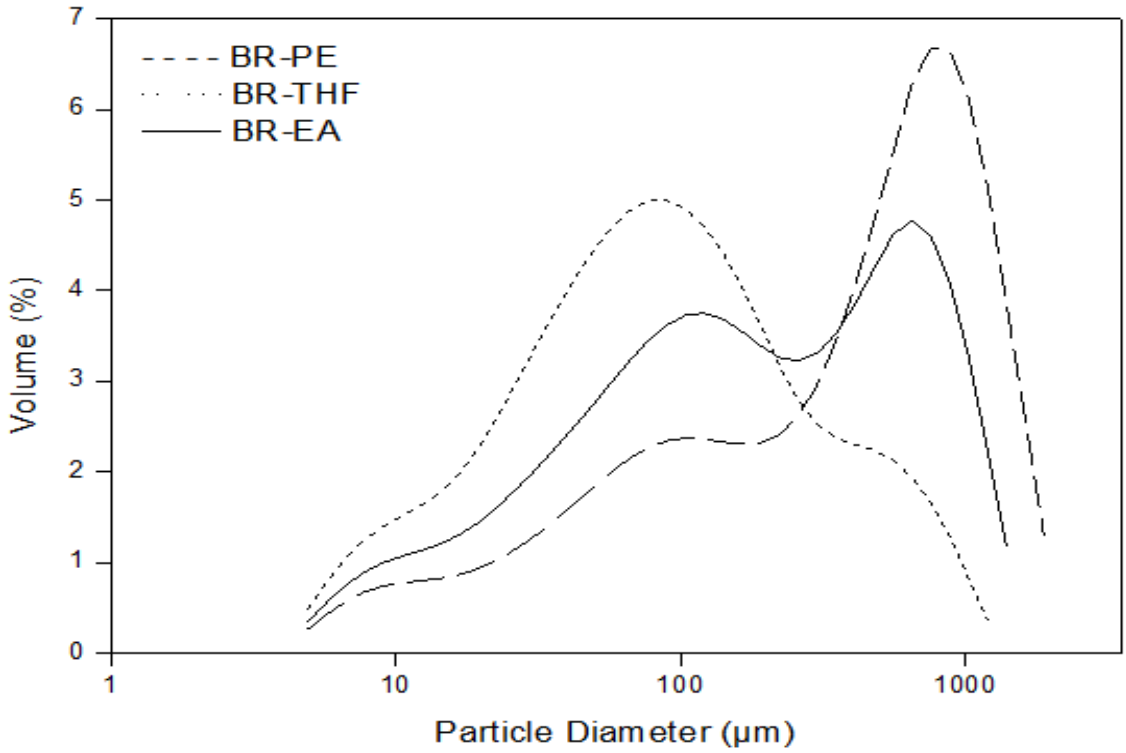

Fig. 4.9 Particle size distribution plot for bio-residue samples obtained using EA, THF and PE.

4.3.5 Textural Properties by Brunauer-Emmett-Teller (BET) and Barret-Joyner-Halenda (BJH) Analysis

From the surface area and porosity analysis (Table 4.10), it was observed that BR-PE had the lowest BET surface area and the highest average pore volume and pore size. The low surface area of BR-PE may be explained by the fact that it also happened to have the highest average particle size as concluded from the particle size distribution data in section 4.3.4. However,

similar behaviours were not observed for the other two bio-residue samples: BR-EA was found to have the highest BET surface area, whereas the surface area for BR-THF was an intermediate value even though BR-THF had the lowest average particle size. The average pore sizes for these two bio-residue samples were almost same (~ 7 nm) but BR-EA had a higher average pore volume (0.37 ± 0.03 cm^3/g) than that of BR-THF (0.29 ± 0.02 cm^3/g). As discussed in section 4.3.4, the amount of unrecovered bio-crude present in each of the bio-residue samples might follow the order: BR-PE > BR-EA > BR-THF. Containing higher amounts of bio-crude traces could be related to having higher average pore volumes and thus, it might provide an explanation as to why the average pore volumes for the bio-residue samples also follow the order: BR-PE > BR-EA > BR-THF. Furthermore, as BR-EA exhibited a higher average pore volume than BR-THF, it could explain why BR-EA, instead of BR-THF, was found to have the highest BET surface area. However, this explanation doesn't stand true for BR-PE which had the lowest BET surface area in spite of having the highest average pore volume. It is quite likely that for BR-PE, the increase in average particle size had more than offset the influence of increase in the average pore volume, thus resulting in a reduced BET surface area.

Table 4.10 Surface area and porosity analysis for bio-residue samples obtained using EA, THF and PE.

Sample	BET Surface Area (m^2/g)	Average Pore Volume (cm^3/g)	Average Pore Size (nm)
BR-EA	249 ± 3	0.37 ± 0.03	7.0 ± 0.2
BR-THF	232 ± 6	0.29 ± 0.02	6.9 ± 0.1
BR-PE	190 ± 4	0.44 ± 0.04	8.5 ± 0.2

4.3.6 Thermogravimetric Analysis (TGA)

Fig. 4.10 represents the loss in weight of all the bio-residue samples when subjected to thermogravimetric analysis (TGA) over a temperature range of ~ 30-800 °C. It was observed that all the bio-residue fractions had almost identical onset temperatures (~ 185 °C). It was also found that BR-EA exhibited the lowest percentage of weight loss (29.03%), whereas BR-PE underwent the highest percentage of weight loss (43.62%). The weight loss observed for BR-THF was an intermediate value of 35.3%. The temperatures at which the bio-residue samples

degrade and lose mass have been provided in Table 4.11. Thus, BR-EA was found to be the most stable bio-residue fraction over the temperature range studied (especially at higher temperatures), whereas BR-PE was the least stable fraction. Consequently, BR-EA would be the most preferred choice for high-temperature catalytic and adsorptive processes.

Table 4.11 Mass loss of bio-residue samples at different degradation temperatures.

Weight Loss (%)	Temperature (°C)		
	BR-EA	BR-THF	BR-PE
10	330.5	382.3	313.2
15	399.2	452.2	379.8
20	448.3	514.1	441.3
25	537.1	577.1	497.9
30	---	656.5	552.2
35	---	784.6	612.8
40	---	---	697.5

The rate of weight loss was also plotted for each of the bio-residue samples and the results were represented as derivative thermogravimetric (DTG) curves as shown in Fig. 4.11. From the DTG curves, it was observed that the rates of weight loss for all the bio-residue samples were quite similar up to 125 °C. The loss in weight from room temperature till 125 °C can be attributed to the evaporation of water/moisture and some low-boiling compounds. It was also observed that for all three bio-residue samples, a sharp peak appeared at around 225 °C which is attributed to the loss of n-alkanes corresponding to heavy naphtha and kerosene fractions. However, the intensity of this peak varies considerably and follows the order: BR-PE (0.77 wt. %/min) > BR-EA (0.61 wt. %/min) > BR-THF (0.38 wt. %/min). This observation strongly supports a remark that was made earlier in section 4.3.4 suggesting that the amount of unrecovered bio-crude present in each of the bio-residue samples also follows a similar order.

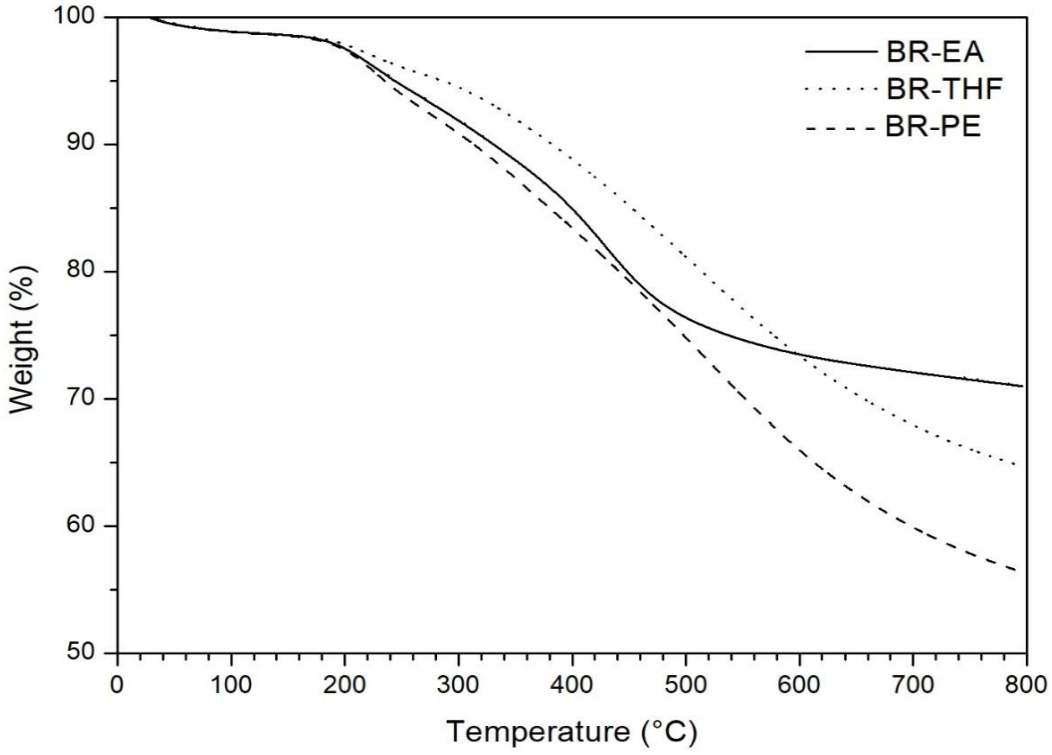

Fig. 4.10 TGA curves depicting weight loss for bio-residue samples with increasing temperature.

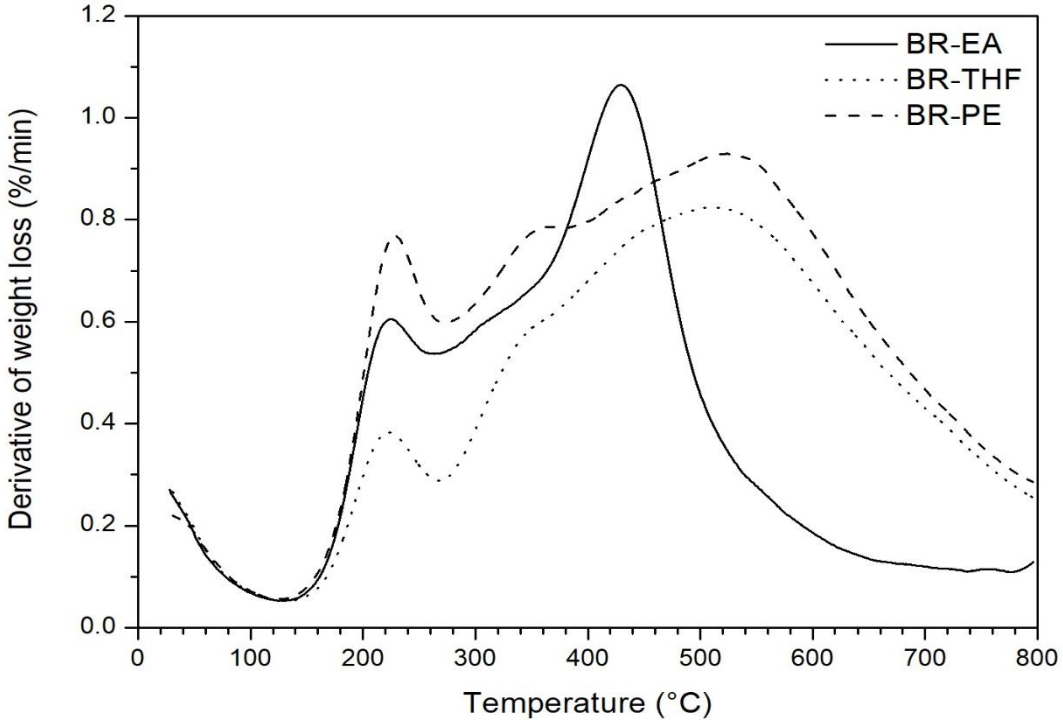

Fig. 4.11 DTG curves depicting the rate of weight loss for bio-residue samples.

One more distinct peak was observed at higher temperatures for each of the bio-residue samples which is attributed to the loss of n-alkanes corresponding to gas oil and vacuum gas oil fractions. For all the bio-residue samples, the loss of weight in the temperature ranges of 120-270 °C (5.17%) and 270-380 °C (6.95%) can also be attributed to the decomposition of hemi-cellulosic carbohydrates and cellulosic polysaccharides, respectively (Wei et al., 2015). Lignin is, however, known to decompose rather slowly over the entire (almost) temperature range of thermogravimetric analysis and hence, a fraction of the weight loss in the temperature range of 100-800 °C can be attributed to the degradation of lignin (Yang et al., 2007). This further implies that the loss of weight observed above 550 °C is predominantly due to lignin degradation.

4.3.7 X-ray Diffraction (XRD) Analysis

The XRD patterns for all the bio-residue samples were quite similar to each other, as shown in Fig. 4.12. All the bio-residue samples exhibited their characteristic peaks at similar values of 2θ. However, the intensity of the respective peaks varied noticeably depending on the solvent used for extraction. For BR-EA, the most intense peak was observed at 2θ = 27.91° corresponding to the calcium mica (calcium aluminium silicate; $Al_3Ca_{0.5}Si_3O_{11}$) phase. The dominant calcium mica phase belonged to monoclinic lattice system. The next major phase in BR-EA was found to be quartz (SiO_2) and it was represented by the peak observed at 2θ = 26.71°. The quartz phase belonged to hexagonal lattice system. In both BR-THF and BR-PE, the most intense peak was observed around a 2θ value of 21.84° which represented the presence of α-cristobalite phase. This cristobalite phase had the same chemical formula as quartz (SiO_2) but belonged to tetragonal lattice system. Trubetskaya et al. (2016) have also reported the presence of cristobalite phase in their study on bio-char samples produced by fast pyrolysis of wheat straw and rice husk. The next major phase in BR-PE was again found to be quartz, while calcium mica was the next dominant phase found in BR-THF. Quartz was also identified as a major phase in BR-THF along with the aforementioned phases. Due to the presence of α-cristobalite and quartz, the bio-residue fractions could be used for road construction, sanding roads during winter, manufacturing glass fibres and ceramics, and also as abrasives and cement additives (Government of Canada, 2013). One particular peak observed at 2θ = 49.78° was quite intense and distinct in the diffractogram of BR-EA, unlike the other two samples. This

peak was associated with the presence of magnesium sulphide (MgS) phase which belonged to the cubic lattice system.

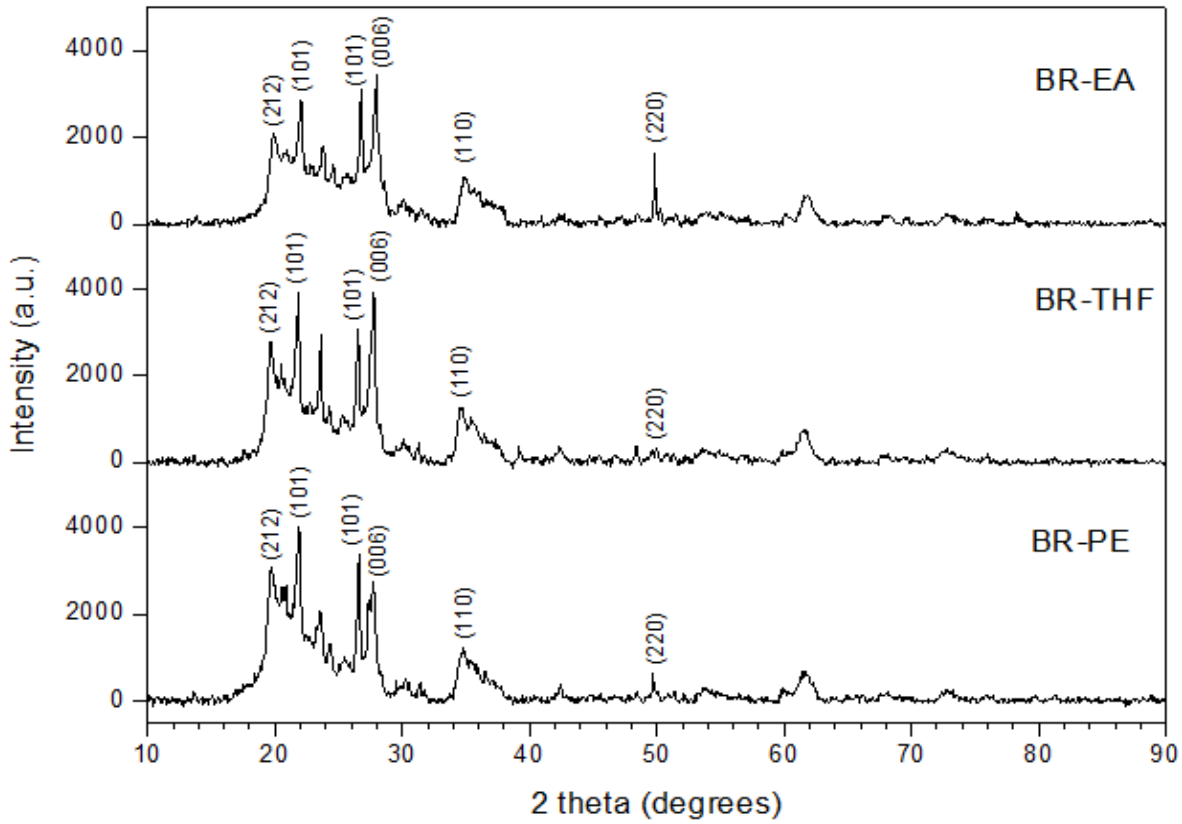

Fig. 4.12 XRD patterns depicting lattice parameters of identified phases for bio-residue samples.

Apart from these phases, magnetite (Fe_3O_4; $2\theta = 19.84°$) and sylvite (KCl; $2\theta = 34.82°$) were two other phases that were identified in all the bio-residue samples. These phases belonged to orthorhombic and cubic lattice systems, respectively and are known to have many industrial applications. Sylvite is predominantly used for producing potassium-rich fertilizers known as Potash (Canpotex, 2019). Magnetite-based catalysts are used for the industrial synthesis of ammonia (Appl, 2011). Owing to their impressive adsorptive properties, magnetite nanoparticles are used for the removal of colloidal particles from drinking water (Blaney, 2007). In addition, magnetite is known to catalyse the decomposition of hydrogen peroxide into hydroxyl free radicals which helps in the consequent degradation of organic pollutants such as *p*-nitrophenol (He et al., 2015). Thus, the bio-residue samples could be used for any of the aforementioned areas of application upon suitable processing. Domingues et al. (2017) had

also reported the presence of quartz and sylvite phases in bio-char samples produced by pyrolysis of coffee husk and pine bark. Further, Clemente et al. (2018) had reported the presence of magnetite, quartz and sylvite phases in their study involving 13 different bio-char samples produced from poultry litter, switchgrass and different types of wood.

4.4 Conclusions

The extraction carried out using ethyl acetate had the most ideal balance between a high bio-crude yield and an easy-to-handle final product. The bio-crude thus obtained had the lowest moisture content, highest gross calorific value, lowest ash content, lowest oxygen content, highest oxidation stability at room temperature and a significantly high percentage of compounds in the C_{13}-C_{24} carbon range. All these factors suggest that the bio-crude extracted using ethyl acetate would be the most suitable candidate for further upgrading processes and bio-diesel applications. Catalytic hydrodeoxygenation would be the most preferred upgrading process for this bio-crude because oxygen was the major heteroatom impurity that was found in the sample.

The oxygen in the bio-crude and bio-residue fractions was present mostly in the form of carboxylic acids and esters. It was also observed that traces of bio-crude were present in each of the bio-residue samples, thus suggesting that the extraction process employed in the current study could not recover 100% of bio-crude present in the hydrothermal liquefaction product mixture. Owing to its high surface area, mesoporosity and high pore volume, the bio-residue obtained using ethyl acetate had more favourable textural properties than the bio-residue fractions obtained using tetrahydrofuran and petroleum ether. Therefore, it can be developed further for use in catalytic applications or as bio-adsorbents. The bio-residue samples, especially the one obtained using ethyl acetate, can also be used as solid bio-fuels for domestic use.

In Chapter 5, the bio-crude extracted using ethyl acetate will be used for blending with hydrotreated heavy gas oil (HHGO) and the prepared bio-crude blend will be subjected to catalytic hydrodeoxygenation in an attempt to upgrade its properties. Additionally, the bio-residue obtained using ethyl acetate will be used as one (labelled as BR) of the carbon supports to synthesize molybdenum catalysts for hydrodeoxygenation of the aforementioned bio-crude blend.

5. CATALYTIC HYDRODEOXYGENATION OF BIO-CRUDE AND HEAVY GAS OIL BLENDS USING CARBON-SUPPORTED MOLYBDENUM CATALYSTS

5.1 Screening of Synthesized Catalysts and Comparative Study with Commercial Hydrotreating Catalysts

5.1.1 Screening of Synthesized Catalysts for Hydrodeoxygenation of Bio-crude Blends

The experiments in the present study were performed in triplicates and the data were reported as the arithmetic mean of all individual results. The standard deviations for such data have also been provided, wherever applicable. The CHNS analysis of bio-crude blends before and after hydrodeoxygenation using each of the three synthesized catalysts has been provided in Table 5.1. The post-hydrodeoxygenation blends were labelled as Blend_Mo/MWCNT, Blend_Mo/AC and Blend_Mo/BR. It was observed that the (H/C) ratios for all the hydrodeoxygenated blends were greater than that of the untreated blend. All the post-HDO blends exhibited significant decreases in the amounts of sulphur and oxygen. However, the reduction in nitrogen content was negligible for all the hydrodeoxygenated blends.

Table 5.1 CHNS analysis for bio-crude blends hydrotreated with prepared Mo/MWCNT, Mo/AC and Mo/BR catalysts (Temp: 300 °C, Pressure: 5 MPa, Catalyst Loading: 3% w/w, Time: 3 h).

Sample	C (wt. %)	H (wt. %)	N (wt. %)	S (wt. %)	O (wt. %) *	Oxygen Reduction (%)
Blend	86.33 ± 0.05	10.54 ± 0.02	0.44 ± 0.02	0.23 ± 0.02	2.46 ± 0.07	
Blend_Mo/ MWCNT	85.98 ± 0.03	11.54 ± 0.05	0.43 ± 0.06	0.12 ± 0.013	1.93 ± 0.08	21.5 ± 1.0
Blend_Mo/ AC	85.89 ± 0.05	11.65 ± 0.05	0.44 ± 0.04	0.11 ± 0.002	1.91 ± 0.10	22.4 ± 1.8
Blend_Mo/ BR	86.47 ± 0.04	11.76 ± 0.07	0.42 ± 0.01	0.10 ± 0.01	1.25 ± 0.11	49.2 ± 3.0

* Calculated by difference

The oxygen reduction percentages observed for Blend_Mo/MWCNT and Blend_Mo/AC were quite close to each other and in the range of 20-24%. On the other hand, the oxygen reduction percentage for Blend_Mo/BR was more than twice as much as those observed for the other two

post-HDO blends. In addition, the percentage of sulphur reduction was the highest for the aforementioned blend. Based on the screening studies, Mo/BR was identified as the best catalyst for carrying out hydrodeoxygenation of the prepared bio-crude blend as the catalyst resulted in the highest percentage of oxygen reduction among the three synthesized catalysts. The higher oxygen reduction percentage observed for Mo/BR could be possibly accredited to more favourable textural properties of the catalyst and a higher concentration of Mo_2C phase on the surface of the said catalyst. To check the validity of the aforementioned hypotheses, all the synthesized catalysts were characterized in detail and analyses of the results thereof are discussed in Section 5.2.

5.1.2 Comparative Study of Best-performing Synthesized Catalyst with Commercial Hydrotreating Catalysts

Commercial CoMo/γ-Al_2O_3 and NiMo/γ-Al_2O_3 catalysts were used for hydrodeoxygenation of the prepared bio-crude blend at the screening conditions and their resultant oxygen reduction percentages were compared to that of the best-performing synthesized catalyst (Mo/BR). Table 5.2 shows that both the commercial hydrotreating catalysts yielded better nitrogen reductions than the Mo/BR catalyst. The amount of sulphur reduction was identical for CoMo/γ-Al_2O_3 and Mo/BR catalysts, whereas the NiMo/γ-Al_2O_3 catalyst exhibited a slightly better sulphur reduction than the previous two.

Table 5.2 CHNS analysis for bio-crude blends hydrotreated with commercial catalysts and prepared Mo/BR catalyst (Temp: 300 °C, Pressure: 5 MPa, Catalyst Loading: 3% w/w, Time: 3 h).

Sample	C (wt. %)	H (wt. %)	N (wt. %)	S (wt. %)	O (wt.%)*	Oxygen Reduction (%)
Blend	86.33 ± 0.05	10.54 ± 0.02	0.44 ± 0.02	0.23 ± 0.02	2.46 ± 0.07	
Blend_CoMo/ γ-Al_2O_3	86.94 ± 0.03	10.62 ± 0.03	0.40 ± 0.02	0.10 ± 0.01	1.94 ± 0.06	21.1 ± 0.2
Blend_NiMo/ γ-Al_2O_3	87.12 ± 0.06	10.59 ± 0.03	0.39 ± 0.01	0.08 ± 0.01	1.82 ± 0.09	26.0 ± 1.5
Blend_Mo/ BR	86.47 ± 0.04	11.76 ± 0.07	0.42 ± 0.01	0.10 ± 0.01	1.25 ± 0.11	49.2 ± 3.0

* Calculated by difference

However, the synthesized Mo/BR catalyst exhibited a much better oxygen reduction percentage than both the commercial catalysts. Furthermore, unlike Blend_Mo/BR, no improvement was observed in the (H/C) ratios of both Blend_CoMo/γ-Al_2O_3 and Blend_NiMo/γ-Al_2O_3. Thus, the synthesized Mo/BR catalyst proved to be more favourable than the commercial catalysts for hydrodeoxygenation of the prepared bio-crude blend. As discussed in Section 2.3.6, the commercial sulphided catalysts are prone to rapid deactivation due to sulphur leaching which changes the micro-structure of the active sites (Li et al., 2018). Furthermore, the thermal stability of γ-Al_2O_3 support worsens due to the high moisture content of bio-crude and in the presence of water that is formed during the HDO process. This results in high coke deposition rates which reduce the surface area and pore volume of the aforementioned support. On the other hand, carbon-based supports, such as bio-residue, are hydrophobic in nature and have better tolerance towards moisture. As a result, they have better thermal stability and lower deactivation rates than γ-Al_2O_3 support (Wang et al., 2016, Patel and Kumar, 2016). Moreover, unlike the sulphide phases, the Mo_2C phase present in Mo/BR catalyst is highly oxophilic in nature which improves the selectivity for oxygen reduction (Wang et al., 2016, Lee et al., 2014). The aforementioned factors could provide a possible explanation as to why the bio-residue based molybdenum catalyst resulted in a higher oxygen reduction percentage than the commercial hydrotreating catalysts.

5.2 Characterization of Synthesized Catalysts

5.2.1 N_2 Physisorption and CO Chemisorption Analysis

The surface area and porosity analysis for the support materials and synthesized catalysts were carried out via N_2 physisorption and the results have been tabulated in Table 5.3. The Mo/AC catalyst had the highest BET surface area but the lowest average pore size. On the other hand, Mo/MWCNT had a much lower surface area but the highest average pore volume and pore size. Mo/BR catalyst had the lowest surface area and average pore volume among the synthesized catalysts. However, the average pore size for Mo/BR was an intermediate value which might be crucial in explaining the catalyst's superior oxygen reduction percentage compared to the other two catalysts. A lower average pore size, as observed in Mo/AC, can make it difficult for bio-crude oxygenates to enter the pores on catalyst surface and take part in the reaction. At the other side of the spectrum, larger average pore sizes cannot effectively

trap the oxygenates long enough for HDO to take place and thus, it might provide an explanation as to why Mo/MWCNT exhibits a lower percentage of oxygen reduction than Mo/BR.

Table 5.3 Surface area, porosity and metal dispersion analysis for synthesized catalysts.

Sample	BET Surface Area (m^2/g)	Average Pore Volume (cm^3/g)	Average Pore Size (nm)	Molybdenum Dispersion (%)	Metallic Surface Area (m^2/g of catalyst)
MWCNT	231 ± 4	1.08 ± 0.04	16.4 ± 0.3	-	-
Mo/MWCNT	202 ± 6	0.93 ± 0.05	16.2 ± 0.2	0.2	0.11
AC	1127 ± 5	0.67 ± 0.03	7.0 ± 0.2	-	-
Mo/AC	1253 ± 8	0.75 ± 0.02	6.8 ± 0.1	3.2	1.92
BR	249 ± 3	0.37 ± 0.03	7.0 ± 0.2	-	-
Mo/BR	118 ± 2	0.27 ± 0.02	9.7 ± 0.3	2.4	1.42

The pore size distributions for the synthesized catalysts have been represented in Fig. 5.1. It was observed that all the carbon-supported catalyst samples had bimodal pore size distributions which is typical for porous carbonaceous materials. The bimodal shape of the curves can be attributed to the presence of micropores in the synthesized catalysts. Monomodal pore size distributions are observed only if the material is strictly microporous in nature (Gauden et al., 2007).

Fig. 5.2 shows the N_2 adsorption-desorption isotherms for the synthesized catalysts. All the samples exhibited type IV isotherms which suggest monolayer-multilayer adsorption and capillary condensation taking place in mesopores. The isotherms for Mo/AC and Mo/BR catalysts had type H4 hysteresis loops which indicate the presence of narrow slit-shaped pores. On the other hand, the isotherm for Mo/MWCNT catalyst had a type H3 hysteresis loop which is generally associated with the presence of non-rigid aggregates of plate-like particles forming slit-shaped pores (Sing et al., 1985).

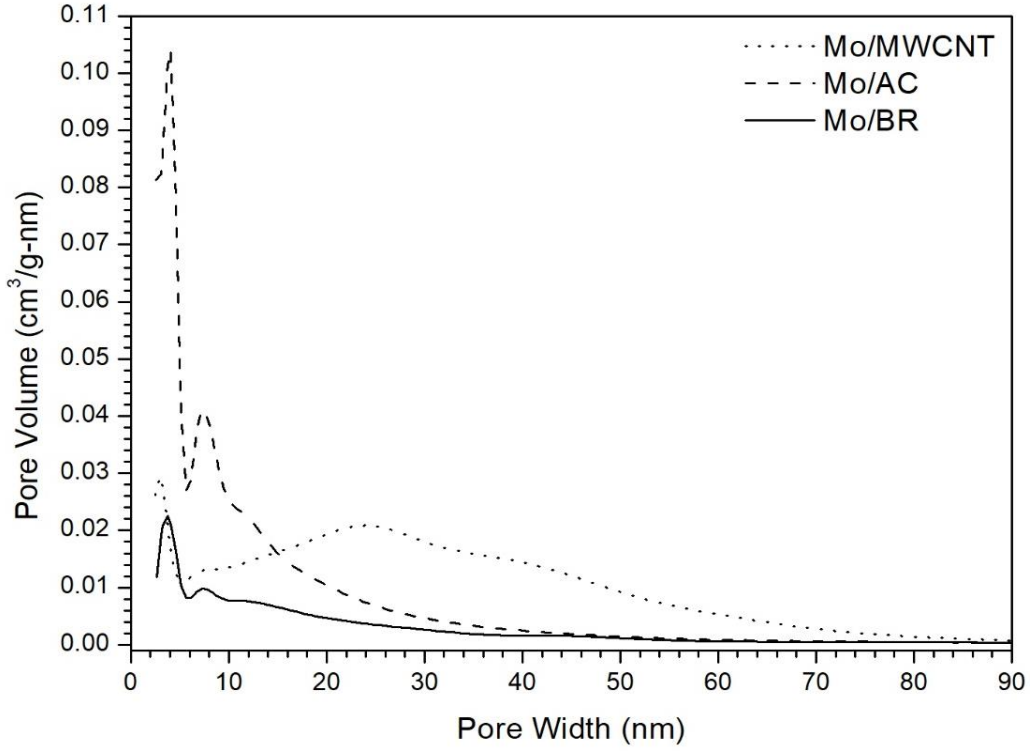

Fig. 5.1 Pore size distribution for prepared catalyst samples.

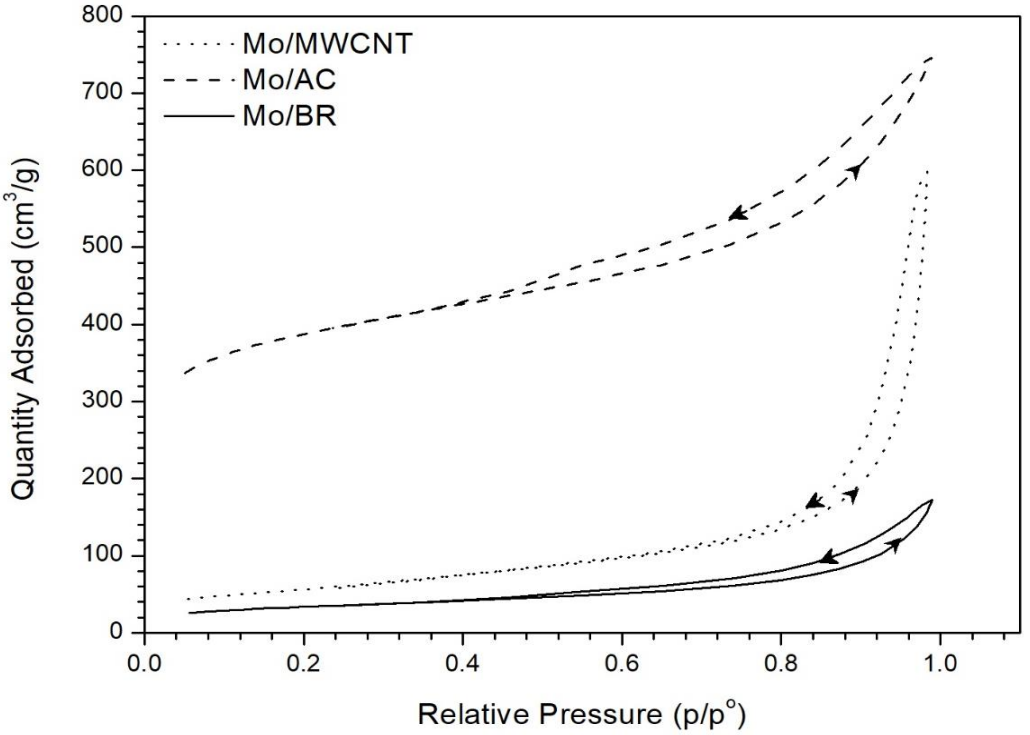

Fig. 5.2 BET isotherm linear plot for prepared catalyst samples.

The molybdenum dispersion over the catalyst samples was determined via CO chemisorption. Mo/AC and Mo/BR exhibited high molybdenum dispersion percentages and metallic surface areas, whereas the values observed for Mo/MWCNT were much lower. This could explain why Mo/MWCNT had the lowest oxygen reduction percentage among the three synthesized catalysts.

5.2.2 Thermogravimetric Analysis (TGA)

Among the three catalysts, Mo/MWCNT underwent the highest percentage of weight loss (17.7%), whereas Mo/BR exhibited the lowest percentage of weight loss (3.94%). The weight loss observed for Mo/AC was an intermediate value of 4.94%. The weight loss patterns for Mo/BR and Mo/AC were quite similar to each other (Fig. 5.3). Thus, Mo/BR was found to be the most stable catalyst over the temperature range studied.

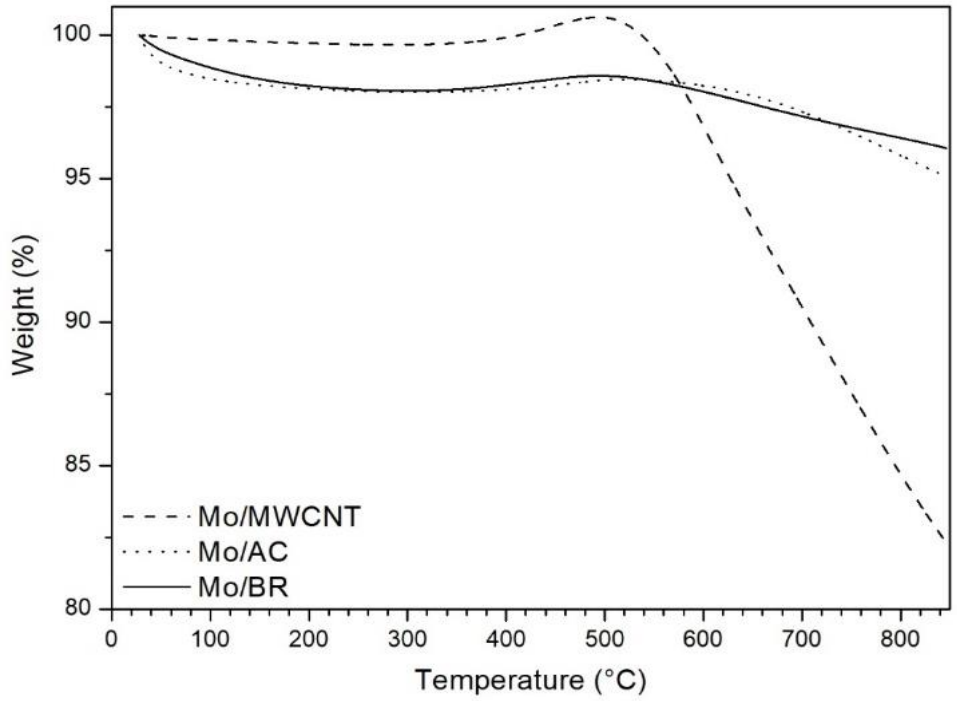

Fig. 5.3 TGA curves depicting weight loss for catalyst samples with increasing temperature.

Interestingly, all the catalyst samples exhibited weight gains between 400 °C and 500 °C (Figs. 5.3 and 5.4). The observed weight gains are lower than 1% and are within the acceptable measurement error range for the TGA instrument. The increase in weight observed for the catalysts can be attributed to the partial oxidation of samples. This can happen if the N_2 used for the purpose is not of the highest purity. Another explanation for the observed weight gains

can be the formation of metal nitrides under the given conditions but this hypothesis needs to be properly justified by XRD analysis of the residue left behind after TGA to check for the presence of nitride phases. However, this is beyond the scope of the current study and therefore, is not discussed any further.

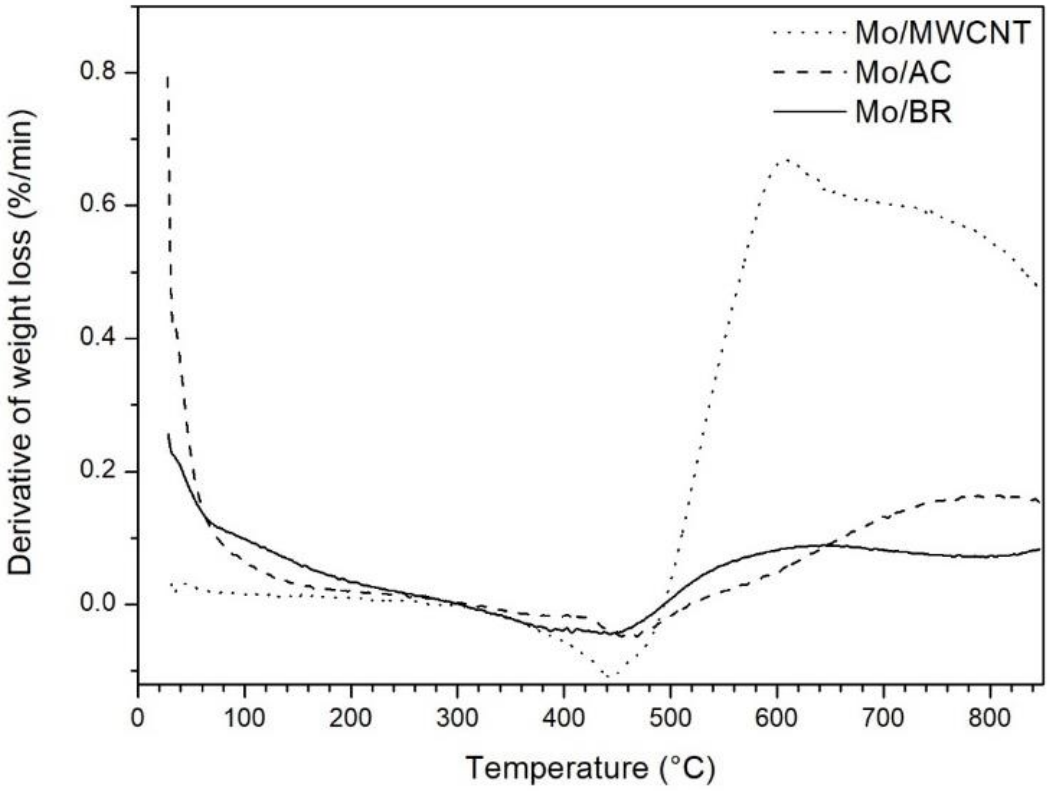

Fig. 5.4 DTG curves depicting the rate of weight loss for catalyst samples.

5.2.3 X-ray Diffraction (XRD) Analysis

The desired β-Mo_2C phase was detected in the XRD spectra of all the catalyst samples (Fig. 5.5). The phase belonged to hexagonal lattice system and its identification validated the selection of the synthesis procedure. In Mo/MWCNT, α-Mo_2C phase was also found and ascribed to the peak at 43.52° (Ren et al., 2013). In addition, SiO_2 and MoO_2 phases were identified in the catalyst sample and corresponded to the peak at 26.08°. The SiO_2 and MoO_2 phases belonged to hexagonal and monoclinic lattice systems, respectively.

In Mo/AC, Mo phase (cubic lattice system) was identified instead of MoO_2 and was attributed to the peaks found at 40.38°, 58.48°, 73.48° and 87.43°. MoO_2 phase was again detected in Mo/BR catalyst and no peaks associated with Mo phase could be identified. SiO_2 was also

present in Mo/AC and Mo/BR catalysts but it existed as a polymorph – quartz (hexagonal lattice system) – in the latter. In addition, calcium aluminum silicate (calcium mica) phase was identified in the Mo/BR catalyst and was ascribed to the peak at 27.71°. The calcium mica phase (monoclinic lattice system) belongs to a family of minerals known as zeolites and its presence in Mo/BR could further explain the high oxygen reduction observed for the said catalyst (Gamliel et al., 2018, Luo et al., 2019).

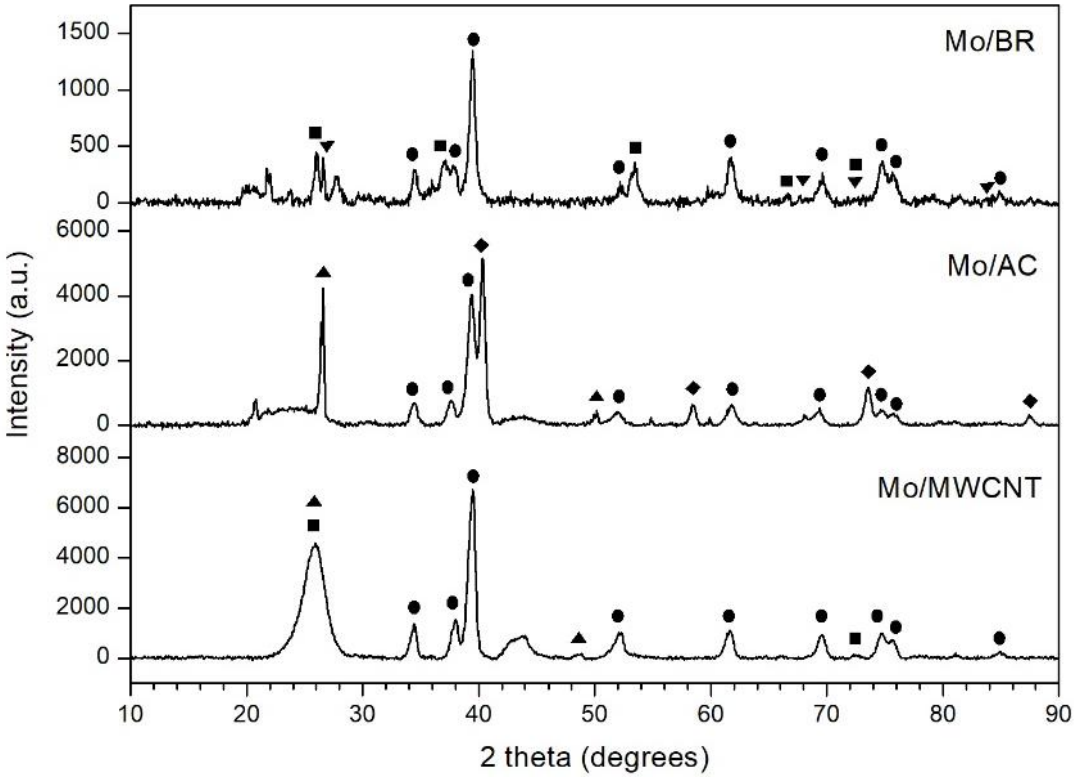

Fig. 5.5 XRD patterns for the synthesized catalyst samples (●: β-Mo_2C, ■: MoO_2, ▲: SiO_2, ▼: Quartz, ♦: Mo).

5.2.4 Ammonia Temperature Programmed Desorption (NH_3-TPD) Analysis

The acidity of catalyst samples was determined by using a basic molecule such as ammonia (NH_3). Ammonia adsorbs strongly on acidic sites and their strength depends on the desorption temperature. The acidic sites are classified as weakly acidic (<200 °C), moderately acidic (200-350 °C) and strongly acidic (>350 °C) (Badoga, 2015). All the catalyst samples exhibited dominant desorption peaks above 650 °C which is characteristic of very strong acid sites. Among the prepared catalysts, Mo/BR was found to have the highest number of such acid sites,

while Mo/MWCNT had the lowest number of acid sites (Fig. 5.6). The amount of acid sites in Mo/AC was intermediate. The high concentration of acidic sites in Mo/BR catalyst could be attributed to the presence of calcium mica which is a zeolitic phase. The zeolitic phase is known to provide Bronsted acidity which promotes the dehydration step during hydrodeoxygenation. In addition, the C–O cleavage during hydrodeoxygenation is known to occur on such acid sites (Luo et al., 2019, Kumar et al., 2018). Therefore, among the three synthesized catalysts, the Mo/BR catalyst is likely to promote hydrodeoxygenation to the highest degree and result in the highest oxygen reduction percentage. This explanation is in agreement with the oxygen reduction percentages observed for the three catalysts (please see Table 5.1 for reference). Hence, the superior oxygen reduction percentage observed for Mo/BR catalyst could be attributed to the presence of higher concentration of strong acidic sites (Luo et al., 2019, Kumar et al., 2018, Moreira et al., 2018, He and Wang, 2012).

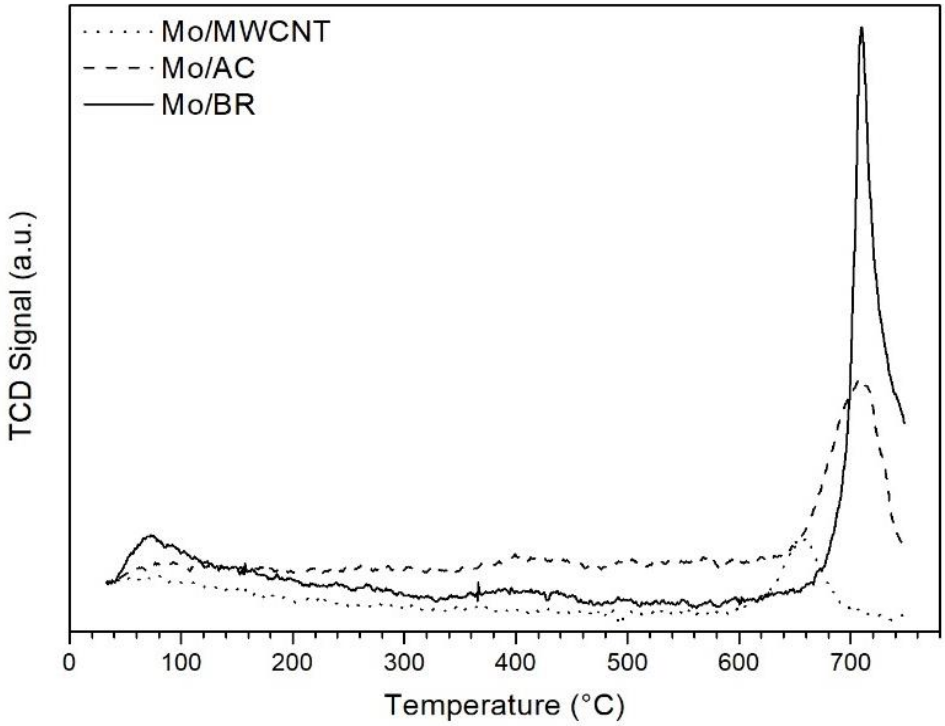

Fig. 5.6 NH_3-TPD curves for the synthesized catalyst samples.

5.2.5 X-ray Photoelectron Spectroscopic (XPS) Analysis

The C 1s peak at 285.0 eV was used as the reference for correcting the spectra of the catalyst samples and to account for charging effects (Wang et al., 2016). The XPS spectra were deconvoluted using CasaXPS (version 2.3.19PR1.0) software. Shirley background subtraction

and Lorentzian Asymmetric (LA) Lineshape functions were used to deconvolute the Mo 3d peaks in the XPS spectra (Figs. 5.7, 5.8 and 5.9). The Mo 3d spectrum for each catalyst was fitted by Mo^{0} at 227.8 eV, Mo^{2+} at 229.0 eV, Mo^{3+} at 229.9 eV, Mo^{4+} at 231.8 eV, Mo^{5+} at 233.1 eV and Mo^{6+} at 233.9 eV. Each oxidation state of molybdenum consists of two peaks resulting from spin-orbit (j-j) coupling: Mo $3d_{5/2}$ and Mo $3d_{3/2}$. The Mo $3d_{5/2}$ and Mo $3d_{3/2}$ peaks have an area ratio of 3:2 and are separated by ~ 3.1 eV (Wang et al., 2016, Li et al., 2004).

Mo/MWCNT and Mo/AC catalysts were found to have carbon, oxygen, silicon and molybdenum on their surfaces with the amount of molybdenum being 0.15 at. % and 0.30 at. %, respectively (Table 5.4). In contrast, Mo/BR catalyst had a much higher amount of molybdenum on its surface (1.56 at. %). Additionally, calcium and aluminium were detected on the surface of Mo/BR catalyst which corroborated the identification of calcium mica phase by XRD analysis.

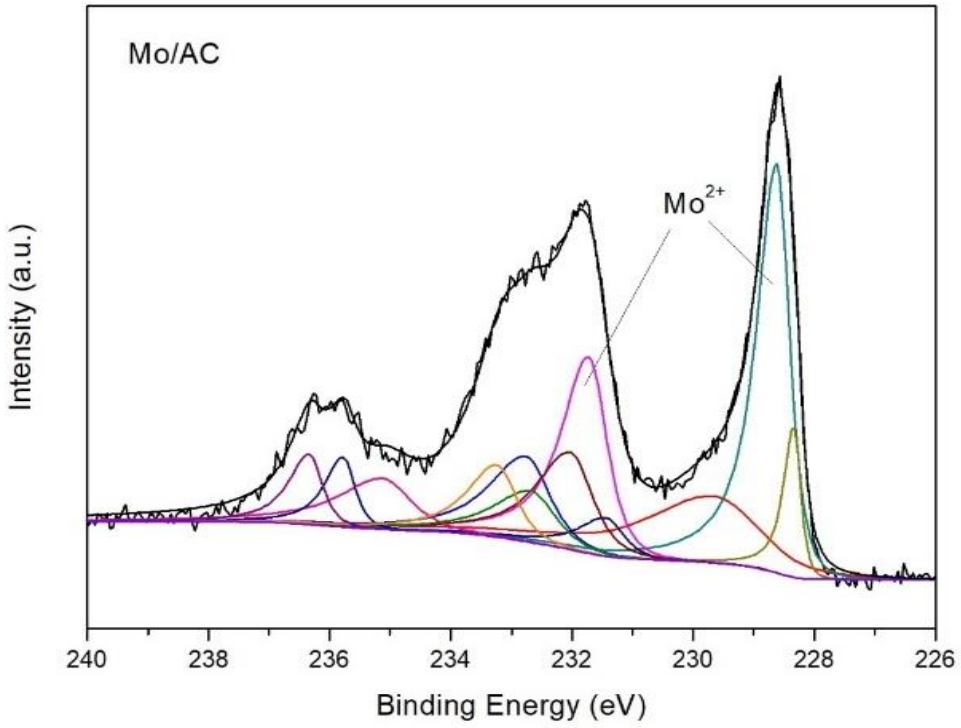

Fig. 5.7 Mo 3d XPS narrow scan spectrum deconvolution of Mo/AC catalyst.

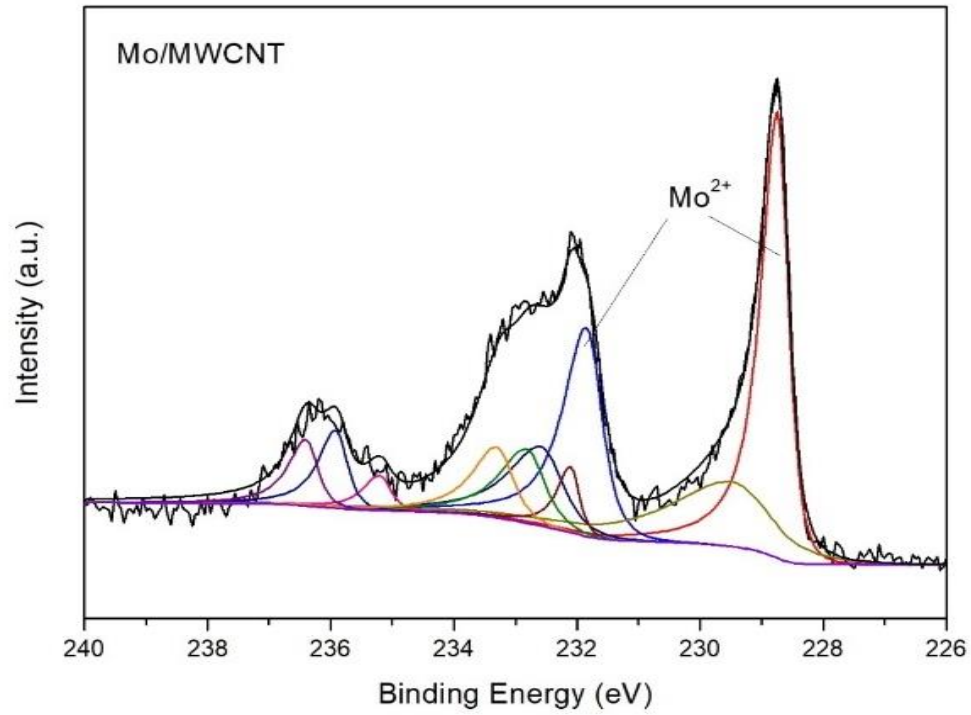

Fig. 5.8 Mo 3d XPS narrow scan spectrum deconvolution of Mo/MWCNT catalyst.

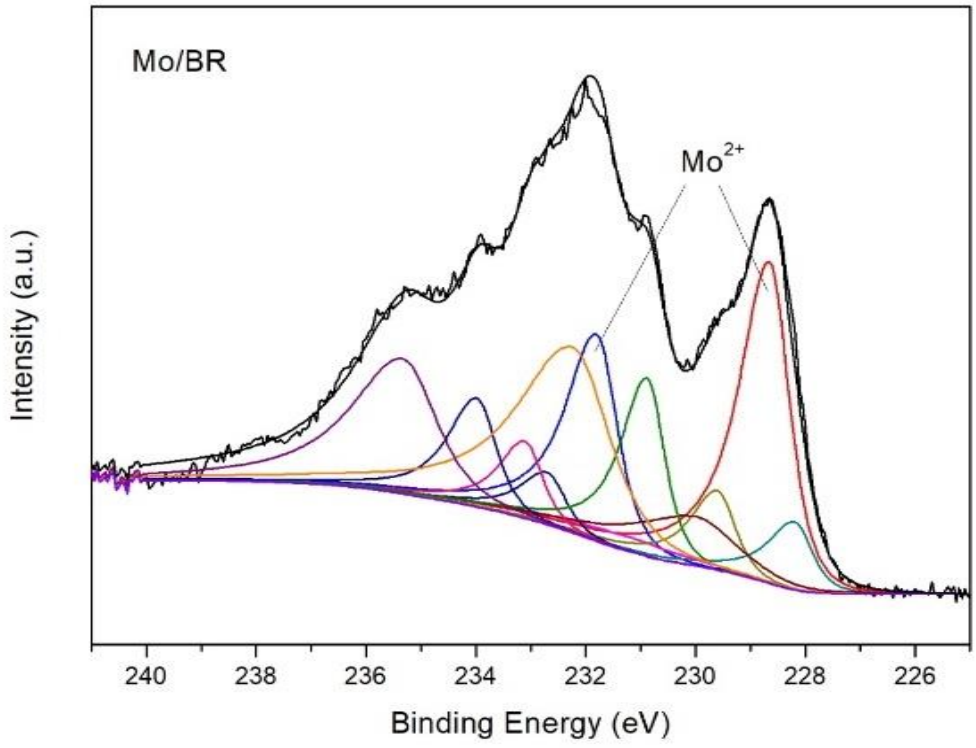

Fig. 5.9 Mo 3d XPS narrow scan spectrum deconvolution of Mo/BR catalyst.

Table 5.4 Surface elemental composition of prepared catalyst samples from XPS wide scan spectra.

Catalyst	Elemental Composition (at. %)					
	C	O	Si	Mo	Al	Ca
Mo/MWCNT	93.00	6.59	0.26	0.15	-	-
Mo/AC	84.13	14.60	0.97	0.30	-	-
Mo/BR	21.70	53.11	20.44	1.56	3.03	0.17

Mo 3d spectrum deconvolution yields the concentration of different oxidation states of molybdenum present in the synthesized catalysts (Table 5.5). The β-Mo_2C phase corresponds to the Mo^{2+} oxidation state of molybdenum and it was observed that the net amount of surface Mo^{2+} species was the highest for Mo/BR catalyst. As a result, it could be inferred that Mo/BR had the highest concentration of β-Mo_2C on its surface which in turn would explain the superior oxygen reduction percentage observed for the said catalyst.

Table 5.5 Distribution of chemical states of Molybdenum from Mo 3d XPS analysis of prepared catalyst samples.

Catalyst	Concentration (at. %)					
	Mo^0	Mo^{2+}	Mo^{3+}	Mo^{4+}	Mo^{5+}	Mo^{6+}
Mo/MWCNT	0	44.35	23.21	8.36	12.72	11.36
Mo/AC	8.24	37.88	21.69	5.65	13.65	12.89
Mo/BR	5.21	32.28	7.19	9.60	14.97	30.75

5.3 Parametric Study for Hydrodeoxygenation Reactions

The prepared bio-crude blend was subjected to hydrodeoxygenation using the synthesized Mo/BR catalyst at different conditions of temperature, pressure, reaction time and catalyst loading. Each parameter was studied individually while keeping the other three parameters constant. The first set of reactions involved varying the pressure while keeping the temperature, reaction time and catalyst loading fixed at the values previously used for screening studies. For each successive set of reactions, the highest oxygen reduction percentage was determined and the corresponding value of the variable parameter was updated and fixed for the next set of reactions. The reaction runs used for the parametric study and the corresponding CHNS analysis of the bio-crude blends along with the oxygen reduction percentages are shown in Tables 5.6, 5.7, 5.8 and 5.9. From the parametric study, the highest percentage of oxygen reduction (59.8 ± 0.9%) was achieved for a reaction that was carried out at 325 °C and 5 MPa for 2 h with a catalyst loading of 4% w/w. The effects of pressure, reaction time, temperature and catalyst loading on the oxygen reduction efficiency of prepared Mo/BR catalyst are shown graphically in Figures 5.10, 5.11, 5.12 and 5.13, respectively.

As shown in Fig. 5.10, the oxygen reduction percentage initially increases with increase in pressure and reaches its maximum value at 5 MPa. The increase in pressure leads to an increase in H_2 partial pressure within the system which facilitates enhanced mass transfer of H_2 molecules into the bulk of bio-crude blend, thus improving the percentage of oxygen reduction. However, the percentage decreases when the pressure is increased beyond 5 MPa. At higher pressures, the hydrodeoxygenated products might not detach efficiently from the catalyst surface which can lead to secondary reactions thereby lowering the oxygen reduction percentage (Ayodele and Daud, 2015, Ayodele et al., 2014).

Increase in reaction time up to 2 h also promotes an increase in the oxygen reduction but for longer reaction times, a decrease in the reduction percentage is observed which can be ascribed to the occurrence of parallel secondary reactions. Similarly, the oxygen reduction improved initially with increases in temperature (up to 325 °C: Fig. 5.12) and catalyst loading (up to 4% w/w: Fig. 5.13) but tapered off due to the dominance of secondary reactions at higher values.

Table 5.6 Effect of pressure on oxygen reduction efficiency of prepared Mo/BR catalyst for bio-crude blends (Temperature: 300 °C, Catalyst Loading: 3% w/w, Reaction Time: 3 h).

Pressure (MPa)	C (wt. %)	H (wt. %)	N (wt. %)	S (wt. %)	O (wt. %) *	Oxygen Reduction (%)
Blend	86.33 ± 0.05	10.54 ± 0.02	0.44 ± 0.02	0.23 ± 0.02	2.46 ± 0.07	
3	86.24 ± 0.02	11.70 ± 0.03	0.34 ± 0.01	0.10 ± 0.003	1.62 ± 0.05	34.2 ± 0.2
4	86.44 ± 0.05	11.58 ± 0.01	0.43 ± 0.003	0.13 ± 0.02	1.42 ± 0.06	42.3 ± 0.8
5	86.47 ± 0.04	11.76 ± 0.07	0.42 ± 0.01	0.10 ± 0.01	1.25 ± 0.11	49.2 ± 3.0
6	86.43 ± 0.05	11.74 ± 0.04	0.39 ± 0.02	0.12 ± 0.001	1.32 ± 0.09	46.3 ± 2.2
7	86.52 ± 0.06	11.57 ± 0.05	0.43 ± 0.06	0.12 ± 0.01	1.36 ± 0.10	44.7 ± 2.6

* Calculated by difference

Table 5.7 Effect of reaction time on oxygen reduction efficiency of prepared Mo/BR catalyst for bio-crude blends (Temperature: 300 °C, Pressure: 5 MPa, Catalyst Loading: 3% w/w).

Reaction Time (h)	C (wt. %)	H (wt. %)	N (wt. %)	S (wt. %)	O (wt. %) *	Oxygen Reduction (%)
Blend	86.33 ± 0.05	10.54 ± 0.02	0.44 ± 0.02	0.23 ± 0.02	2.46 ± 0.07	
1	85.92 ± 0.08	11.64 ± 0.03	0.41 ± 0.01	0.19 ± 0.02	1.84 ± 0.10	25.2 ± 2.0
2	86.69 ± 0.07	11.71 ± 0.05	0.36 ± 0.01	0.11 ± 0.001	1.13 ± 0.12	54.1 ± 3.6
3	86.47 ± 0.04	11.76 ± 0.07	0.42 ± 0.01	0.10 ± 0.01	1.25 ± 0.11	49.2 ± 3.0
4	86.41 ± 0.01	11.77 ± 0.06	0.42 ± 0.02	0.10 ± 0.001	1.30 ± 0.07	47.2 ± 1.3
5	86.48 ± 0.03	11.62 ± 0.07	0.44 ± 0.06	0.12 ± 0.01	1.34 ± 0.10	45.5 ± 2.6

* Calculated by difference

Table 5.8 Effect of temperature on oxygen reduction efficiency of prepared Mo/BR catalyst for bio-crude blends (Pressure: 5 MPa, Reaction Time: 2 h, Catalyst Loading: 3% w/w).

Temperature (°C)	C (wt. %)	H (wt. %)	N (wt. %)	S (wt. %)	O (wt. %) *	Oxygen Reduction (%)
Blend	86.33 ± 0.05	10.54 ± 0.02	0.44 ± 0.02	0.23 ± 0.02	2.46 ± 0.07	
250	85.91 ± 0.09	11.88 ± 0.03	0.39 ± 0.002	0.09 ± 0.001	1.73 ± 0.12	29.7 ± 2.9
275	86.25 ± 0.05	11.74 ± 0.02	0.44 ± 0.04	0.12 ± 0.01	1.45 ± 0.07	41.1 ± 1.2
300	86.69 ± 0.07	11.71 ± 0.05	0.36 ± 0.01	0.11 ± 0.001	1.13 ± 0.12	54.1 ± 3.6
325	86.63 ± 0.02	11.80 ± 0.02	0.42 ± 0.04	0.11 ± 0.005	1.04 ± 0.04	57.7 ± 0.5
350	86.57 ± 0.06	11.75 ± 0.02	0.38 ± 0.002	0.13 ± 0.003	1.17 ± 0.08	52.4 ± 2.0

* Calculated by difference

Table 5.9 Effect of catalyst loading on oxygen reduction efficiency of prepared Mo/BR catalyst for bio-crude blends (Temperature: 325 °C, Pressure: 5 MPa, Reaction Time: 2 h).

Catalyst Loading (% w/w)	C (wt. %)	H (wt. %)	N (wt. %)	S (wt. %)	O (wt. %) *	Oxygen Reduction (%)
Blend	86.33 ± 0.05	10.54 ± 0.02	0.44 ± 0.02	0.23 ± 0.02	2.46 ± 0.07	
1	86.06 ± 0.03	11.71 ± 0.04	0.44 ± 0.003	0.22 ± 0.05	1.57 ± 0.07	36.2 ± 1.0
2	86.38 ± 0.05	11.66 ± 0.01	0.40 ± 0.01	0.09 ± 0.004	1.47 ± 0.06	40.2 ± 0.8
3	86.63 ± 0.02	11.80 ± 0.02	0.42 ± 0.04	0.11 ± 0.005	1.04 ± 0.04	57.7 ± 0.5
4	86.68 ± 0.04	11.78 ± 0.01	0.38 ± 0.004	0.17 ± 0.01	0.99 ± 0.05	59.8 ± 0.9
5	86.58 ± 0.06	11.74 ± 0.04	0.42 ± 0.01	0.12 ± 0.01	1.14 ± 0.10	53.7 ± 2.8

* Calculated by difference

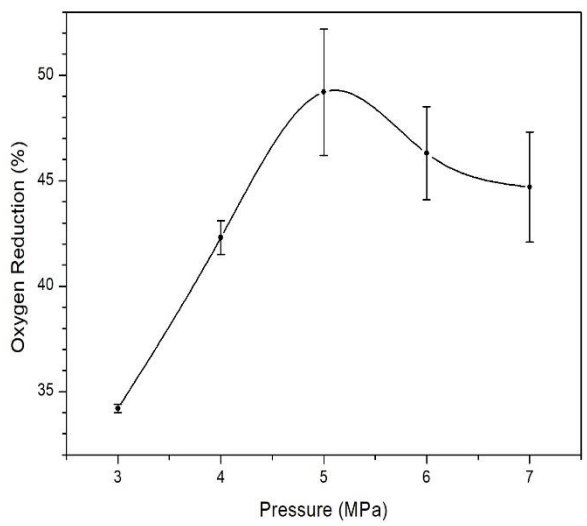

Fig. 5.10 Effect of pressure on oxygen reduction (Temperature: 300 °C, Reaction Time: 3 h, Catalyst Loading: 3% w/w).

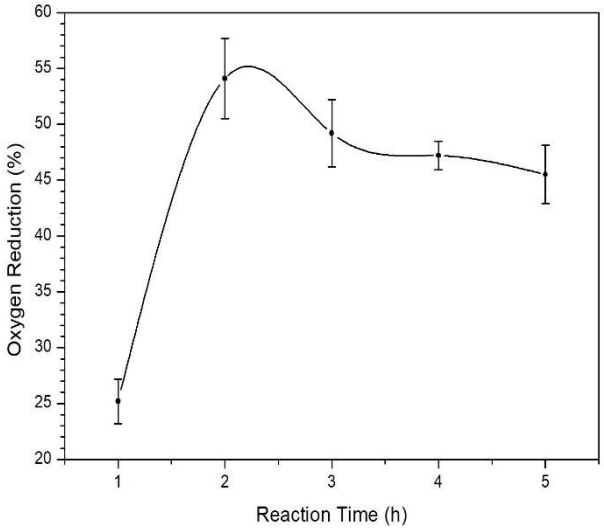

Fig. 5.11 Effect of reaction time on oxygen reduction (Temperature: 300 °C, Pressure: 5 MPa, Catalyst Loading: 3% w/w).

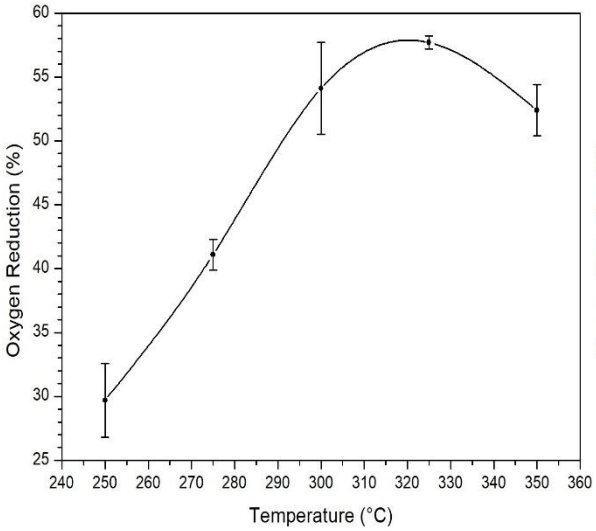

Fig. 5.12 Effect of temperature on oxygen reduction (Pressure: 5 MPa, Reaction Time: 2 h, Catalyst Loading: 3% w/w).

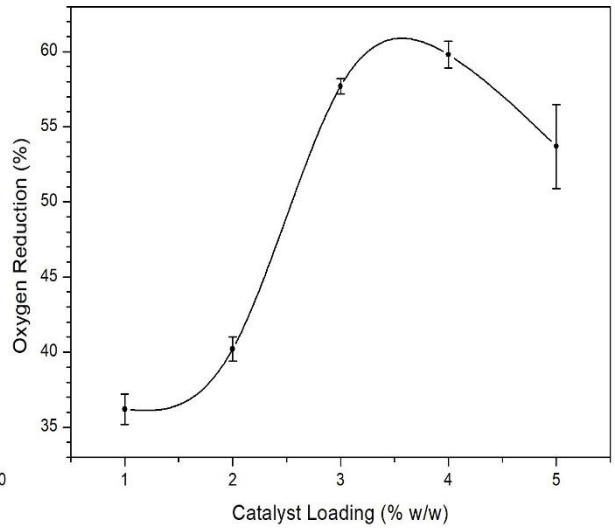

Fig. 5.13 Effect of catalyst loading on oxygen reduction (Temperature: 325 °C, Pressure: 5 MPa, Reaction Time: 2 h).

The increase in oxygen reduction percentage observed up to 325 °C can be attributed to the increase in kinetic energy of the reactant molecules which promotes faster collisions and thereby higher rates of hydrodeoxygenation. Catalyst loading up to 4% w/w provides increasingly more active sites for HDO reaction but any further increase results in introduction of redundant active sites which favour secondary reactions and therefore, a decrease in oxygen reduction percentage is observed (Arend et al., 2011, Ayodele and Daud, 2015, Ayodele et al., 2014). Thus, the desirable values of the process parameters for carrying out hydrodeoxygenation of a bio-crude blend using Mo/BR catalyst were 325 °C (temperature), 5 MPa (pressure), 2 h (reaction time) and 4% w/w (catalyst loading).

5.4 Characterization of Bio-crude Blends

5.4.1 Moisture Content Analysis

The moisture content in the bio-crude blends was determined by Karl-Fischer coulometric titration and the results were reported as weight percentages of moisture. Prior to hydrodeoxygenation, the bio-crude blend contained 0.021 ± 0.002 wt. % of moisture, whereas the hydrodeoxygenated bio-crude blend contained 0.025 ± 0.001 wt. % of moisture. The increase in moisture content can be attributed to the formation of H_2O molecules during the hydrodeoxygenation reaction. In spite of the slight increase, the moisture content in the hydrodeoxygenated bio-crude blend was well within the permissible limit of 0.05 wt. % (Costenoble, 2006).

5.4.2 Boiling Point Distribution Analysis

The boiling point distributions of the bio-crude blends (Blend and HDO Blend) have been shown in Fig. 5.14. The Sim-Dist data was calibrated using n-alkane standards and it was observed that before hydrodeoxygenation, the bio-crude blend contained no n-alkanes in the C_7-C_{13} carbon range. The majority (72.3 wt. %) of n-alkanes were found in the C_{24}-C_{36} range. However, the hydrodeoxygenated blend contained a small fraction (1.45 wt. %) of n-alkanes in the C_{11}-C_{13} range while none could be found in the C_7-C_{10} range. It was also observed that the percentage of n-alkanes (67.86 wt. %) in the C_{24}-C_{36} range decreased after hydrodeoxygenation.

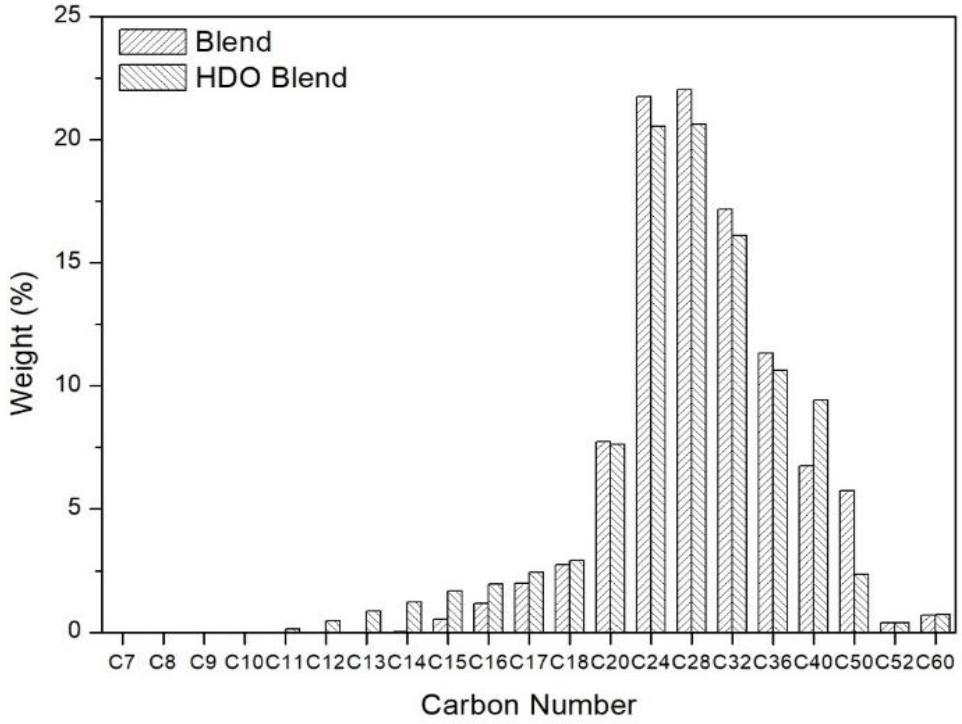

Fig. 5.14 Distribution of n-alkanes in bio-crude blends before and after hydrodeoxygenation.

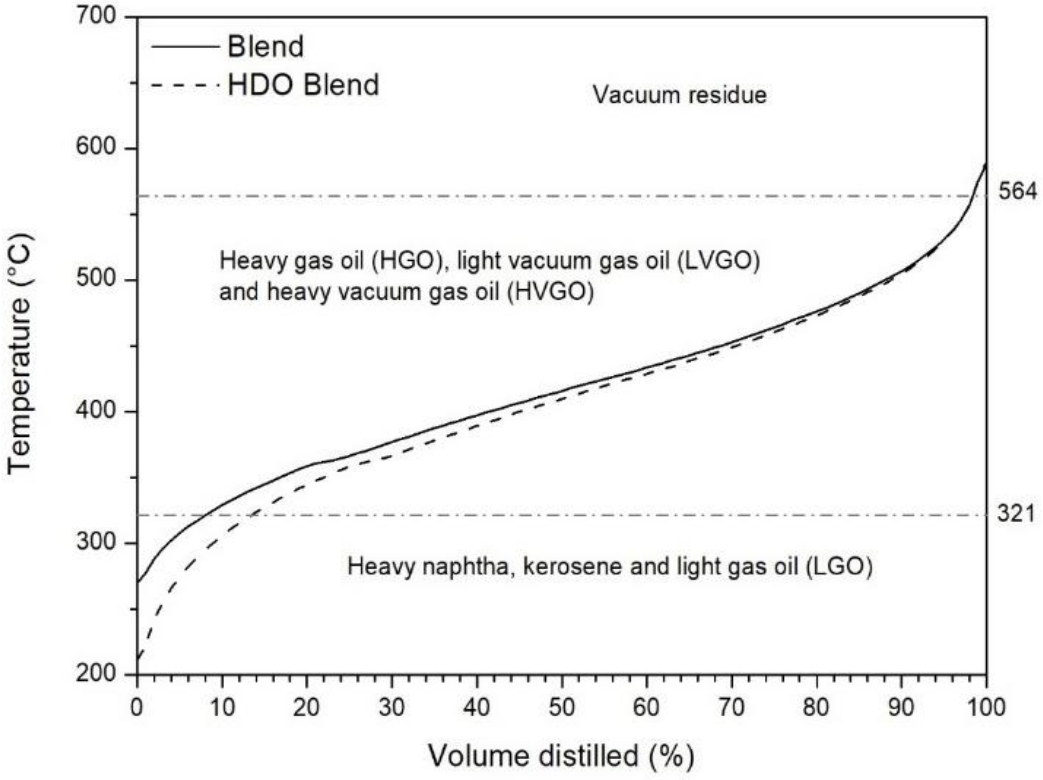

Fig. 5.15 Change in volume of bio-crude blends as a function of boiling point.

On the other hand, the fraction of n-alkanes in the C_{13}-C_{24} range (Blend: 35.9 wt. %, HDO Blend: 39.2 wt. %) and C_{15}-C_{20} range (Blend: 14.1 wt. %, HDO Blend: 16.6 wt. %) increased in the bio-crude blend after undergoing hydrodeoxygenation which suggests that hydrocracking also took place during the HDO reaction (Figs. 5.14 and 5.15). Thus, HDO Blend contained a greater fraction of its n-alkanes in the bio-diesel range and hence, is more suitable for related applications (Bharti et al., 2014).

5.4.3 ^{1}H NMR Spectroscopic Analysis

The ^{1}H NMR spectra of the bio-crude blends before and after hydrodeoxygenation are shown in Fig. 5.16 and the quantitative percentages of different types of hydrogen present in the samples are reported in Table 5.10.

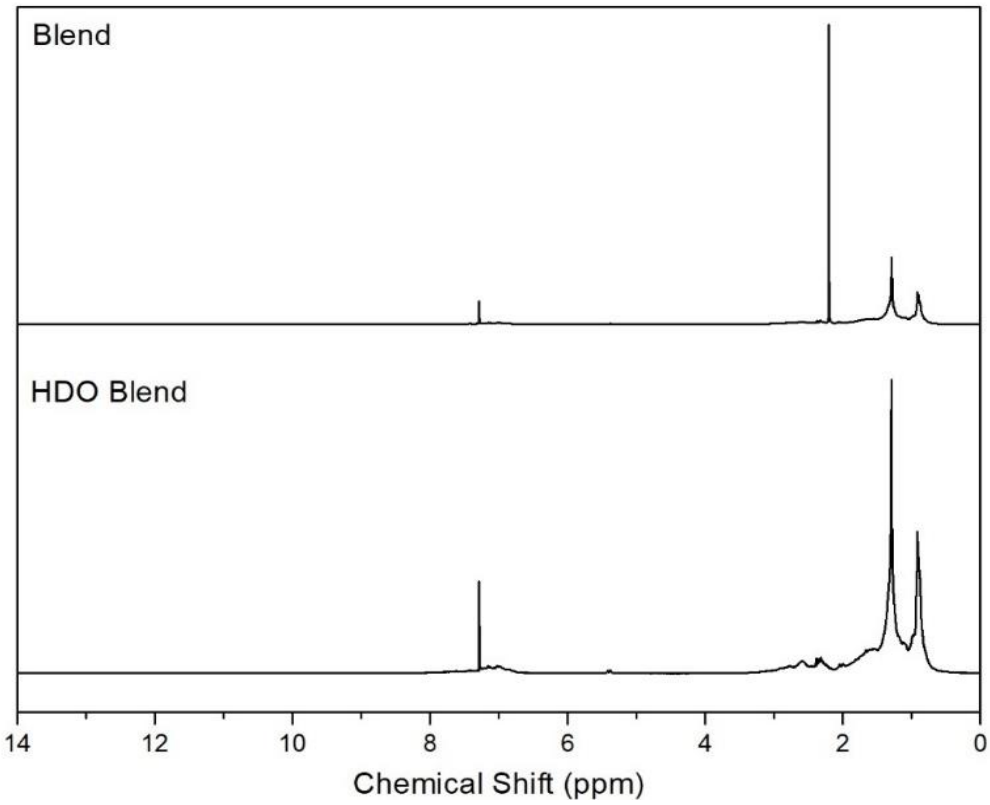

Fig. 5.16 ^{1}H NMR spectra for bio-crude blends before and after hydrodeoxygenation.

The chemical shift ranges were assigned to different types of protons based on previous studies carried out by Joseph et al. (2010) and Ingram et al. (2008). It was observed that the concentration of aliphatic protons increased from 63.8% to 71.6%, whereas the quantity of aliphatic hydroxyl protons decreased slightly after the reaction. The hydrodeoxygenated blend

also contained lower concentrations of aromatics and ethers than the untreated blend. Phenolic hydroxyl groups and non-conjugated alkenes were not detected in both the bio-crude blends. The chemical shift range of 2.2-3.0 ppm was assigned to protons located alpha to ketones, aldehydes and carboxylic groups and benzylic protons. The intensity in this range is related to the intensity observed in the chemical shift range of 8.0-13.0 ppm which was assigned to protons located on aldehydes, carboxylic acids and downfield aromatics. The hydrogen concentrations in both these ranges reduced after hydrodeoxygenation which indicates effective removal of the aforementioned bio-crude oxygenates and aromatics.

Table 5.10 Quantitative percentages of different types of hydrogen present in bio-crude blends based on ^{1}H NMR spectra.

Chemical Shifts (ppm)	Assignment of Protons	Hydrogen Content (% of all hydrogen)	
		Blend	HDO Blend
0 - 1.6	Aliphatic (-C**H**$_3$, -C**H**$_2$-)	63.8	71.6
1.6 - 2.2	Aliphatic Hydroxyls (-O**H**)	12.5	11.5
2.2 - 3.0	C**H**$_3$C=O, C**H**$_3$Ar, -C**H**$_2$Ar	16.0	10.2
3.0 - 4.2	C**H**$_3$O-, -C**H**$_2$O-, =C**H**O-	0.9	0.8
4.2 - 6.5	ArO**H**, non-conjugated alkenes (**H**C=C)	BD	BD
6.5 - 8.0	Ar**H**, conjugated alkenes (**H**C=C)	6.6	5.9
8.0 - 13.0	-COO**H**, -C**H**O, downfield Ar**H**	0.1	BD

*BD: Below Detection

5.4.4 ^{13}C NMR Spectroscopic Analysis

The ^{13}C NMR spectra of Blend and HDO Blend are compared in Fig. 5.17 and the quantitative percentages of different classes of compounds present in the bio-crude blends are reported in Table 5.11. The assignment of different chemical shift ranges in the ^{13}C NMR spectra was accomplished according to Joseph et al. (2010) and Ingram et al. (2008), which facilitated the identification of different types of chemical functional groups present in bio-crude blends.

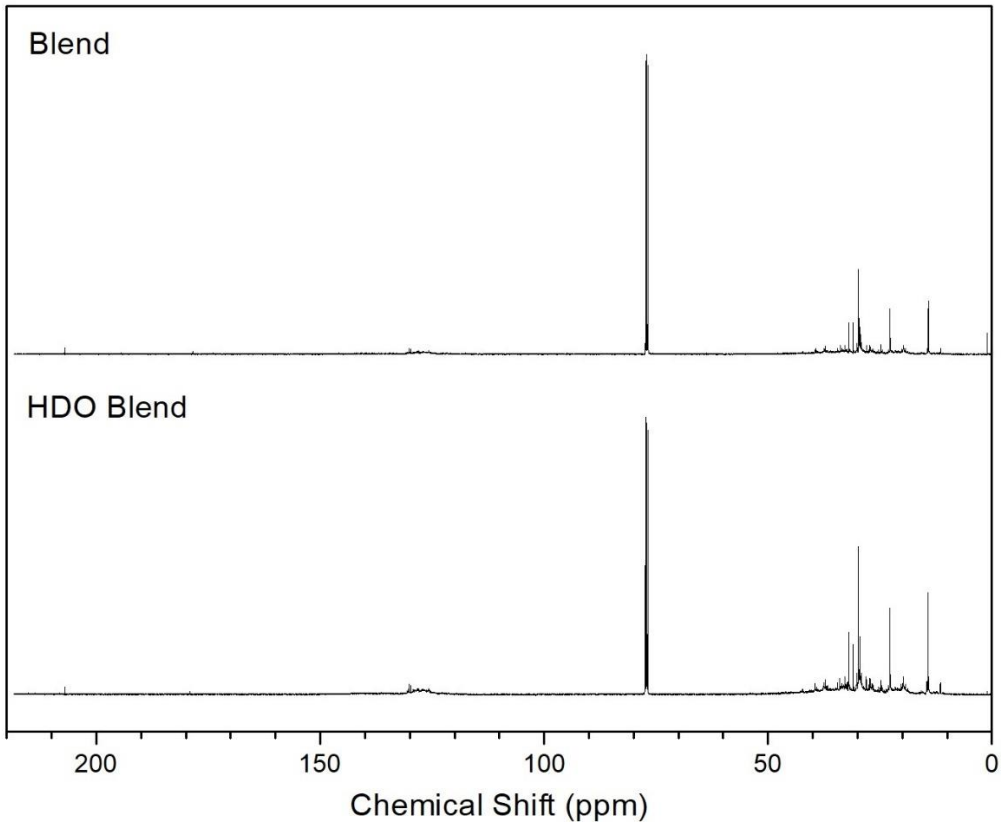

Fig. 5.17 ^{13}C NMR spectra for bio-crude blends before and after hydrodeoxygenation.

Before hydrodeoxygenation, the bio-crude blend contained 57.3% of aliphatic carbons which then increased to 65.6% after the HDO reaction. The concentration of aliphatic carbons was determined by integrating the spectra in the region between 6 ppm and 55 ppm. The carbons present in alcohols, ethers and carbohydrates are normally detected in the spectral region between 55 ppm and 103 ppm. For the bio-crude blends, no carbons were detected in the aforementioned spectral region which indicates that alcohols, ethers and carbohydrates might be present in extremely low quantities. However, in Section 5.4.3, detectable quantities of alcohols and ethers were recorded from ^{1}H NMR spectroscopic analysis and this discrepancy could be explained by the fact that ^{13}C NMR spectroscopy is a less sensitive technique than ^{1}H NMR spectroscopy (Joseph et al., 2010). The spectral region between 103 ppm and 163 ppm is associated with carbons present in aromatic and olefinic compounds and it was found that the concentration of these carbons decreased after the bio-crude blend underwent hydrodeoxygenation. Similar observations were also recorded for the spectral region between 163 ppm and 215 ppm: it was found that the carbons present in carbonyl group-containing

compounds such as esters, carboxylic acids, ketones and aldehydes decreased after the bio-crude blend was subjected to hydrodeoxygenation. These observations complement the findings from ^{1}H NMR spectroscopic analysis (Section 5.4.3) and corroborate the effectiveness of the hydrodeoxygenation process.

Table 5.11 Quantitative percentages of different types of carbon present in bio-crude blends based on ^{13}C NMR spectra.

Sample	Carbon type (% of all carbon)			
	Aliphatics	Alcohols, Ethers and Carbohydrates	Aromatics and Olefins	Esters, Carboxylic acids, Ketones and Aldehydes
	6-55 ppm	55-103 ppm	103-163 ppm	163-215 ppm
Blend	57.3	BD	40.4	2.3
HDO Blend	65.6	BD	33.2	1.2

*BD: Below Detection

5.5 Conclusions

For the prepared bio-crude blend, the molybdenum catalyst synthesized using bio-residue as the support exhibited a higher oxygen reduction percentage than the catalysts synthesized using commercial multi-walled carbon nanotubes and commercial activated carbon. The bio-residue-based catalyst also performed much better than commercial CoMo/γ-Al_2O_3 and NiMo/γ-Al_2O_3 catalysts in terms of oxygen reduction efficiency. Carbothermal hydrogen reduction method was used to synthesize the carbon-supported catalysts and as intended, β-Mo_2C phase was formed in all the synthesized catalysts. The bio-residue-based molybdenum catalyst had a high percentage of molybdenum dispersion, the highest number of strongly acidic sites, highest concentration of β-Mo_2C on its surface and an optimum average pore size. The aforementioned characteristics might explain the superior oxygen reduction efficiency of the said catalyst. Additionally, calcium mica phase was identified in the bio-residue-based catalyst which could have possibly enhanced the effectiveness of the catalyst towards oxygen reduction. The highest oxygen reduction percentage using the bio-residue-based catalyst was achieved for a given set of reaction conditions: temperature – 325 °C, pressure – 5 MPa, reaction time – 2 h and catalyst loading – 4% w/w.

6. CONCLUSION AND RECOMMENDATIONS

6.1 Conclusion

Chapter 4

Ethyl acetate was identified as the most favourable option for solvent-extraction even though none of the solvents could recover 100% of bio-crude present in the hydrothermal liquefaction product mixture. The extraction carried out using ethyl acetate yielded significantly large amounts (bio-crude yield: 31.8 wt. %) of an easy-to-handle, high quality bio-crude that is most suitable for further upgrading processes and eventual bio-diesel applications. The bio-crude extracted using ethyl acetate had a higher heating value of 46.0 MJ/kg, an oxygen content of 9.2 wt. % and an ash content of 0.1 wt. %. The aforementioned bio-crude exhibited the highest oxidation stability at room temperature with an induction period of 86.5 days and had a significant percentage of its compounds in the C_{13}-C_{24} carbon range. The amounts of nitrogen and sulphur were quite low in all the bio-crude samples. Catalytic hydrodeoxygenation was determined to be the most preferred upgrading process for the bio-crude samples because oxygen was the major heteroatom impurity found in them. Carboxylic acids and esters were the predominant oxygen-containing compounds found in the bio-crude and bio-residue fractions. Silica polymorphs such as quartz and α-cristobalite, along with calcium mica, were the dominant phases in all the bio-residue samples. The bio-residue obtained using ethyl acetate had the highest specific surface area (249 m^2/g) among the three bio-residue samples with an average pore volume of 0.37 cm^3/g and an average pore size of 7 nm. In addition, the aforementioned bio-residue underwent the lowest percentage of weight loss (29.03%) when subjected to thermogravimetric analysis over a temperature range of ~ 30-800 °C. Due to its favourable textural properties and superior thermal stability, the bio-residue extracted using ethyl acetate was earmarked for potential use as catalyst supports or as bio-adsorbents.

Chapter 5

The desired β-Mo_2C phase was detected in all the synthesized catalyst samples. The synthesized catalysts were screened for their oxygen reduction efficiency and the bio-residue-based catalyst was identified as the best-performing catalyst at the screening conditions. Commercial hydrotreating catalysts such as CoMo/γ-Al_2O_3 and NiMo/γ-Al_2O_3 were also used

for hydrodeoxygenation of the bio-crude blend to provide comparisons with the bio-residue-based catalyst. The bio-residue-based catalyst exhibited a higher oxygen reduction percentage (49.2%) than both CoMo/γ-Al_2O_3 (21.1%) and NiMo/γ-Al_2O_3 (26.0%) catalysts. In petroleum refineries, the bio-crude blend can be introduced just before the hydrotreating unit so that the blend of bio-crude and petroleum crude can be co-processed in the hydrotreater using suitable catalysts. This would improve the oxygen reduction efficiency of the hydrotreating unit without significantly disrupting the economics and infrastructure of petroleum industries. For hydrotreating a bio-crude blend that has 10 wt. % of bio-crude, the synthesized Mo/BR catalyst would be suitable. However, if the amount of bio-crude is less than 1 wt. % in petroleum feedstock, then the petroleum industries may not choose to substitute the conventional catalysts with a new synthesized catalyst. Among the synthesized catalysts, the bio-residue-supported molybdenum catalyst had the highest number of strongly acidic sites and the highest concentration of β-Mo_2C on its surface. The aforementioned catalyst had a molybdenum dispersion of 2.4%, BET surface area of 118 m^2/g and an average pore size of 9.7 nm. The oxygen reduction percentage for the said catalyst improved and reached the maximum value of 59.8% for a reaction that was carried out at 325 °C and 5 MPa for 2 h with a catalyst loading of 4% w/w. The hydrodeoxygenated bio-crude blend obtained using the aforementioned reaction conditions exhibited a slight increase in the moisture content which is characteristic of the HDO process. However, the observed moisture content was within the permissible limit of 0.05 wt. %. The bio-crude blend also underwent hydrocracking during the hydrodeoxygenation process and as a result, the fraction of n-alkanes in the C_{13}-C_{24} and C_{15}-C_{20} ranges increased after hydrodeoxygenation. Furthermore, the concentration of aliphatic compounds increased and that of carbonyl-group containing oxygenates and aromatics decreased in the bio-crude blend after hydrodeoxygenation. Thus, the hydrodeoxygenated bio-crude blend was found to be more suitable for further co-processing and eventual application as a transportation fuel.

6.2 Recommendations

- The solvent recovery for the extraction process can be further improved to make the process more economic. This would involve either modifying the existing vacuum evaporation method or finding an alternative for the same.

- Instead of using solvents discretely for the extraction process, different combinations of organic solvents can be investigated in an attempt to increase the bio-crude yield and manipulate the boiling point distribution of the said product.
- The synthesized catalysts can be modified and further developed to improve the sulphur, nitrogen and oxygen reduction. This could be done by changing the molybdenum loading on the catalysts and/or introducing a promoter metal to enhance the overall catalytic activity.
- An effective method needs to be developed to recover the catalyst after hydrodeoxygenation reaction is over. The recovered catalyst can then be studied to evaluate the extent of deactivation and the potential for regeneration and reuse.
- Techno-economic analysis and study of reaction kinetics need to be carried out in order to facilitate industrial scale-up.

7. REFERENCES

Akhtar J, Amin NAS. A review on process conditions for optimum bio-oil yield in hydrothermal liquefaction of biomass. Renew. Sust. Energy Rev. 2011; 15; 1615–24.

Appl M. Ammonia, 2. Production Processes. In Ullmann's Encyclopaedia of Industrial Chemistry, (Ed.) 2011. DOI: 10.1002/14356007.o02_o11.

Ardiyanti AR, Khromova SA, Venderbosch RH, Yakovlev VA, Heeres HJ. Catalytic hydrotreatment of fast-pyrolysis oil using non-sulfided bimetallic Ni-Cu catalysts on a δ-Al_2O_3 support. Appl. Catal., B 2012; 117-118; 105–17.

Arend M, Nonnen T, Hoelderich WF, Fischer J, Groos J. Catalytic deoxygenation of oleic acid in continuous gas flow for the production of diesel-like hydrocarbons. Appl. Catal., A 2011; 399 (1–2); 198–204.

ASTM Standard D2887, 2018, "Boiling range Distribution of Petroleum Fractions by Gas Chromatography", ASTM International, West Conshohocken, PA, 2018, DOI: 10.1520/D2887-18, www.astm.org.

ASTM Standard D482, 2013, "Ash from Petroleum Products", ASTM International, West Conshohocken, PA, 2013, DOI: 10.1520/D0482-13, www.astm.org.

Ayodele OB, Abbas HF, Daud WMAW. Hydrodeoxygenation of stearic acid into normal and iso-octadecane biofuel with zeolite supported palladium-oxalate catalyst. Energy Fuels 2014; 28 (9); 5872–81.

Ayodele OB, Daud WMAW. Optimization of catalytic hydrodeoxygenation of oleic acid into biofuel using fluoroplatinum oxalate zeolite supported catalyst. J. Taiwan Inst. Chem. Eng. 2015; 47; 113–24.

Badoga S. Synthesis and characterization of NiMo supported mesoporous materials with EDTA and phosphorous for hydrotreating of heavy gas oil. PhD Thesis 2015. Retrieved from http://hdl.handle.net/10388/ETD-2015-04-2019.

Baloch UK. Wheat: Post-harvest operations. In Mejia D, Lewis B (Eds.). INPhO – Post-harvest Compendium, AGSI/FAO. 1999.

Bardet M, Hediger S, Gerbaud G, Gambarelli S, Jacquot JF, Foray MF, Gadelle A. Investigation with C-13 NMR, EPR and magnetic susceptibility measurements of char residues obtained by pyrolysis of biomass. Fuel 2007; 86; 1966–76.

Bharti RK, Srivastava S, Thakur IS. Production and characterization of biodiesel from carbon dioxide concentrating chemolithotrophic bacteria, Serratia sp. ISTD04. Bioresour. Technol. 2014; 153; 189–97.

Blaney L. Magnetite (Fe_3O_4): Properties, synthesis, and applications. The Lehigh Review 2007; 15 (5).

Boateng AA, Mullen CA, Goldberg N, Hicks KB, Jung HG, Lamb JFS. Production of bio-oil from alfalfa stems by fluidized-bed fast pyrolysis. Ind. Eng. Chem. Res. 2008; 47; 4115–22.

Boocock DGB, Sherman KM. Further aspects of powdered poplar wood liquefaction by aqueous pyrolysis. Can J. Chem. Eng. 2009; 63; 627–33.

Borges ME, Diaz L, Gavin J, Brito A. Estimation of the content of fatty acid methyl esters (FAME) in biodiesel samples from dynamic viscosity measurements. Fuel Process Tech. 2011; 92; 597–99.

Botchwey C. Two-stage hydrotreating of heavy gas oil with inter-stage hydrogen sulphide removal. Master Thesis 2003. Retrieved from https://harvest.usask.ca/handle/10388/etd-07192010-092232.

Boullosa-Eiras S, Lødeng R, Bergem H, Stocker M, Hannevold L, Blekkan EA. Catalytic hydrodeoxygenation (HDO) of phenol over supported molybdenum carbide, nitride, phosphide and oxide catalysts. Catal. Today 2014; 223; 44–53.

Cai Z, Wang F, Zhang X, Ahishakiye R, Xie Y, Shen Y. Selective hydrodeoxygenation of guaiacol to phenolics over activated carbon supported molybdenum catalysts. Mol. Catal. 2017; 441; 28–34.

Canpotex. What is Potash? Retrieved from https://www.canpotex.com/our-potash/what-potash. Last accessed on November 17, 2019.

Cao X, Ro SK, Chappell M, Li Y, Mao J. Chemical structure of swine manure chars produced under different carbonization conditions investigated by advanced solid-state ^{13}C Nuclear Magnetic Resonance (NMR) spectroscopy. Energy Fuels 2011; 25; 388–97.

Casséus L. Canola: a Canadian success story. Canadian Agriculture at a Glance. 2009. Retrieved from https://www150.statcan.gc.ca/n1/en/catalogue/96-325-X200700010778. Last accessed on November 17, 2019.

Chaiwat W, Gunawan R, Gholizadeh M, Li X, Lievens C, Hu X, et al. Upgrading of bio-oil into advanced biofuels and chemicals. Part II. Importance of holdup of heavy species during the hydrotreatment of bio-oil in a continuous packed-bed catalytic reactor. Fuel 2013; 112; 302–10.

Chen C-J, Lee W-S, Bhan A. Mo_2C catalyzed vapor phase hydrodeoxygenation of lignin-derived phenolic compound mixtures to aromatics under ambient pressure. Appl. Catal., A 2016; 510; 42–8.

Chornet E, Overend RP. Biomass liquefaction: An overview. In: Overend RP, Milne TA, Mudge LK (Eds.). Fundamentals of Thermochemical Biomass Conversion. Springer 1985.

Clemente JS, Beauchemin S, Thibault Y, MacKinnon T, Smith D. Differentiating inorganics in biochars produced at commercial scale using principal component analysis. ACS Omega 2018; 3; 6931–44.

Costenoble O. Overview of specifications and regulations on (bio)fuels. Worldwide Fuels Standards. NEN Report 2006.

Degen T, Sadki M, Bron E, König U, Nénert G. The HighScore suite. Powder Diffraction 2014; 29; S13–S18.

Demirbas A. Competitive liquid biofuels from biomass. Appl. Energy 2011; 88; 17–28.

Dhandapani B, St. Clair T, Oyama ST. Simultaneous hydrodesulfurization, hydrodeoxygenation, and hydrogenation with molybdenum carbide. Appl. Catal., A 1998; 168; 219–28.

Dimitriadis A, Bezergianni S. Hydrothermal liquefaction of various biomass and waste feedstocks for biocrude production: A state of the art review. Renew. Sust. Energy Rev. 2017; 68; 113–25.

Domingues RR, Trugilho PF, Silva CA, de Melo ICNA, Melo LCA, Magriotis ZM, Sanchez-Monedero MA. Properties of biochar derived from wood and high-nutrient biomasses with the aim of agronomic and environmental benefits. PLoS ONE 2017; 12; e0176884.

El-Rub AZ, Bramer EA, Brem G. Review of catalysts for tar elimination in biomass gasification processes. Ind. Eng. Chem. Res. 2004; 43; 6911–9.

Eser S. Lesson 4 - Cut Points. FSC 432: Petroleum Processing. John A. Dutton e-Education Institute. Retrieved from https://www.e-education.psu.edu/fsc432/content/cut-points. Last accessed on November 17, 2019.

European Committee for Standardization (2003) Fat and oil derivatives—fatty acid methyl esters (FAME)—determination of oxidation stability (accelerated oxidation test). European Committee for Standardization Press, Brussels, Method EN 14112:2003.

Filippis PD, Caprariis BD, Scarsella M, Petrullo A, Verdone N. Biocrude production by hydrothermal liquefaction of olive residue. Int. J. Sust. Dev. Plann. 2016; 11; 700–7.

Fundamentals of Hydrotreating Part 1. What-When-How. Retrieved from http://what-when-how.com/petroleum-refining/fundamentals-of-hydrotreating-part-1/. Last accessed on November 25, 2019.

Furimsky E. Metal carbides and nitrides as potential catalysts for hydroprocessing. Appl. Catal., A 2003; 240; 1–28.

Gai C, Zhang Y, Chen W-T, Zhang P, Dong Y. Energy and nutrient recovery efficiencies in biocrude oil produced *via* hydrothermal liquefaction of *Chlorella pyrenoidosa*. RSC Adv. 2014; 4; 16958–67.

Gamliel DP, Baillie BP, Augustine E, Hall J, Bollas GM, Valla JA. Nickel impregnated mesoporous USY zeolites for hydrodeoxygenation of anisole. Microporous Mesoporous Mater. 2018; 261; 18-28.

Gary HJ, Handwerk GE, Kaiser MJ. Petroleum Refining: Technology and Economics; 5th ed. CRC Press: N.Y. 2007.

Gauden PA, Terzyk AP, Jaroniek M, Kowalczyk P. Bimodal pore size distributions for carbons: Experimental results and computational studies. J. Colloid Interface Sci. 2007; 310 (1); 205–16.

Girgis MJ, Gates BC. Reactivities, reaction networks, and kinetics of high-pressure catalytic hydroprocessing. Ind. Eng. Chem. Res. 1991; 30; 2021–58.

Gollakota ARK, Kishore N, Gu S. A review on hydrothermal liquefaction of biomass. Renew. Sust. Energy Rev. 2018; 81; 1378–92.

Gollakota ARK, Reddy M, Subramanyam MD, Kishore N. A review on the upgradation techniques of pyrolysis oil. Renew. Sust. Energy Rev. 2016; 58; 1543–68.

Goudriaan F, Beld B. van de, Boerefijn FR, Bos GM, Naber JE, Wal S et al. Thermal efficiency of the HTU process for biomass liquefaction. In: Proceedings of the Progress in Thermochemical Biomass Conversion Conference 2000; pp. 1312–25.

Government of Canada. “Challenge” for chemical substances that are high priority for action: Chemical substances in Batch 12 of the Challenge. 2013. Retrieved from https://www.canada.ca/en/health-canada/services/chemical-substances/challenge/batch-12/cristobalite-quartz.html. Last accessed on November 17, 2019.

Grilc M, Veryasov G, Likozar B, Jesih A, Levec J. Hydrodeoxygenation of solvolysed lignocellulosic biomass by unsupported MoS_2, MoO_2, Mo_2C and WS_2. Appl. Catal., B 2015; 163; 467–77.

Gruia A. Chapter 8: Hydrotreating. In: Jones DSJ, Pujadó PR (Eds.). Handbook of Petroleum Processing. Springer Netherlands 2006.

Gutierrez A, Kaila RK, Honkela ML, Slioor R, Krause AOI. Hydrodeoxygenation of guaiacol on noble metal catalysts. Catal. Today 2009; 147; 239–46.

Hachemi I, Jenistova K, Maki-Arvela P, Kumar N, Eranen K, Hemming J, Murzin DY. Comparative study of sulfur-free nickel and palladium catalysts in hydrodeoxygenation of different fatty acid feedstocks for production of biofuels. Catal. Sci. Technol. 2016; 6; 1476–87.

Han JX, Duan JZ, Chen P, Lou H, Zheng XM. Molybdenum carbide-catalyzed conversion of renewable oils into diesel-like hydrocarbons. Adv. Synth. Catal. 2011; 353; 2577–83.

He H, Zhong Y, Liang X, Tan W, Zhu J, Wang CY. Natural Magnetite: an efficient catalyst for the degradation of organic contaminant. Sci. Rep. 2015; 5: 10139.

He Z, Wang X. Hydrodeoxygenation of model compounds and catalytic systems for pyrolysis bio-oils upgrading. Catal. Sustainable Energy 2012; 1; 28–52.

Ingram L, Mohan D, Bricka M, Steele P, Strobel D, Crocker D, Mitchell B, Mohammad J, Cantrell K, Pittman CU Jr. Pyrolysis of wood and bark in an auger reactor: physical properties and chemical analysis of the produced bio-oils. Energy Fuels 2008; 22 (1); 614–25.

Jahirul MI, Rasul MG, Chowdhury AA, Ashwath N. Biofuels production through biomass pyrolysis – A technological review. Energies 2012; 5; 4952–5001.

Jensen CU, Hoffmann J, Rosendahl LA. Co-processing potential of HTL bio-crude at petroleum refineries. Part 2: A parametric hydrotreating study. Fuel 2016; 165; 536–43.

Jin F. Application of hydrothermal reactions to biomass conversion. Springer 2014. ISBN:978-3-642-54457-6.

Jongerius AL, Jastrzebski R, Bruijnincx PCA, Weckhuysen BM. CoMo sulphide-catalyzed hydrodeoxygenation of lignin model compounds: An extended reaction network for the conversion of monomeric and dimeric substrates. J. Catal. 2012; 285 (1); 315−23.

Joseph J, Baker C, Mukkamala S, Beis SH, Wheeler MC, DeSisto WJ, Jensen BL, Frederick BG. Chemical shifts and lifetimes for nuclear magnetic resonance (NMR) analysis of biofuels. Energy Fuels 2010; 24 (9); 5153–62.

Kader EA, Hussein HS, Hussien NH, Diwani GE, Hawash SI. Effect of extractive solvents on bio-oil production from microalgae via hydrothermal liquefaction. Chem. Process. Eng. Res. 2015; 38; 1-7.

Khader BFY, Yigezu YA, Duwayri MA, Niane AA, Shideed K. Where in the value chain are we losing the most food? The case of wheat in Jordan. Food Secur. 2019; 11 (5); 1009–27.

Kim SK, Yoon D, Lee S-C, Kim J. Mo_2C/graphene nanocomposite as a hydrodeoxygenation catalyst for the production of diesel range hydrocarbons. ACS Catalysis 2015; 5; 3292–303.

Kimura T, Imai H, Li XH, Sakashita K, Asaoka S, Al-Khattaf SS. Hydroconversion of triglycerides to hydrocarbons over Mo-Ni/γ-Al_2O_3 catalyst under low hydrogen pressure. Catal. Lett. 2013; 143; 1175–81.

Kumar A, Phadke S, Bhan A. Acetic acid hydrodeoxygenation on molybdenum carbide catalysts. Catal. Sci. Technol. 2018; 8; 2938–53.

Kumar G, Panda AK, Singh RK. Optimization of process for the production of bio-oil from eucalyptus wood. J. Fuel Chem. Technol. 2010; 38; 162–7.

Laurent E, Delmon B. Study of the hydrodeoxygenation of carbonyl, carboxylic and guaiacyl groups over sulfided CoMo/γ-Al_2O_3 and NiMo/γ-Al_2O_3 catalysts: I. Catalytic reaction schemes. Appl. Catal., A 1994; 109; 77–96.

Lee JW, Kidder M, Evans BR, Paik S, Buchanan III AC, Garten CT, Brown RC. Characterization of biochars produced from cornstovers for soil amendment. Environ. Sci. Technol. 2010; 44; 7970–4.

Lee W-S, Wang Z, Wu RJ, Bhan A. Selective vapor-phase hydrodeoxygenation of anisole to benzene on molybdenum carbide catalysts. J. Catal. 2014; 319; 44–53.

Li F, Shen K, Long X, Wen J, Xie X, Zeng X, Liang Y, Wei Y, Lin Z, Huang W, Zhong R. Preparation and characterization of biochars from *Eichornia crassipes* for cadmium removal in aqueous solutions. PLoS ONE 2016a; 11; e0148132.

Li R, Shahbazi A, Wang L, Zhang B, Hung AM, Dayton DC. Graphite encapsulated molybdenum carbide core/shell nanocomposite for highly selective conversion of guaiacol to phenolic compounds in methanol. Appl. Catal., A 2016b; 528; 123–30.

Li X, Luo X, Jin Y, Li J, Zhang H, Zhang A, Xie J. Heterogeneous sulfur-free hydrodeoxygenation catalysts for selectively upgrading the renewable bio-oils to second generation biofuels. Renew. Sust. Energy Rev. 2018; 82; 3762–97.

Li Y, Fan Y, He J, Xu B, Yang H, Miao J, Chen Y. Selective liquid hydrogenation of long chain linear alkadienes on molybdenum nitride and carbide modified by oxygen. Chem. Eng. J. 2004; 99 (3); 213–8.

Lian X, Xue Y, Zhao Z, Xu G, Han S, Yu H. Progress on upgrading methods of bio-oil: A review. Int. J. Energy Res. 2017; 41; 1798–1816.

Liang C, Ying P, Li C. Nanostructured β-Mo2C prepared by carbothermal hydrogen reduction on ultrahigh surface area carbon material. Chem. Mater. 2002; 14; 3148–51.

Liang J, Ding R, Wu Y, Chen Y, Wu K, Meng Y, Yang M, Wang Y. Effective conversion of heteroatomic model compounds in microalgae-based bio-oils to hydrocarbons over β-Mo_2C/CNTs catalyst. J. Mol. Catal. A: Chem. 2016; 411; 95–102.

Lin F, Waters CL, Mallinson RG, Lobban LL, Bartley LE. Relationships between biomass composition and liquid products formed via pyrolysis front. Energy Res. 2015; 3; 45.

Lin Z, Wan W, Yao S, Chen JG. Cobalt-modified molybdenum carbide as a selective catalyst for hydrodeoxygenation of furfural. Appl. Catal., B 2018; 233; 160-6.

Lu H, Zhang W, Yang Y, Huang X, Wang S, Qiu R. Relative distribution of Pb^{2+} sorption mechanisms by sludge-derived biochar. Water Res. 2012; 46; 854–62.

Luo W, Cao W, Bruijnincx PCA, Lin L, Wang A, Zhang T. Zeolite-supported metal catalysts for selective hydrodeoxygenation of biomass-derived platform molecules. Green Chem. 2019; 21; 3744–68.

Manya JJ. Pyrolysis of biochar purposes: A review to establish current knowledge gaps and research needs. Environ. Sci. Technol. 2012; 46; 7939–54.

Mapiour M. Kinetics and effects of H_2 partial pressure on hydrotreating of heavy gas oil. Master Thesis 2009. Retrieved from http://hdl.handle.net/10388/etd-12092009- 123009.

Moreira R, Ochoa E, Pinilla JL, Portugal A, Suelves I. Liquid-phase hydrodeoxygenation of guaiacol over Mo_2C supported on commercial CNF. Effects of operating conditions on conversion and product selectivity. Catalysts 2018; 8; 127.

Mortensen PM, Grunwaldt J-D, Jensen PA, Knudsen KG, Jensen AD. A review of catalytic upgrading of bio-oil to engine fuels. Appl. Catal., A 2011; 407; 1–19.

Patel M, Kumar A. Production of renewable diesel through the hydroprocessing of lignocellulosic biomass-derived bio-oil: A review. Renew. Sust. Energy Rev. 2016; 58; 1293–1307.

Puente GDL, Gil A, Pis JJ. Effects of support surface chemistry in hydrodeoxygenation reactions over CoMo/activated carbon sulfided catalysts. Langmuir 1999; 15; 5800–6.

Qu Y, Wei X, Zhong C. Experimental study on the direct liquefaction of *Cunninghamia lanceolata* in water. Energy 2003; 28; 597–606.

Rana R. Depositions of fines entrained in bitumen-derived light gas oil on hydrotreating catalyst: Impact of process parameters. Master Thesis 2016. Retrieved from http://hdl.handle.net/10388/7619.

Regmi P, Moscoso JLC, Kumar S, Cao X, Mao J, Schafran G. Removal of copper and cadmium from aqueous solution using switchgrass biochar produced via hydrothermal carbonization process. J. Environ. Manage. 2012; 109; 61–9.

Reichardt C. Solvents and solvent effects in organic chemistry. Wiley-VCH Publishers. 3rd edition. 2003.

Ren H, Yu W, Salciccioli M, Chen Y, Huang Y, Xiong K, Vlachos DG, Chen JG. Selective hydrodeoxygenation of biomass-derived oxygenates to unsaturated hydrocarbons using molybdenum carbide catalysts. Chem. Sus. Chem. 2013 ; 6 ; 798–801.

Reusch W. Infrared Spectroscopy. 2013. Retrieved from https://www2.chemistry.msu.edu/faculty/reusch/virttxtjml/spectrpy/infrared/infrared.htm. Last accessed on November 17, 2019.

Rocha JD, Luengo CA, Snape CE. Hydrodeoxygenation of oils from cellulose in single and two-stage hydropyrolysis. Renew. Energy 1996; 9; 950–3.

Ross AB, Biller P, Kubacki ML, Li H, Lea-Langton A, Jones JM. Hydrothermal processing of microalgae using alkali and organic acids. Fuel 2010; 89; 2234–43.

Sangon S, Ratanavaraha S, Ngamprasertsith S, Prasassarakich P. Coal liquefaction using supercritical toluene-tetralin mixture in a semi-continuous reactor. Fuel Process Technol. 2006; 87; 201–7.

Santos RM, Santos AO, Sussuchi EM, Nascimento JS, Lima AS, Freitas LS. Pyrolysis of mangaba seed: Production and characterization of bio-oil. Bioresour. Technol. 2015; 196; 43–8.

Satterfield CN. Heterogeneous catalysis in industrial practice. Charles N. Satterfield, 2nd E. 1996.

Sauvanaud L, Mathieu Y, Corma A, Humphreys L, Rowlands W, Maschmeyer T. Co-processing of lignocellulosic biocrude with petroleum gas oils. Appl. Catal., A 2018; 551; 139–45.

Shang N-C, Liu R-Z, Chen Y-H, Chang C-Y, Lin R-H. Characterization of fatty acid methyl esters in biodiesel using high-performance liquid chromatography. J. Taiwan Inst. Chem. Eng. 2012; 43; 354–59.

Sing KSW, Everett DH, Haul RAW, Moscou L, Pierotti RA, Rouquérol J, Simemieniewska T. Reporting physisorption data for gas/solid systems with special reference to the determination of surface area and porosity. Pure Appl. Chem. 1985; 57 (4); 603–19.

Singh R, Prakash A, Balagurumurthy B, Bhaskar T. Chapter 10 – Hydrothermal liquefaction of biomass. In: Pandey A, Bhaskar T, Stöcker M, Sukumaran RK (Eds.). Recent Advances in Thermo-Chemical Conversion of Biomass. Elsevier 2015, p. 269–91. ISBN: 978-0-444-63289-0.

Smirnov AA, Geng Z, Khromova SA, Zavarukhin SG, Bulavchenko OA, Saraev AA, Kaichev VV, Ermakov DY, Yakovlev VA. Nickel molybdenum carbides: Synthesis, characterization, and catalytic activity in hydrodeoxygenation of anisole and ethyl caprate. J. Catal. 2017; 354; 61–77.

Sorrell S, Speirs J, Bentley R, Brandt A, Miller R. Global oil depletion: A review of the evidence. Energy Policy 2010; 38; 5290–5.

Stanislaus A, Marafi A, Rana MS. Recent advances in the science and technology of ultra-low sulfur diesel (ULSD) production. Catal. Today. 2010; 153; 1–68.

Statistics Canada. Table 32-10-0359-01: Estimated areas, yield, production, average farm price and total farm value of principal field crops, in metric and imperial units. Retrieved from https://www150.statcan.gc.ca/t1/tbl1/en/tv.action?pid=3210035901. Last accessed on November 17, 2019.

Suguihiro TM, de Oliveira PR, de Rezende EIP, Mangrich AS, Junior LHM, Bergamini MF. An electroanalytical approach for evaluation of biochar adsorption characteristics and its application for Lead and Cadmium determination. Bioresour. Technol. 2013; 143; 40–5.

Toba M, Abe Y, Kuramochi H, Osako M, Mochizuki T, Yoshimura Y. Hydrodeoxygenation of waste vegetable oil over sulfide catalysts. Catal. Today 2011; 164; 533–7.

Torri IDV, Paasikallio V, Faccini CS, Huff R, Caramão EB, Sacon V, Oasmaa A, Zini CA. Bio-oil production of softwood and hardwood forest industry residues through fast and intermediate pyrolysis and its chromatographic characterization. Bioresour. Technol. 2016; 200; 680–90.

Trubetskaya A, Jensen PA, Jensen AD, Steibel M, Spliethoff H, Glarborg P, Larsen FH. Comparison of high temperature chars of wheat straw and rice husk with respect to chemistry, morphology and reactivity. Biomass Bioenergy 2016; 86; 76–87.

Tzanetis KF, Posada JA, Ramirez A. Analysis of biomass hydrothermal liquefaction and biocrude-oil upgrading for renewable jet fuel production: The impact of reaction conditions on production costs and GHG emissions performance. Renew. Energy 2017; 113; 1388–98.

Valdez PJ, Dickinson JG, Savage PE. Characterization of product fractions from hydrothermal liquefaction of *Nannochloropsis* sp. and the influence of solvents. Energy Fuels 2011; 25; 3235–43.

Vardon DR, Sharma BK, Scott J, Yu G, Wang Z, Schideman L, Zhang Y, Strathmann TJ. Chemical properties of biocrude oil from the hydrothermal liquefaction of Spirulina algae, swine manure, and digested anaerobic sludge. Bioresour. Technol. 2011; 102; 8295–303.

Vassilev SV, Baxter D, Andersen LK, Vassileva CG. An overview of the composition and application of biomass ash. Part 1. Phase–mineral and chemical composition and classification. Fuel 2013; 105; 40–76.

Wandas R, Surygała J, Śliwka E. Conversion of cresols and naphthalene in the hydroprocessing of three-component model mixtures simulating fast pyrolysis tars. Fuel 1996; 75; 687–94.

Wang F, Xu J, Jiang J, Liu P, Li F, Ye J, Zhou M. Hydrotreatment of vegetable oil for green diesel over activated carbon supported molybdenum carbide catalyst. Fuel 2018; 216; 738–46.

Wang H, Liu S, Smith KJ. Synthesis and hydrodeoxygenation activity of carbon supported molybdenum carbide and oxycarbide catalysts. Energy Fuels 2016; 30 (7); 6039−49.

Wang H, Yan S, Salley SO, Simon Ng KY. Support effects on hydrotreating of soybean oil over NiMo carbide catalyst. Fuel 2013; 111; 81-7.

Wang K, Zhang J, Shanks BH, Brown RC. Catalytic conversion of carbohydrate-derived oxygenates over HZSM-5 in a tandem micro-reactor system. Green Chem. 2015; 17; 557–64.

Wei L, Liang S, Guho NM, Hanson AJ, Smith MW, Garcia-Perez M, McDonald AG. Production and characterization of bio-oil and biochar from the pyrolysis of residual bacterial biomass from a polyhydroxyalkanoate production process. J. Anal. Appl. Pyrolysis 2015; 115; 268–78.

Wildschut J, Mahfud FH, Venderbosch RH, Heeres HJ. Hydrotreatment of fast pyrolysis oil using heterogeneous noble-metal catalysts. Ind. Eng. Chem. Res. 2009; 48; 10324–34.

Xiu S, Shahbazi A. Bio-oil production and upgrading research: A review. Renew. Sust. Energy Rev. 2012; 16; 4406–14.

Xu Y, Wang T, Ma L, Chen G. Upgrading of fast pyrolysis liquid fuel from biomass over Ru/γ-Al_2O_3 catalyst. Energy Convers. Manage. 2012; 55; 172–7.

Yang H, Yan R, Chen H, Lee DH, Zheng C. Characteristics of hemicellulose, cellulose and lignin pyrolysis. Fuel 2007; 86; 1781–8.

Yang X, Lyu H, Chen K, Zhu X, Zhang S, Chen J. Selective extraction of bio-oil from hydrothermal liquefaction of *Salix Psammophila* by organic solvents with different polarities through multistep extraction separation. BioResources 2014; 9; 5219–33.

Zhang C, Xing J, Song L, Xin H, Lin S, Xing L, et. al. Aqueous-phase hydrodeoxygenation of lignin monomer eugenol: Influence of Si/Al ratio of HZSM-5 on catalytic performances. Catal. Today 2014; 234; 145–52.

Zhao S-X, Ta N, Wang X-D. Effect of temperature on the structural and physicochemical properties of biochar with apple tree branches as feedstock material. Energies 2017; 10; 1293.

Zou XW, Qin TF, Huang LH, Zhang XL, Yang Z, Wang Y. Mechanisms and main regularities of biomass liquefaction with alcoholic solvents. Energy Fuels 2009; 23; 5213–8.

APPENDIX A: Permission to use Journal Article

Permission to use the following paper in thesis:

Chand R, Borugadda VB, Qiu M, Dalai AK. Evaluating the potential for bio-fuel upgrading: A comprehensive analysis of bio-crude and bio-residue from hydrothermal liquefaction of agricultural biomass. Applied Energy 2019; 254; 113679.

DOI: https://doi.org/10.1016/j.apenergy.2019.113679.

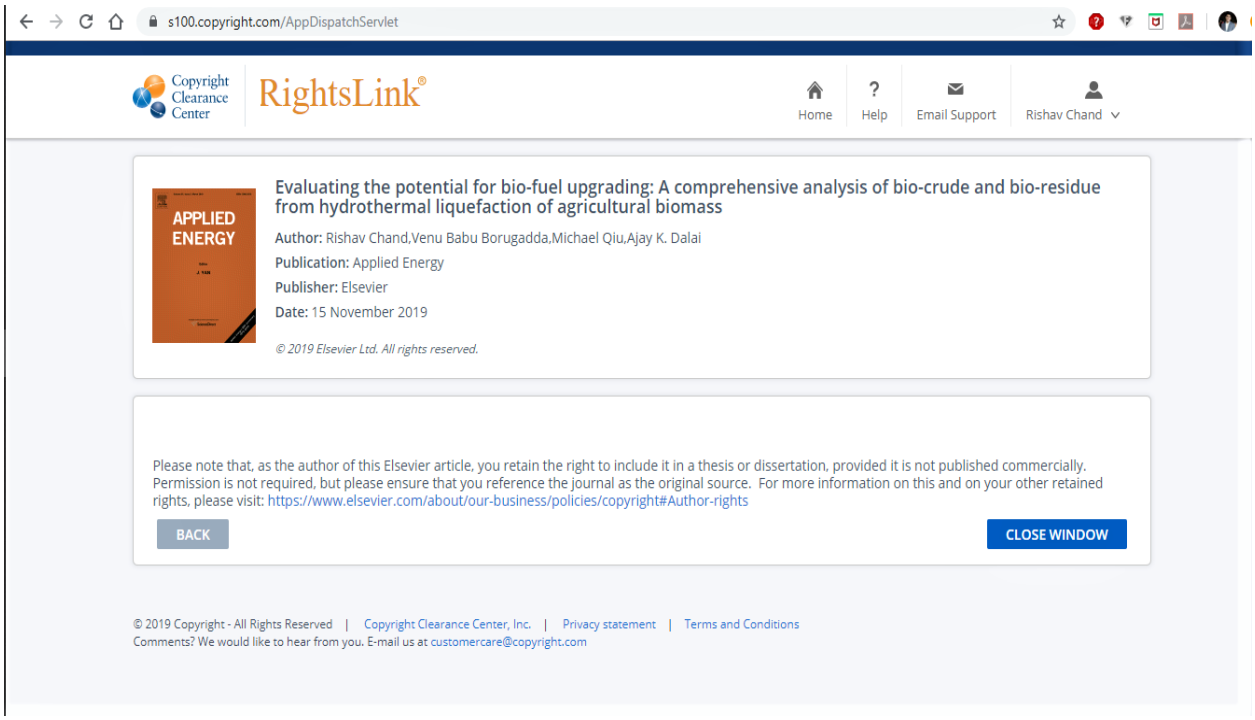

Copyright

Describes the rights related to the publication and distribution of research. It governs how authors (as well as their employers or funders), publishers and the wider general public can use, publish and distribute articles or books.

Journal author rights Government employees Elsevier's rights Protecting author rights Open access

Journal author rights

In order for Elsevier to publish and disseminate research articles, we need publishing rights. This is determined by a publishing agreement between the author and Elsevier. This agreement deals with the transfer or license of the copyright to Elsevier and authors retain significant rights to use and share their own published articles. Elsevier supports the need for authors to share, disseminate and maximize the impact of their research and these rights, in Elsevier proprietary journals* are defined below:

For subscription articles	For open access articles
Authors transfer copyright to the publisher as part of a journal publishing agreement, but have the right to: • Share their article for Personal Use, Internal Institutional Use and Scholarly Sharing purposes, with a DOI link to the version of record on ScienceDirect (and with the Creative Commons CC-BY-NC- ND license for author manuscript versions) • Retain patent, trademark and other intellectual property rights (including research data). • Proper attribution and credit for the published work.	Authors sign an exclusive license agreement, where authors have copyright but license exclusive rights in their article to the publisher**. In this case authors have the right to: • Share their article in the same ways permitted to third parties under the relevant user license (together with Personal Use rights) so long as it contains a CrossMark logo, the end user license, and a DOI link to the version of record on ScienceDirect. • Retain patent, trademark and other intellectual property rights (including research data). • Proper attribution and credit for the published work.

APPENDIX B: Highlights of the Solvent-extraction Process

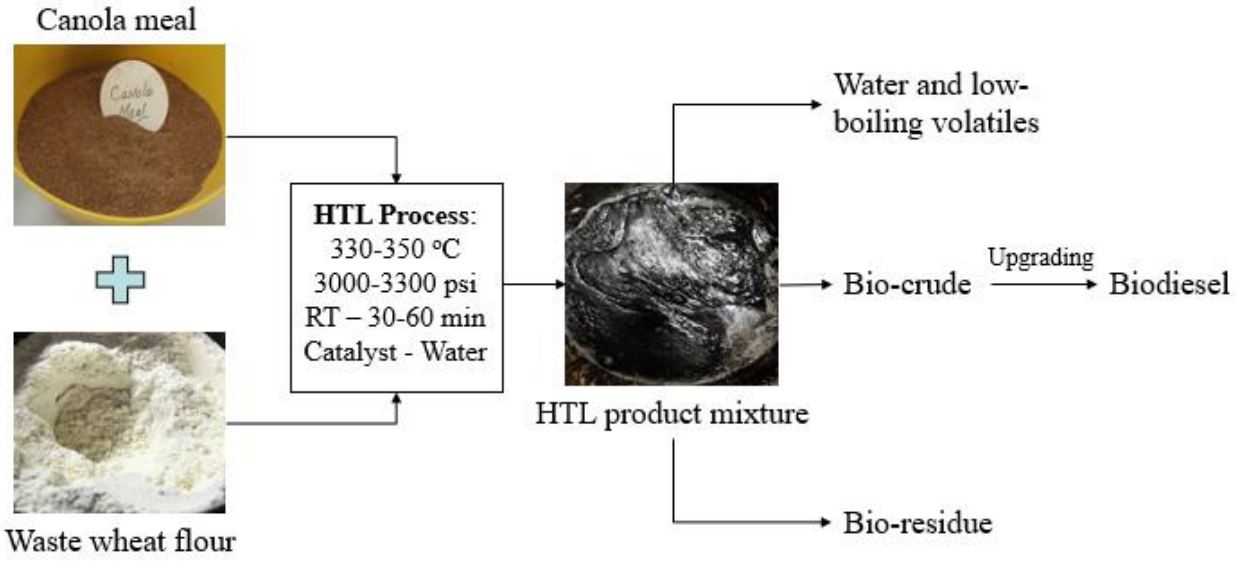

Fig. B.1 Process outline for the production and extraction of HTL bio-crude and bio-residue.

Fig. B.2 Bio-crude samples (from left to right): BC-EA, BC-THF and BC-PE.

Fig. B.3 Bio-residue samples (from left to right): BR-EA, BR-THF and BR-PE.